

Nanoparticle-Cell Interactions
in a Dynamic *In Vitro*
Lung Model

Dissertation
zur Erlangung des Grades
der Doktorin der Naturwissenschaften der
Naturwissenschaftlich-Technischen Fakultät
der Universität des Saarlandes

Von
Carmen Beate Schmitz

Saarbrücken
Mai 2022

Tag des Kolloquiums: 09. September 2022

Dekan: Prof. Dr. Jörn Walter

1. Berichterstatter: Priv.-Doz. Dr. Annette Kraegeloh

2. Berichterstatter: Prof. Dr. Alexandra K. Kiemer

Vorsitz: Prof. Dr. Marc Schneider

Akademischer Mitarbeiter: Dr. Stefan Boettcher

Table of Content

Table of Content	III
Abbreviations	V
1 Abstract	1
2 Zusammenfassung in deutscher Sprache	3
3 Background: Nanoparticles in the human lungs	5
3.1 Nanomaterials and nanotoxicology	7
3.2 Entry routes into the body	8
3.3 Mechanisms of nanoparticle toxicity	11
3.4 Anatomy and physiology of the respiratory tract	13
3.5 Mechanical forces in the lung	14
3.6 Current <i>in vitro</i> lung models	16
4 Aim of this study	19
5 Materials and Methods	21
5.1 Synthesis and characterization of nanomaterials	23
5.1.1 <i>Colloidal amorphous silica nanoparticles</i>	23
5.2 Cell Culture	24
5.3 Mechanical strain	26
5.4 Exposition of cells to nanomaterials	27
5.5 RNA isolation for gene array and qPCR	28
5.5.1 <i>RNA isolation</i>	28
5.5.2 <i>DNase digestion and purification</i>	28
5.6 Microarray analysis and bioinformatics	29
5.6.1 <i>RNA quality control</i>	30
5.7 Gene Expression Analysis by Quantitative Real-Time PCR	30
5.7.1 <i>Reverse Transcription</i>	30
5.7.2 <i>Primer Design</i>	30
5.7.3 <i>qPCR protocol</i>	31
5.7.4 <i>Primer validation by agarose gel electrophoresis</i>	31
5.7.5 <i>Determination of PCR efficiency and optimization</i>	32
5.7.6 <i>qPCR data evaluation</i>	32
5.8 Membrane integrity	32
5.9 IL8 secretion (ELISA)	33
5.10 Microscopy	33
5.10.1 <i>Sample preparation for confocal microscopy</i>	33
5.10.2 <i>Confocal laser scanning microscopy</i>	34
5.10.3 <i>Image processing with ImageJ 1.51j8</i>	35
5.10.4 <i>Statistical analysis</i>	36
6 Part I: Mechanical strain alters gene expression in A549 cells treated with 25 nm silica particles	37
6.1 Introduction	39
6.2 Results	41
6.2.1 <i>SiO₂ nanoparticle properties</i>	41
6.2.2 <i>Compatibility of the culture conditions (matrix coating, strain, and nanoparticles)</i>	43
6.2.3 <i>Membrane integrity is not affected by SiO₂ nanoparticles, mechanical strain or both</i>	45
6.2.4 <i>Determination of treatment exposition time to analyze short term changes in gene expression</i>	46
6.2.5 <i>Genome-wide gene expression alterations</i>	46
6.2.6 <i>Nanoparticle exposure under mechanical strain increases expression of inflammation-associated genes</i>	47
6.2.7 <i>Nanoparticle exposure under mechanical strain decreases expression of proliferation-associated genes</i>	48
6.2.8 <i>Confirmation of cytokine expression by qPCR</i>	50
6.2.9 <i>Nanoparticle exposure under mechanical strain increases IL8 secretion</i>	50
6.2.10 <i>Cellular accumulation of Si25 nanoparticles is not affected by stretching</i>	51
6.2.11 <i>No NF-κB translocation upon Si25 treatment, stretching or both</i>	54
6.3 Discussion	57

6.3.1	<i>SiO₂ nanoparticle uptake is not enhanced under mechanical strain</i>	57
6.3.2	<i>The pro-inflammatory response of A549 cells induced by SiO₂ nanoparticles under mechanical strain seems independent from the canonical NF-κB pathway</i>	58
6.3.3	<i>Mechanical strain amplifies Si25-induced effects on expression of genes related to inflammation in A549 cells</i>	59
7	Part II: Influence of silica nanoparticle size and stretching amplitude on cytokine release in alveolar type II cells	63
7.1	Introduction	65
7.1.1	<i>Particle size</i>	65
7.1.2	<i>Mechanical strain in in vitro models</i>	66
7.2	Results	69
7.2.1	<i>Silica nanoparticles of 25 or 80 nm in diameter cause similar responses in A549 cells</i>	69
7.2.2	<i>Increasing stretching amplitude from 15% to 25% does not lead to stronger inflammatory response of A549 cells</i>	70
7.3	Discussion	73
7.3.1	<i>Particle delivery</i>	73
7.3.2	<i>Interplay between stretch and nanoparticles may take place at the cell membrane</i>	74
7.3.3	<i>Cell type specific robustness to mechanical strain needs to be considered for in vitro models</i>	75
8	Part III: Experimental reproducibility with the dynamic lung <i>in vitro</i> model	79
8.1	Introduction	81
8.2	Results	83
8.2.1	<i>Nanoparticles and fetal bovine serum</i>	83
8.2.2	<i>Culture conditions may alter particle-induced effects on cytokine expression</i>	83
8.2.3	<i>Impact of FBS change on NF-κB translocation</i>	87
8.3	Discussion	89
9	Conclusion and Outlook	93
10	References	97
11	Supplementary Information	107
11.1	Identity verification of A549 cell line	109
11.2	Intracellular nanoparticle localization	109
11.3	Validation of elongation in stretching setup	110
11.4	Primer validation	111
11.5	LDH degradation	112
11.6	Leaching of fluorescent SiO ₂ nanoparticles	113
11.7	Stretch and Si25 induced IL8 secretion	113
11.8	Cell morphology under different fetal bovine sera	114
11.9	Cell morphology under supplementation with heat-inactivated FBS	114
11.10	Cytokine expression under supplementation with heat-inactivated FBS	115
11.11	Effect of nanoparticles and stretch on human pulmonary alveolar epithelial cells	115
11.12	Translocation kinetics of NF-κB subunits	116
11.12.1	<i>NF-κB p65</i>	116
11.12.2	<i>NF-κB2 p100/p52</i>	117
11.12.3	<i>NF-κB1 p105/p50</i>	118
Danksagung		VII

Abbreviations

μl	Microliter
3T3	Murine embryo fibroblast cell line
a.u.	Arbitrary units
A549	Human adenocarcinomic cell line with properties of type II alveolar epithelial cells (Lieber <i>et al.</i> , 1976)
AE-I	Type 1 alveolar epithelial cells
AE-II	Type 2 alveolar epithelial cells
ALI	Air-liquid interface
AM	Alveolar macrophages
aRNA	Amplified ribonucleic acid
BEAS-2B	Bronchial epithelium transformed with Ad12-SV40 2B
bp	Base pairs
BSA	Bovine serum albumin
CCL20	CC-chemokine ligand 20, also known as Liver Activation Regulated Chemokine (LARC) or Macrophage Inflammatory Protein-3 (MIP3A)
cDNA	Complementary deoxyribonucleic acid
CEL file	data file created by Affymetrix DNA microarray image analysis software
cm	Centimeter
Cq	Cycle of quantification
CXCL8	Chemokine ligand 8
DMEM	Dulbecco's modified Eagle medium
DNA	Deoxyribonucleic acid
EA.hy926	Human endothelial somatic cell hybrid
EDTA	Ethylenediaminetetraacetic acid
FBS	Fetal bovine serum (short: serum)
fwd	Forward
GAPDH	Glyceraldehyde 3-phosphate dehydrogenase
h	Hour
HBEC3-KT	Human bronchial epithelial cells immortalized with CDK4 and hTERT
IL1β	Interleukin 1 beta
IL8	Interleukin 8 (product of <i>CXCL8</i>)
J774	Murine macrophage cell line
KCl	Potassium chloride
LB	Lamellar bodies
LD540	Lipophilic dye based on the Bodipy fluorophore (lipid droplet stain)
LDH	Lactate dehydrogenase
LIGHT	Tumor necrosis factor superfamily member 14 (TNFSF14)
LPS	Lipopolysaccharides
MIAME	Minimum Information About a Microarray Experiment
min	Minute
ml	Milliliter
mm	Millimeter
N	Number of independent experiments (biological replicates) included in analysis
NF-κB	Nuclear factor 'kappa-light-chain-enhancer' of activated B-cells
nm	Nanometer
NP(s)	Nanoparticle(s)
p38 MAPK	p38 mitogen-activated protein kinases

PBS	Phosphate-buffered saline
pg	Picogram
PMT	Photomultiplier tube
qPCR	Quantitative real time polymerase chain reaction
rev	Reverse
RNA	Ribonucleic acid
RT	Room temperature (≈ 20 °C)
sec	Seconds
SAS	Synthetic amorphous silica (aggregated)
SD	Standard deviation
Si25	SiO ₂ nanoparticles with diameter of ≈ 25 nm (colloidal, monodisperse)
Si25-FD	Fluorescently labelled SiO ₂ nanoparticles with diameter of ≈ 25 nm (colloidal, monodisperse)
Si80	SiO ₂ nanoparticles with diameter of ≈ 80 nm (colloidal, monodisperse)
SR-A1	Scavenger receptor class A1
SR-B1	Scavenger receptor class B1
STR	Short tandem repeats
t	Time
TACE	Also known as: ADAM metallopeptidase domain 17
TLC	Total lung capacity
TNF	Tumor necrosis factor
V	Volt
WGA	Wheat germ agglutinin
ΔS_A	Area expansion of the flexible cell culture substrate under tension
ϵ	Linear elongation

1 Abstract

The effects of engineered nanomaterials on human health are intensively studied in order to facilitate their safe application. However, relatively little is known how mechanical strain (stretching), as induced in alveolar epithelial cells by breathing dynamics, modifies biological responses to nanoparticles. In this study, A549 cells as a model for human type II alveolar epithelial cells were exposed to 25 nm amorphous colloidal silica nanoparticles (Si25) under dynamic or static culture conditions. Gene array data, qPCR, and ELISA revealed that stretching, in order to mimic breathing, can amplify the inflammatory responses to nanoparticle exposure. Treatment of cells with either stretching or nanoparticles alone led to minor changes in gene expression or cytokine secretion. The amplifying effect from stretching was not influenced by nanoparticle size or an intensified stretching, but by varying fetal bovine sera for medium supplementation. The type of fetal bovine serum used as medium supplement determined the occurrence of the amplifying effect, affecting both baseline cytokine production, as well as cellular response to nanoparticles.

Gene expression alterations induced by combined exposure to nanoparticles plus stretching showed a high similarity to those known to be induced by TNF and mediated by NF κ B. However, translocation of NF κ B-p65, NF- κ B2-p100/p52, and NF- κ B1-p105/p50 subunits upon Si25, stretch, or a combined treatment could not be observed. Confocal microscopy revealed that stretching did not lead to an increased internalization of nanoparticles in this simplified lung model, indicating that the observed response amplification was not caused secondary to an elevated intracellular nanoparticle accumulation.

This study suggests that mechanical strain, which constantly affects lung epithelial cells *in vivo*, significantly determines cell response and should therefore be implemented in all *in vitro* models for pulmonary toxicity tests.

2 Zusammenfassung in deutscher Sprache

Die Auswirkungen menschengemachter Nanopartikel sind im Fokus vieler wissenschaftlicher Studien, um zukünftig deren sichere Handhabung und Anwendung zu gewährleisten. Wenig ist bisher darüber bekannt, wie sich mechanische Belastung, die beispielsweise während der Atmung in unseren Lungen stattfindet, auf die zelluläre Reaktion gegenüber inhalierter Nanopartikel auswirkt.

In dieser Arbeit wurden A549 Zellen als Modell für humane alveoläre Typ II Epithelzellen mit kolloidalen amorphen Siliziumdioxid-Nanopartikeln behandelt und währenddessen entweder mit oder ohne mechanische Dehnung kultiviert. Genexpressionsanalysen mittels Microarrays und quantitativer Echtzeit-Polymerase-Kettenreaktion (qPCR) sowie Sekretionsanalysen durch Enzymimmunoassays (ELISA) zeigten, dass atmungssimulierende mechanische Dehnung *in vitro* die inflammatorische Zellantwort auf Nanopartikelexposition verstärken kann. Die Behandlung der Zellen mit entweder mechanischer Dehnung oder Nanopartikeln allein verursachte nur schwache Veränderungen der Genexpression und Sekretion bestimmter Zytokine. Der beobachtete verstärkende Effekt der mechanischen Dehnung auf die Zytokinexpression schien unabhängig von der Größe der eingesetzten Nanopartikel zu sein. Auch das Steigern der mechanischen Dehnung von 15% auf 25% Flächenexpansion veränderte den verstärkenden Effekt nicht. Jedoch führte die Verwendung eines anderen fötalen Kälberserums (FBS) in der Zellkultur zum Ausbleiben dieses Effekts von mechanischer Dehnung. Sowohl die grundlegende Zytokinproduktion, als auch die Reaktion auf die Nanopartikel waren vom Einfluss des FBS betroffen.

Das durch Siliziumdioxid-Nanopartikel plus mechanische Dehnung veränderte Genexpressionsmuster der Zellen wies Ähnlichkeit mit der Zellantwort auf, die NF κ B-abhängig durch den Tumornekrosefaktor (TNF) induziert wird. Mithilfe von Konfokalmikroskopie konnte die Translokation der NF κ B-p65, NF- κ B2-p100/p52 und NF- κ B1-p105/p50 Untereinheiten durch Behandlung mit Nanopartikeln, Dehnung oder einer Kombination aus beidem nicht nachgewiesen werden.

Die Vermutung, dass mechanische Dehnung die zelluläre Aufnahme von Siliziumdioxid-Nanopartikeln steigert und damit indirekt zu einer stärkeren

inflammatorischen Reaktion führt, konnte für dieses Lungenmodell mithilfe von Konfokalmikroskopie widerlegt werden.

Diese Arbeit bestätigt, dass mechanische Belastung ein integraler Bestandteil der *in vivo* Situation von alveolaren Epithelzellen ist und deren Zellantwort auf Nanopartikel signifikant beeinflusst. Mechanische Belastung sollte daher in allen *in vitro*-Modellen für Pneumotoxizitätstests implementiert werden.

3 Background: Nanoparticles in the human lungs

3.1 Nanomaterials and nanotoxicology

Humans have always been exposed to naturally occurring nano-sized materials, for example from volcanic ashes or dust from desert storms (Strambeanu *et al.*, 2015b). Unintended exposition to anthropogenic nano-sized or ultra-fine particles (e.g. from mining, milling, and fuel combustion), however, has increased with industrialization (Strambeanu *et al.*, 2015a). Awareness of the hazardous potential of such small particles compared to larger ones rose in the nineteen-nineties with the realization of their stronger inflammatory potential and more efficient interstitial translocation (Donaldson *et al.*, 2004; Kagan *et al.*, 2005; Oberdörster *et al.*, 2005; Oberdörster *et al.*, 2009). Nowadays, more and more types of engineered nanomaterials (ENM) are being used for a diversity of applications. The most prominent examples are certainly titanium dioxide in sunscreen, nano-silver for its antibacterial effect in medical plasters or clothing, quantum dots in optical electronics, carbon black in printer toner or mascara, and nano-scaled synthetic amorphous silicon dioxide (SAS) as a food additive (Karlsruher Institut für Technologie, 2021a). It is not surprising that nanotoxicology as a research field at the transition between materials science and toxicology has gained increasing interest over the past two decades (Miller and Poland, 2020). Initially, the common understanding and nomenclature of 'nano-sized', 'nano-scaled' or 'ultra-fine' particles was inconsistent. Many attempts have been made to establish a definition for nanomaterials with regard to their origin, primary particles size, agglomeration and aggregation behaviour, or their volume-specific surface area (Kreyling *et al.*, 2010). In 2011, the European Commission recommended the following definition: *“‘Nano-material’ means a natural, incidental or manufactured material containing particles, in an unbound state or as an aggregate or as an agglomerate and where, for 50% or more of the particles in the number size distribution, one or more external dimensions is in the size range 1 nm-100 nm. [...] ‘Particle’ means a minute piece of matter with defined physical boundaries [...].”*

3.2 Entry routes into the body

Depending on the way of exposure, nanoparticles can enter the human body through several routes (Stern and McNeil, 2008). The dermal route (intercellularly, transcellularly, or *via* hair follicles) is especially relevant for nanoparticulate components of cosmetics, dermatics and clothing. Healthy human skin is an effective protection and prevents most of these nanoparticle types from entering the body (Nohynek *et al.*, 2007).

The gastrointestinal tract (GIT) may come into contact with nano sized components of food additives^a and packaging material (e.g. nano-silver as an antimicrobial agent, TiO₂^b as a food pigment, SiO₂ as a thickening agent), but also unintended consumption of nanoparticles through contaminated food or water matters. Medical applications, such as contrast agents for radiology, also require ingestion of nanoparticles (e.g. barium sulphate or iron oxide). Inside the GIT, nanoparticles encounter saliva, gastric acid, enzymes, mucus, bacteria and food components leading to chemical and physical transformation, disruption and eventually elimination. On their way from the gut lumen into the tissue or blood stream, nanoparticles first have to penetrate a layer of mucosa before entering the tissue *via* cellular or paracellular transport. Data on gastrointestinal nanoparticle entry vary substantially between *in vitro* and *in vivo* studies as well as nanoparticle types. Estimating realistic exposition doses and translating and applying these in cell culture or animal models are difficult challenges (Sohal *et al.*, 2018; da Silva *et al.*, 2020).

In contrast to dermal and gastrointestinal nanoparticle entry, the inhalative entry route is especially important when it comes to unintended occupational exposure to nanoparticles. Many types of nanoparticles are suspected to cause respiratory diseases such as inflammation, fibrosis or cancer (Nho, 2020). With global annual production of SiO₂ being vaguely estimated between 10⁵-10⁶ tons and expected to increase (Janković and Plata, 2019), these materials represent an important unintended way of exposure to production workers. Inhalative uptake can also become relevant when nanoparti-

^a Currently, in the European Union no food additives that are intentionally produced in nano size are approved. (Karlsruher Institut für Technologie, 2021b. *Nanomaterialien in Lebensmitteln* [online].

<https://nanopartikel.info/basics/querschnittsthemen/nanomaterialien-in-lebensmitteln/>, [September 10, 2021].)

^b Since 2021, the food additive E171, which contains nano-sized TiO₂, is no longer considered safe by the European Food Safety Authority. (European Food Safety Authority, 2021. *Titanium dioxide: E171 no longer considered safe when used as a food additive* [online]. <https://www.efsa.europa.eu/en/news/titanium-dioxide-e171-no-longer-considered-safe-when-used-food-additive>, [November 15, 2021].)

cles that are usually bound within composite materials are subject to degradation and thus released into the air. In 2015, ambient particulate matter was the cause for 4.2 million deaths; occupational exposure to particulate matter caused 0.4 million deaths (Global Burden of Disease (GBD) 2015 Risk Factors Collaborators, 2016). Inhalation of nanoparticles, e.g. as drug delivery system, has also gained increasing interest. Potential applications, some already under clinical investigation, use e.g. aerosolized liposomes, polymers, or silica as carriers to target lung cancer, acute respiratory distress syndrome (ARDS), asthma, respiratory infections, or diabetes (Osman *et al.*, 2020; Praphawatvet *et al.*, 2020).

During inhalation, airborne particles enter the respiratory tract through nose or mouth. Depending on size, shape and density, they deposit in different sections of the lung. Particles in the size range of approximately 10 μm deposit in the nasal and laryngopharyngeal region, mainly upon impaction, but hardly reach the alveolar space. Particles sized 10-100 nm reach the bronchial and alveolar space almost unhindered *via* diffusion. Deposition of nanoparticles in the lung also depends on capacity, flow rate and frequency of inhalation (Heyder and Svartengren, 2002; Oberdörster *et al.*, 2005; Nho, 2020). Particles that deposit in the upper and conducting airways are subject to mucociliary clearance. In the alveolar space, deposited particles can be phagocytosed by alveolar macrophages. However, large parts retain in close contact with lung surfactant and the alveolar epithelium where they can accumulate and eventually transition to the interstitium, the lymphatic system, or into the blood stream from where systemic distribution is possible (Oberdörster *et al.*, 2005; Riediker *et al.*, 2019).

Cellular entry mechanisms (Figure 1) include endocytic processes, such as caveolin or clathrin dependent endocytosis, clathrin independent endocytosis, phagocytosis and macropinocytosis, as well as direct nanoparticle translocations. Endocytic uptake is strictly regulated and incorporates nanoparticles within endocytic or phagocytic vesicles, thereby determining their intracellular or even transcellular fate and potential immune responses. Direct nanoparticle translocations result in a vesicle-free penetration through the cell membrane, which is an important mechanism in drug delivery research (Donahue *et al.*, 2019).

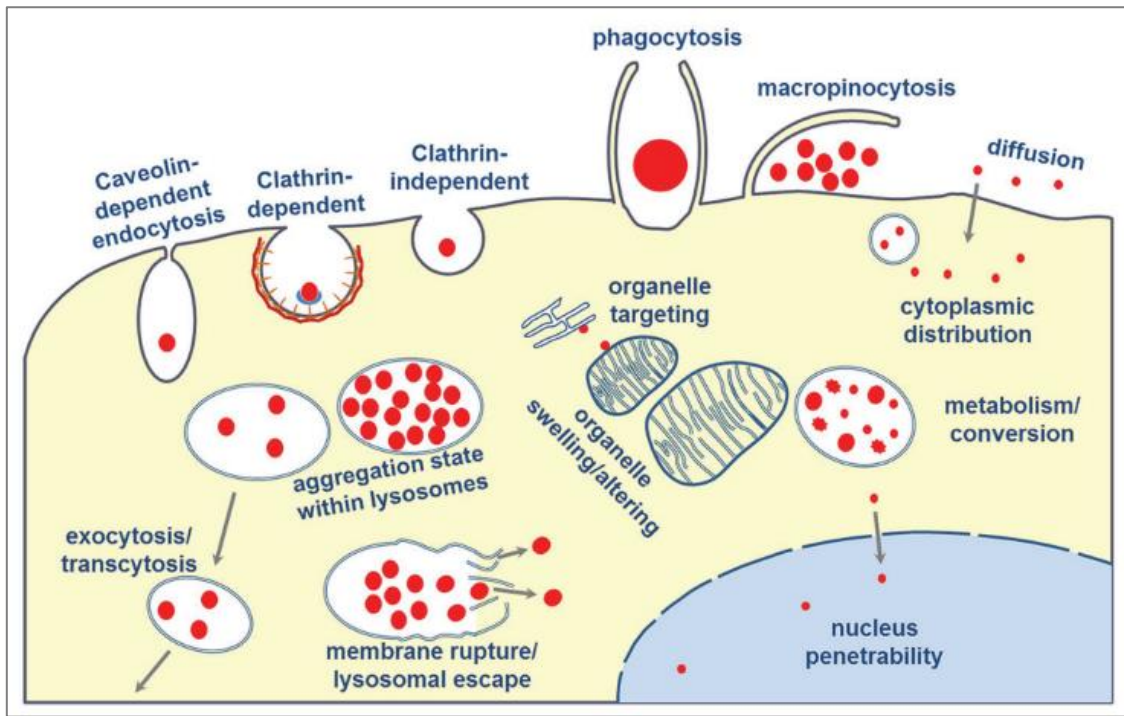


Figure 1: Cellular entry mechanisms and intracellular fate of nanoparticles. Reproduced from Reifarth et al. (2018) with permission from John Wiley and Sons.

3.3 Mechanisms of nanoparticle toxicity

Many attempts have been made to identify specific nanoparticle properties that cause toxicity. However, depending on particle type and the cells or tissues involved in this interaction, the nano-bio interface can differ and 'toxicity' can have many faces.

Physicochemical properties like charge or functional groups determine the characteristics of the nanoparticle surface which is the first component of the nano-bio interface. The interaction between the particle surface and its surrounding presents the second component of the nano-bio interface – the solid-liquid interface, which will finally be in contact with tissue or cells. All three parts of the nano-bio interface can thereby impair the biological entity – even before any direct contact (Nel *et al.*, 2009). The following paragraphs will briefly introduce relevant cellular effects that can be triggered by nanoparticles (Osman *et al.*, 2020).

Cell membrane damage may be caused by mechanisms like frustrated phagocytosis (Donaldson *et al.*, 2010), membrane depolarization, lipid leakage, production of reactive oxygen species (ROS) causing lipid peroxidation, or impaired membrane transport. Major factors can be nanoparticle size, shape, surface charge, and chemical composition.

Oxidative stress upon nanoparticle exposition may be caused by their physicochemical properties like dissolution behaviour or ion release, or by their ability to damage the mitochondrial membrane. Depending on the damage done by free radicals that interact with cellular components (e.g. DNA), cells react with inflammation, apoptosis or necrosis.

Once nanoparticles have passed the cell membrane they may damage organelles directly. Examples are loss of energy production when mitochondria are affected, or enzymatic spilling when lysosomes rupture (Reifarth *et al.*, 2018).

Inflammatory response upon nanoparticle exposition has not only been observed in alveolar macrophages, but also in alveolar epithelial cells (Muehlfeld *et al.*, 2008). Prolonged or excessive inflammation can lead to fibrosis and cancer. The inflammatory potential of nanoparticles depends on properties like size, shape, agglomeration behaviour, or surface chemistry, as those determine the probability of macrophage recognition and complete phagocytosis, biopersistence, and pulmonary retention. In-

flammasome activation has also been considered a possible inflammatory mechanism upon nanoparticle exposure (Sharma and Jha, 2020).

Genotoxic effects may directly result from interaction between nanoparticle and DNA, or indirectly after inflammatory processes, oxidative stress, or activation of membrane receptors that are involved in DNA repair or other pathways (Yang *et al.*, 2012; Doak and Dusinska, 2017; Singh *et al.*, 2017).

Cell death scenarios like necrosis, apoptosis and autophagy have been observed upon nanoparticle exposure. Not only the definition of death modes varies strongly, but cell death pathways also have significant crosstalk and depend on exposure intensity (Mohammadinejad *et al.*, 2019).

3.4 Anatomy and physiology of the respiratory tract

The lungs can be divided into the upper (conducting) airways and the lower (respiratory) airways, also called lung parenchyma. The process of breathing can also be divided into ventilation and respiration. Ventilation of the lungs (in a relaxed state) is driven by contraction of the diaphragm, resulting in a negative pressure inside the lungs that causes air inflow. The conducting airways (pharynx, larynx, trachea, bronchi and bronchioles) aerate the respiratory zone (respiratory bronchioles, alveolar ducts, alveolar sacs and alveoli) (Lang, 2020). Alveoli are the smallest functional entity in this hierarchically or tree-structured organ. In contrast to the conductive airways, which are lined with ciliated columnar epithelium, mucus and surfactant (together $\approx 60 \mu\text{m}$ thick), the alveolar wall merely presents a $2 \mu\text{m}$ or thinner barrier between air and blood (Gehr *et al.*, 1978). Oxygen in the air-filled alveoli diffuses through a lining of surfactant, a squamous epithelium, the alveolar interstitium, and the capillary endothelium before reaching the (deoxygenated) blood where it is, in large parts, bound to the erythrocytes' haemoglobin.

The epithelial layer is built from alveolar epithelial cells of types I and II (AE-I, AE-II). Type I cells are very flat and cover the greater part of the alveolar surface ($\approx 90\%$) to minimize the diffusion barrier for respiratory gases. Cuboidal AE-II cells are twice as numerous but cover only small portions of the alveolar surface ($<10\%$) and have the ability to differentiate and replace AE-I cells (Crapo *et al.*, 1982; Crapo *et al.*, 1983). AE-II cells contain lamellar bodies that secrete surfactant, mainly composed of surface active lipids and proteins, onto the alveolar epithelium to reduce surface tension, thereby preventing the alveoli from collapsing and facilitating normal breathing dynamics (Perez-Gil and Weaver, 2010). Alveolar macrophages are the first defence line against inhaled pathogens that reach the alveoli, and involved in inflammatory activation (Hoppstädter *et al.*, 2010).

3.5 Mechanical forces in the lung

Our lungs are permanently under mechanical stress: an adult takes 12-20 breaths per minute, inhaling 400-600 ml of air per breath. This equals 4.8-12 l of air that pass the lungs each minute (Lang, 2020) under significant mechanical deformations. Knudsen and Ochs (2018) reviewed current knowledge on surfactant lining and integrity of the inter-alveolar septum, which facilitate mechanical stability in the alveolar space: during inhalation and exhalation, alveoli experience deformation (Figure 2), which is commonly described as ‘strain’. Under normal breathing within 40-80% of total lung capacity (TLC), reduced alveolar surface tension from surfactant lining and stability from the connective tissue fibre network prevent the alveoli from collapsing at low lung volumes, and from overdistention at higher lung volumes, thereby enabling energy efficient breathing. As epithelial cells are overall connected to the stress-bearing connective tissue fibre network, they experience stress even in a healthy lung, for example during physical exercise (this aspect will be further discussed in chapter 7.1.2). To a certain degree, resulting damages to the plasma membrane or to cell-cell interactions can be compensated by the cells. When it comes to diseased lungs or scenarios of invasive mechanical ventilation, pulmonary micromechanical properties as well as pressure ratios can change and cause imbalances in these complex structures, leading to lung injuries (Slutsky and Ranieri, 2013; Brochard *et al.*, 2017).

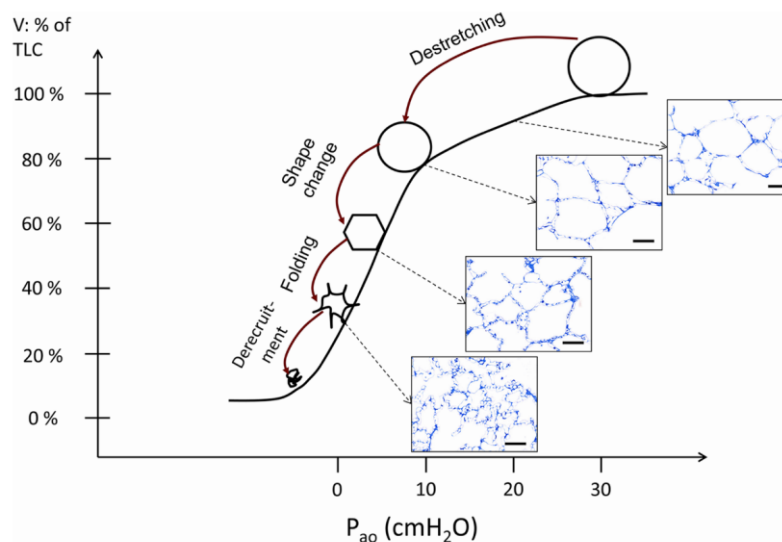


Figure 2: Suggested alveolar deformation mechanisms originally postulated by Gil *et al.* (1979), here associated with more recent observations (Bachofen *et al.*, 1987; Tschumperlin and Margulies, 1999; Knudsen *et al.*, 2018) by Knudsen and Ochs (2018). De-recruitment is unlikely during normal breathing where the residual volume ($\approx 20\text{-}40\%$ of TLC (Ruppel, 2012)) remains in the lungs. Alveolar wall folding, change of shape, and isotropic balloon-like stretching occur with increasing pressure. Figure

reproduced from Knudsen and Ochs (2018) under the terms of the Creative Commons Attribution 4.0 International License (CC BY 4.0) (<http://creativecommons.org/licenses/by/4.0/>).

Basic cellular responses to normal or excessive mechanical forces in the lungs are still not entirely understood. As access to alveoli is limited *in vivo*, many attempts have been made to simulate breathing or ventilation movement *in vitro*.

3.6 Current *in vitro* lung models

Research in life sciences depends on *in vitro* models. Despite many efforts, results from *in vitro* models and associated *in vivo* or *ex vivo* data often lack correlation. Complex *in vitro* models that also address biophysical aspects are a recent development in toxicology that may help to close the gap between *in vitro* and *in vivo* scenarios (Del Favero and Kraegeloh, 2020). With the knowledge gained from the previous chapters, it can be summarized that modelling the human lung *in vitro* involves many challenges. Focussing on the alveoli as functional units of the lungs, it should be considered that i) multiple interacting cell and tissue types are involved; ii) the alveolar barrier is situated at the interface between air and blood; iii) the alveoli are exposed to mechanical stress and deformation. This work focussed on the latter, using a stretchable submerge monoculture model.

The simplified lung model allowed easy handling of cells and uncomplicated medium-carried nanoparticle exposure. Vacuum-driven equibiaxial strain and a 6-well format ensured that a large proportion of cells experienced strain – this is of importance for any analysis that includes all cells of a well (e.g. well-based toxicity assays). In addition, when preparing microscopy samples, one well is sufficient to prepare 4-6 different samples. Complex immuno staining with multiple antibodies and labels can be avoided. However, a big well size requires large numbers of cells which can be a disadvantage when attempting to culture primary cells.

This subchapter will illustrate current modelling approaches that address one or multiple of these aspects. Permeable cell culture dishes (e.g. Transwell systems) can serve as a connection between epithelial cells and macrophages on the upper (apical) side with endothelial cells on the lower (basolateral) side. Depending on the liquid level, the epithelial cells on the apical side of the transwell are submerged or in direct contact with air (Kasper *et al.*, 2017; Costa *et al.*, 2019). Culturing alveolar epithelial cells at the air-liquid interface (ALI) is an important approach when it comes to research on pulmonary surfactant or inhalation toxicology (Lacroix *et al.*, 2018). So far, these systems were limited to static cultivation.

First attempts to mimic strain *in vitro* used stretchable cell substrates like silicone membranes or gelatine sponges (Wirtz and Dobbs, 1990; Liu *et al.*, 1992). A commercial system based on elastic silicone substrates that are stretched *via* vacuum applica-

tion was introduced in the nineteen-nineties and revealed effects of stretching on, for instance, epithelial repair, cytokine release and ROS production (Savla and Waters, 1998; Vlahakis *et al.*, 1999; Chapman *et al.*, 2005). Permeable and at the same time elastic cell substrates can mimic the air-blood interface and dynamic conditions in one system. Huh *et al.* (2010) even added microfluidic components to recreate blood flow in the endothelial compartment of their system. Stucki *et al.* (2018) presented a lung-on-a-chip system that additionally addresses easy handling regarding sterility, medium supply, sample taking and measurement of transepithelial resistance as well as suitability for microscopy analysis. Biological membranes made of collagen and elastin may resemble the air-blood barrier even more realistically (Zamprogno *et al.*, 2019). Typical parameters for validation of such alveolar epithelial models are, for instance, surfactant production, presence of tight junctions, transepithelial resistance or permeability for small hydrophilic molecules.

4 Aim of this study

The aim of this work was to elucidate how mechanical strain, mimicking normal breathing, affects the cellular response of type II alveolar epithelial cells upon exposition to amorphous colloidal silica nanoparticles.

The first part focussed on gene expression alterations caused by treating the model cells (A549) with nanoparticles, mechanical strain, or both. It was analyzed if mechanical strain influenced the amount of nanoparticles that the cells internalized during the experiments.

The second part investigated whether this dynamic *in vitro* model was able to mimic more extensive mechanical strain as occurs, for instance, in the diseased or ventilated lung. The established model was also tested with a larger type of nanoparticles to see whether the interaction between stretch and particles is affected by particle size.

The last part of this work addressed experimental robustness of the system. Experiments of parts I and II were repeated under new experimental conditions such as batch variations of nanoparticles and fetal bovine serum for cell culture supplementation.

Results from this work may help to identify how nanoparticles, cells, and their way of interacting are affected by mechanical stimuli.

5 Materials and Methods

5.1 Synthesis and characterization of nanomaterials

All nanomaterials, if not stated otherwise, were synthesized and characterized at Leibniz Institute for New Materials gGmbH (Saarbrücken, Germany) by colleagues from the program divisions *Nano Cell Interactions*, *Chemical Analytics* and *Physical Analytics*.

5.1.1 Colloidal amorphous silica nanoparticles

Labeled and unlabeled amorphous colloidal SiO₂ nanoparticles with a target diameter of 25 nm or 80 nm were synthesized as described previously (Hartlen *et al.*, 2008; Tavernaro *et al.*, 2017) through L-arginine-catalyzed hydrolysis of tetraethoxysilane (TEOS) in a biphasic water/cyclohexane system. For preparation of fluorescently labeled SiO₂ nanoparticles, the dye ATTO 647N (ATTO-TEC GmbH, Germany), a carbopyronine derivative, was covalently coupled into the SiO₂ nanoparticle matrix after a pre-synthesis modification with cysteic acid and (3-aminopropyl)triethoxysilane. The particles were purified by dialysis against ultrapure water for 24 hours and subsequently filtered through a sterile 0.2 µm cellulose acetate filter. As reported before by Kucki *et al.* (2014), SiO₂ nanoparticle dispersions prepared by this route do not contain detectable levels of endotoxins.

The primary particle size and size distribution of the SiO₂ nanoparticles were estimated by analysis of TEM micrographs (Philips CM200 FEG, FEI Company, Netherlands) using the ImageJ software (<http://rsb.info.nih.gov/ij/>). Nanoparticle samples were prepared by drying nanoparticle dispersions on a carbon coated copper grid.

The average hydrodynamic diameter (Dz) of unlabeled nanoparticles dispersed in water was determined by dynamic light scattering (DLS) at 25 °C using a Zetasizer NanoZSP (Malvern Instruments, Worcestershire, UK). Samples were diluted 1:10 in ultrapure water and were irradiated with a HeNe laser ($\lambda = 633$ nm). The intensity fluctuation of the scattered light, detected at a backscattering angle of 173°, was analyzed in automatic mode to obtain the autocorrelation function. To determine the average hydrodynamic diameter (Dz) of fluorescently labelled nanoparticles (Si25-FD) a Nanotrak NPA 250 (Microtrac GmbH, Germany) with a semiconductor laser ($\lambda = 780$ nm) in backscattering angle mode was used. Three independent measurements were performed. The average hydrodynamic diameter (Dz) is given as z-average, the intensity based harmonic mean.

DLS measurements were also performed to determine the stability and agglomerate content of labeled and unlabeled SiO₂ nanoparticles dispersed in cell culture medium. The particle dispersions were diluted to a concentration of 100 µg SiO₂ ml⁻¹ in Dulbecco's modified Eagle medium (DMEM, PAN-Biotech GmbH, Germany) supplemented with 10% fetal bovine serum (FBS, PAN-Biotech GmbH, Germany) and for comparison in ultrapure water. The pH value of the water was adjusted to 7.4. After 48 hours of incubation at 20 °C, measurements were performed using three independent samples each. Using a regularisation scheme by number, the number weighted distribution of the particle diameters was calculated (hydrodynamic diameter D_n). The agglomerate content was calculated assuming that agglomerates have a hydrodynamic diameter larger than 90 nm.

The zeta potential of nanoparticles was determined using a Zetasizer NanoZSP (Malvern Instruments, UK). In water, measurements were taken at 150 V using 10 mM KCl as background electrolyte. Three independent measurements including several sub runs were performed for each sample at room temperature.

In order to estimate leaching of the covalently bound Atto 647N dye from the nanoparticles, samples were diluted 1:100 and subsequently ultra-filtered through a modified polyethersulfone membrane with a molecular weight cut-off at 30 kDa (Pall, Germany) by centrifugation (9,000 x g, 15 minutes). The fluorescence of the filtrate and the diluted particle dispersions were then measured in a spectral range of 658-800 nm, using a spectrofluorometer Spex FluoroMax-3 (HORIBA Jobin Yvon, Germany) and an excitation wavelength of 645 nm. Measurements were performed in triplicate.

The SiO₂ concentration of nanoparticle dispersions was obtained by ICP-OES analysis (Ultima 2, Horiba Jobin Yvon, Japan).

5.2 Cell Culture

A549 cells, as *in vitro* model for human type II alveolar epithelial cells, were obtained from the German Collection of Microorganisms and Cell Culture (# ACC107, DSMZ, Germany). Authenticity of A549 cells was verified by STR (Short Tandem Repeat) analysis (data not shown) and regular monitoring of the presence of lamellar bodies (Suppl. Figure 31). Cultures were maintained in DMEM (PAN-Biotech GmbH, Germany) supplemented with 10% FBS (PAN-Biotech GmbH, Germany or PAA Laboratories, Austria)

(Table 1) at pH 7.4 and 37 °C in a humidified atmosphere (9% CO₂). At ≈80% confluence, cells were detached using 0.05% trypsin / 0.02% EDTA in PBS (PAN-Biotech GmbH, Germany). Routine testing for mycoplasma contamination was performed with the PCR Mycoplasma Test Kit II (PromoCell, Germany).

Table 1: Overview of fetal bovine sera used in experiments.

Chapter	Experiment	Serum
Part I	Proliferation (Figure 7)	FBS Gold (PAN-Biotech) → Serum B
	Membrane integrity (Figure 8)	FBS Gold (PAN-Biotech) → Serum B
	Determination of treatment exposition time (Figure 9)	FBS Standard (PAA Laboratories) → Serum A
	Gene array and cytokine expression analysis (Figure 10, Figure 11, Table 7, Table 8)	FBS Standard (PAA Laboratories) → Serum A
	IL8 secretion analysis (Figure 12)	FBS Standard (PAA Laboratories) → Serum A
	Nanoparticle uptake (Figure 13, Figure 14, Figure 15)	FBS Gold (PAN-Biotech) → Serum B
	NF-κB translocation (Figure 16, Figure 17, Figure 18)	FBS Gold (PAA Laboratories) → Serum C
Part II	Effect of nanoparticle size (Figure 19, Figure 20)	FBS Standard (PAA Laboratories) → Serum A
	Effect of stretching intensity (Figure 21, Figure 22)	FBS Standard (PAA Laboratories) → Serum A
Part III	Reproducibility of cytokine expression experiments (Figure 23, Figure 25, Figure 26)	FBS Standard (PAA Laboratories) → Serum A vs. FBS Gold (PAN-Biotech) → Serum B
	NF-κB translocation (Figure 28, Figure 29, Figure 30)	FBS Gold (PAA Laboratories) → Serum C vs. FBS Gold (PAN-Biotech) → Serum B

Table 2: Fetal bovine serum components according to manufacturers' quality certificates.

Fetal bovine serum batch	Serum A* Cat: A15-151 Lot: A15109-2859	Serum B Cat: P40-37500 Lot: P132104	Serum C Cat: A11-101 Lot: A10-11-1725
pH	7.1	7.3	7.1
Osmolality [mOsmol / kg]	324	321	311
Albumin [g / 100 ml]	3.0	3.2	1.8
α-Globulin [g / 100 ml]	0.2	0.6	9.0
β-Globulin [g / 100 ml]	0.4	0.8	1.1
γ-Globulin [g / 100 ml]	0.2	unknown	0.1
IgG [μg / ml]	88	411	63
Total protein [g / 100 ml]	3.8	4.7	3.9
Haemoglobin [mg / 100 ml]	14.7	15.5	17.0
Endotoxins [ng / ml]	0.1*	0.1	0.4*

*Converted from EU/ml to ng/ml assuming that one EU equals approximately 0.15 ng endotoxin per ml of solution.

5.3 Mechanical strain

Two-dimensional mechanical strain was applied with a Flexcell FX-5000™ Tension System (Flexcell® International Corporation, USA). The Flexcell FX-5000 Tension System consists of a software controlled vacuum pump, a tubing system that connects the pump with a base plate, loading posts with different geometries for various stretching setups, as well as special well plates with flexible silicone membranes serving as cell substrates. Membranes are available with various protein coatings for improved cell growth. For equibiaxial strain (equivalent degree of elongation in all directions), circular loading posts are inserted into the baseplate. Silicone lubricant spread on the loading posts guarantees non-destructive sliding of the flexible membranes over the loading posts. BioFlex 6-well culture plates with already adhering cells are fixed on top of the loading posts into the baseplate and sealed with rubber gaskets to allow for vacuum development. Negative pressure applied from the bottom of the base plate pulls the flexible membranes down, thereby stretching them over the fixed loading posts and causing the cell substrate to expand to the predefined extent. Negative pressure and loading post diameter define how far the membrane is pulled down and therefore determine the final extent of area expansion. Curve shape and frequency can also be controlled *via* software. The base plate can be stored inside an incubator.

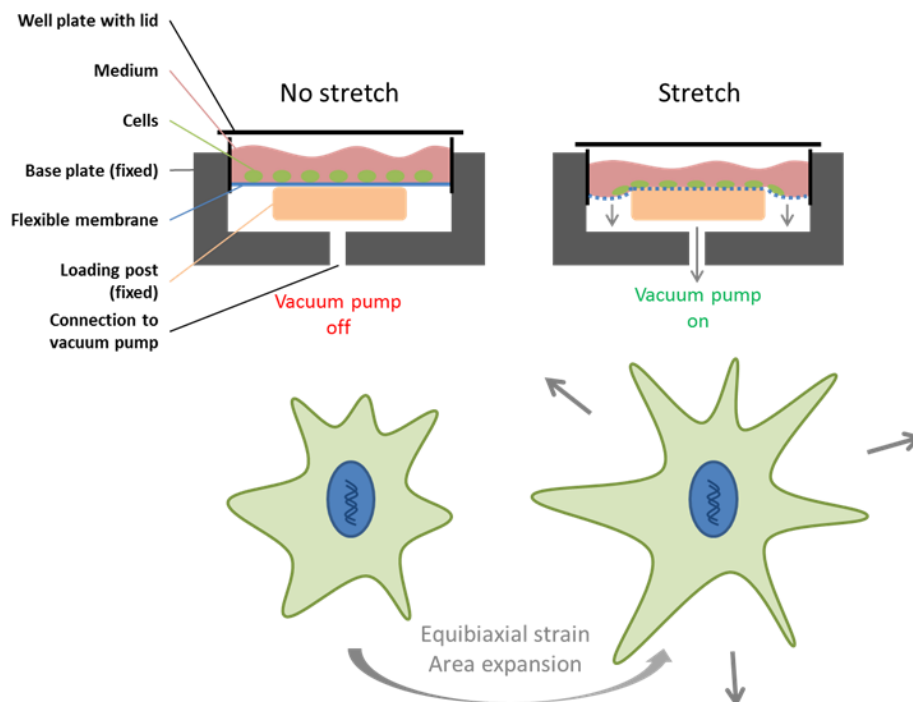


Figure 3: Schematic principle of cell stretching setup.

The nominal surface area expansion values were validated by measuring the distances between several reference points on the membrane at 0% nominal stretch and 15% or 25% nominal stretch (Suppl. Figure 33). Given this linear elongation (ϵ), surface area expansion (ΔS_A , further on referred to as “stretch”) can be calculated (Roan and Waters, 2011):

When L_f is final length and L_0 is initial length at zero stretch, linear elongation equals

$$\epsilon = \frac{(L_f - L_0)}{L_0}$$

or

$$\epsilon = (1 + \Delta S_A)^{\frac{1}{2}} - 1$$

meaning that surface area expansion equals

$$\Delta S_A = (\epsilon + 1)^2 - 1.$$

Cells were seeded onto laminin-coated BioFlex 6-well culture plates (Flexcell® International Corporation, USA) at a density of 10^5 cells per square centimeter and allowed to attach for 24 hours. Cells experienced cyclic sinusoidal equibiaxial strain (Figure 3) with stretch of 15% or 25% at a frequency of 0.25 Hz, simulating the mechanical strain during ventilation (Waters *et al.*, 2012). Stretching was maintained over the given period (2 - 24 h). Control cells did not experience strain but were also grown on laminin-coated BioFlex 6-well culture plates.

5.4 Exposition of cells to nanomaterials

For exposition of cells to nanomaterials, the particle suspensions were vortexed for 30 seconds. Re-dispersed nanoparticles were then diluted in full medium^c, followed by another short vortexing step. Medium from the attachment period of the cells was removed and replaced by the particle-burdened medium. Si25 and Si80 particles were applied in a final SiO₂ concentration of 100 $\mu\text{g ml}^{-1}$ if not stated otherwise. The final medium volume in 6-well culture plates was 3 ml.

^c DMEM with 10% FBS supplementation is considered full medium.

5.5 RNA isolation for gene array and qPCR

Sample generation and preparation for the gene microarray as well as sample generation for expression analysis comparing Si25 vs. Si80 and 15% vs. 25% stretch were performed by Jennifer Welck (*Nano Cell Interactions* at Leibniz Institute for New Materials, Saarbrücken, Germany).

5.5.1 RNA isolation

For isolation of total RNA, cells were detached by trypsin treatment and harvested by centrifugation. For quantitative PCR, RNA was isolated using the RNeasy Mini Kit (QIAGEN GmbH, Germany) according to the manufacturer's instructions.

For gene arrays, RNA was isolated using QIAzol treatment according to the following protocol: the cell pellets were dispersed in 700 μ l QIAzol lysis reagent (QIAGEN GmbH, Germany), transferred into a QIAShredder column and centrifuged. Lysates were then either stored at -80 °C, or processed further. After adding 200 μ l of chloroform, samples were vortexed for 15 seconds, incubated for 2 minutes at room temperature and centrifuged for 15 minutes at $12,000 \times g$ and 4 °C. For precipitation of the RNA, 500 μ l isopropanol were added to the aqueous phase, the mixture was incubated for 10 minutes at room temperature and centrifuged as before. The precipitate was consecutively washed by adding 1 ml 75% ethanol and 96% ethanol and centrifugation for 5 minutes at $7,500 \times g$ at 4 °C. After drying, the RNA was eluted in 50 μ l RNase-free water.

5.5.2 DNase digestion and purification

Contaminating DNA was removed by DNase I digestion using the RNase-free DNase Set (QIAGEN GmbH, Germany). Finally, RNA was purified using the RNeasy Mini Kit (QIAGEN GmbH, Germany). Isolated RNA samples were stored at -80 °C. The RNA concentration was determined by absorption measurement at 260 nm (NanoDrop™ One, Thermo Fisher, Germany). The quality of RNA preparations was checked by determination of the absorption ratio at 260 nm/280 nm and only samples with a ratio > 1.8 were used.

5.6 Microarray analysis and bioinformatics

Microarray and bioinformatics were performed by colleagues at *IfADo—Leibniz Research Centre for Working Environment and Human Factors*, Dortmund (Germany) and *Department of Statistics, TU Dortmund* (Germany).

Analysis of gene expression in A549 cells was performed with Affymetrix GenChip® Human Genome HG-U133 plus 2.0 chips (Affymetrix, Inc., CA, USA) as previously described (Krug *et al.*, 2013). Briefly, the RNA was quantified using a NanoDrop N-1000 spectrophotometer (Thermo Fisher, Germany) and the integrity of RNA was confirmed by an automated gel electrophoresis system (Experion, Bio-Rad, CA, USA). First-strand cDNA (complementary DNA) was synthesised from 100 ng total RNA using an oligo-dT primer with an attached T7 promoter sequence, followed by the complementary second strand. The double-stranded cDNA molecule was used for *in vitro* transcription (IVT, standard Affymetrix procedure) using Genechip 3' IVT Express Kit. During synthesis of the aRNA (amplified RNA, also commonly referred to as cRNA), a biotinylated nucleotide analogue was incorporated, which serves as a label for the message. After amplification, aRNA was purified with magnetic beads and 15 µg of aRNA was incubated with fragmentation buffer as per the manufacturer's instructions. Then, 12.5 µg fragmented aRNA was hybridised with Affymetrix Human Genome U133 plus 2.0 arrays as per the manufacturer's instructions. The chips were placed in a GeneChip Hybridization Oven-645 for 16 hours at 60 rpm and 45 °C. For staining and washing, Affymetrix HWS kits were used on a Genechip Fluidics Station-450. For scanning, the Affymetrix Gene-Chip Scanner-3000-7G was used, and the image and quality control assessments were performed with Affymetrix GCOS software. All reagents and instruments were acquired from Affymetrix (Affymetrix, CA, USA). The generated CEL files were used for further statistical analysis. The authors declare that microarray data were produced according to MIAME guidelines and will be deposited in ArrayExpress upon acceptance of the manuscript.

The following biostatistical analyses were performed using the statistical programming language 'R-version 3.2.4'. Normalisation was performed with the method Robust Multichip Average (RMA) (Irizarry *et al.*, 2003). Differential expression was calculated using the R package limma (Smyth, 2005). The resulting *p*-values were multiplicity-adjusted to control the false discovery rate (FDR) by the Benjamini–Hochberg

procedure with a p -value smaller than 0.05 and fold change equal to or larger than two. As a result, for each combination of centre (= test system), compound and concentration, a probeset/ gene list was obtained, with corresponding estimates for \log fold change and p -values of the Limma t test (unadjusted and FDR-adjusted). Probesets not matching a particular gene in the database were annotated NA and counted as single genes in the Venn diagrams. Probesets assigned to the same gene were treated as dupli- or triplicates and counted as single gene in the Venn diagrams and tables.

5.6.1 RNA quality control

The absence of DNA was confirmed by PCR for Alu elements (Abdel-Halim *et al.*, 2016) on a random basis. Per PCR reaction, 12.5 μ l Dream Taq PCR Mastermix (2x, Thermo Scientific, Germany), 5 μ l A1S primer (5 μ M; 5'-TCA TGT CGA CGC GAG ACT CCA TCT CAA A-3'; Eurofins, Germany), 1000 ng RNA (or 100 ng genomic DNA as positive control) and nuclease-free water ad 25 μ l were added. Samples were initially denatured at 94°C for 5 minutes. Then, 30 cycles of denaturing (1 min, 94 °C), primer annealing (1 min, 56 °C) and elongation (2 min, 72 °C) were run. Twenty microliters of the resulting PCR product mixed with 4 μ l loading dye (6x, Fermentas, USA) was pipetted into a 1% agarose gel stained with SYBR® Safe DNA Gel Stain (Thermo Fisher, Germany). The 1 kB DNA Gene Ruler (Fermentas, USA) was used as a reference. Electrophoresis was run for 40 minutes at 6 V cm^{-1} (data not shown).

5.7 Gene Expression Analysis by Quantitative Real-Time PCR

5.7.1 Reverse Transcription

Three micrograms of RNA were reverse-transcribed using oligo-dT18 primers and the RevertAid First Strand cDNA Synthesis Kit (Thermo Fisher Scientific, Germany) according to the manufacturer's instructions. The obtained cDNA was diluted to 10 ng μ l⁻¹ by addition of RNase free water and stored at -80 °C.

5.7.2 Primer Design

Primers for amplification of *CXCL8*, *CCL20*, and glyceraldehyde 3-phosphate dehydrogenase (*GAPDH*), which served as reference gene, were purchased from Eurofins (Germany) (Table 3).

Table 3: qPCR primers

Primer	Sequence 5'-3'	Products on target templates	Product length [bp]	Melting temperature [°C]	Final concentration in PCR [µM]
<i>CCL20</i> fwd	TCAGTGCTGCTACTCC ACCT	Homo sapiens C-C motif chemokine ligand 20 (<i>CCL20</i>), transcript variant 1, mRNA	116	60.54	0.7
<i>CCL20</i> rev	TGCCGTGTGAAGCCCA CAAT			62.97	0.7
<i>CXCL8</i> fwd	TAGCCAGGATCCACAA GTCC	Homo sapiens C-X-C motif chemokine ligand 8 (<i>CXCL8</i>), transcript variants 1 and 2, mRNA	91	58.80	0.5
<i>CXCL8</i> rev	TGTGAGGTAAGATGG TGGCT			58.34	0.5
<i>GAPDH</i> fwd	CAAATTCATGGCACC GTCA	Homo sapiens glyceraldehyde-3-phosphate dehydrogenase (<i>GAPDH</i>), transcript variant 1, 2, 3, 4, mRNA	146	59.11	0.5
<i>GAPDH</i> rev	TGAAGACGCCAGTGG ACTC			59.33	0.5

5.7.3 qPCR protocol

Per PCR reaction 10 µl iTaq Universal SYBR Green Supermix (Biorad, Germany), primers (final concentrations are given in Table 3), 50 ng cDNA templates and PCR water *ad* 20 µl were added. Samples were analysed at least in technical duplicates. A control without template (no template control, NTC) was run in every analysis for each target. PCR was initiated with a 30 seconds hot start at 95 °C followed by 40 cycles of denaturation (5 sec, 95 °C), annealing and elongation (30 sec, 60 °C) and a plate read. Finally, the melting curve was documented from 65 °C to 95 °C in 0.5 °C steps (Suppl. Figure 34). Low profile qPCR plates in combination with qPCR sealing tape (both Brand, Germany) were used. Cycling, detection and analysis were performed with a CFX96 Touch Real-Time PCR Detection System (Biorad, Germany).

5.7.4 Primer validation by agarose gel electrophoresis

PCR products from TNF treated A549 cells that express *CXCL8* and *CCL20* were fractionated by electrophoresis to determine amplicon length and thereby verify primer specificity. Twenty microliters of PCR product mixed with 4 µl loading dye (6x, Fermentas, USA) were pipetted into a 3% agarose gel stained with SYBR® Safe DNA Gel Stain (Thermo Fisher, Germany). GeneRuler DNA-Ladder (Low Range; Thermo Fisher, Germany) was used for reference. Electrophoresis was run for 60 minutes at 4.6 V cm⁻¹ (Suppl. Figure 34).

5.7.5 Determination of PCR efficiency and optimization

To determine the amplification efficiency of the qPCR, a ten-fold serial dilution was prepared from cDNA obtained from TNF α treated A549 cells (calibration template). According to the protocol described above, qPCR was performed with 600 ng to 0 ng calibration template. Biorad CFX Manager 3.1 was used to determine PCR efficiency (E) by calculating the calibration curve's slope (m) (Pfaffl, 2001; Pfaffl and Riedmaier, 2011) (Suppl. Figure 34).

$$E = 10^{-1/m}$$

5.7.6 qPCR data evaluation

Quantitative PCR data was analyzed using the efficiency (E) correcting Pfaffl method (Pfaffl, 2001). Here, the cycle of quantification is referred to as Cq value. *GAPDH* served as reference gene. *CCL20* or *CXCL8* were target genes. Change in gene expression equals the ratio (R) between efficiency corrected ΔCq values of target and reference genes. Delta Cq can be calculated by subtracting Cq values of test samples from Cq value of control sample. Samples were measured as duplicates or triplicates. Mean values and standard deviations were calculated from at least 3 independent experiments where cells from one 6-well represent one biological replicate.

$$R = \frac{(E_{Target})^{\Delta Cq_{Target}(control-test)}}{(E_{Reference})^{\Delta Cq_{Reference}(control-test)}}$$

5.8 Membrane integrity

Membrane integrity as an indicator for cell membrane damage was determined on the basis of lactate dehydrogenase (LDH) activity in the cell culture medium, using the CytoTox-ONE Homogeneous Membrane Integrity Assay (Promega, Germany). For the LDH assay, cells were either cultivated in BioFlex 6-well culture plates for the dynamic setup as described above, or in 96-well plates for the static setup (seeding density 10^5 cells cm^{-2}). After 24 h, the medium was replaced with particle-containing or control medium and cells were kept under static (0% stretch) or dynamic (15% stretch) conditions for further 24 h. 100 μl of the culture medium were then added to an equal volume of the assay reagent, mixed and incubated for 10 minutes according to manufac-

turer's instructions. Fluorescence was recorded at 590 nm using an Infinite M200 pro microplate reader (Tecan, Switzerland) at an excitation wavelength of 560 nm. The background fluorescence of the medium was measured using control wells without cells and the obtained fluorescence was subtracted from all other samples. Cells incubated with medium only served as untreated controls. Cells treated with 0.2% Triton X-100 (Carl Roth, Germany) for 30 minutes served as positive controls for increased LDH leakage. In order to exclude false negative results caused by potential degradation/deactivation of released LDH within 24 h, the activity of the control samples at $t = 0$ hour and $t = 24$ hour was also determined (Suppl. Figure 35). These values were used to estimate the maximum degradation/deactivation and the evaluation of cytotoxicity. For the determination of membrane integrity, unlabeled nanoparticles were used.

5.9 IL8 secretion (ELISA)

For quantification of IL8 secreted by A549 cells, the Human IL8 Chemiluminescent ELISA (Thermo Fisher Scientific, Germany) was used according to the manufacturer's instructions. Supernatants were transferred into wells of a black 96-well plate (Greiner Bio-One, Germany). Chemiluminescence was measured using an Infinite 200Pro microplate reader (Tecan, Switzerland). Cells treated for 24 hours with TNF (2 ng ml^{-1}) served as positive controls. Untreated cells served as negative controls. IL8 levels were expressed as picograms per milliliter supernatant.

5.10 Microscopy

5.10.1 Sample preparation for confocal microscopy

All microscopy experiments were performed with fixed cells. Samples on BioFlex membranes or glass coverslips were washed two times with PBS before fixation with 4% paraformaldehyde (PFA; Electron Microscopy Sciences, USA) in PBS for 20 minutes. PFA was removed by washing with PBS. Immunostaining was performed in 12-well plates with a volume of 300 μl per sample. For intracellular targets, cells were permeabilized with 0.2% Triton X-100 (Carl Roth GmbH + Co. KG, Germany) in PBS for 10 minutes. Five percent bovine serum albumin fraction V (BSA, Carl Roth, Germany) in PBS was used to block unspecific binding (1 hour, RT). Primary antibodies were applied

in 1% BSA in PBS for 2 hours at RT (room temperature ≈ 23 °C), or overnight at 4 °C. Excess antibodies were washed away with PBS (3 x 5 minutes) before labeled secondary antibodies were applied for 1 hour at RT. Again, samples were washed thoroughly with PBS (3 x, 5 minutes) before nuclei were stained with the DNA binding dye Hoechst (Sigma-Aldrich, Germany). Finally, samples were washed (3 x 5 minutes) and embedded with Aqua-Poly/Mount (Polysciences, Germany). Information on antibodies and dyes can be taken from Table 4.

Table 4: Immunocytochemistry

Target	Antibody/Stain	Provider
Cell membrane (sialic acid and <i>N</i> -acetylglucosaminy residues)	Wheat Germ Agglutinin, Alexa Fluor™ 488 Conjugate, #W11261	Invitrogen
Nucleus (dsDNA)	Höchst 33342, #H3570	Invitrogen
NF- κ B p65	NF- κ B p65 (D14E12) XP® Rabbit mAb, #8242	Cell Signaling Technology
NF- κ B1 p105/p50 (total)	NF- κ B1 p105/p50 (D4P4D) Rabbit mAb, #13586	Cell Signaling Technology
NF- κ B2 p100/p52	NF- κ B2 p100/p52 (18D10) Rabbit mAb, #3017	Cell Signaling Technology

5.10.2 Confocal laser scanning microscopy

Samples were imaged using a Leica TCS SP5 STED (Leica Microsystems, Germany) confocal laser scanning microscope, equipped with an HCX PL APO CS 63.0 x 1.40 oil immersion objective. The 488 nm laser line of an argon laser was used for excitation of Alexa Fluor 488. The ATTO 647N labeled nanoparticles were excited using a 633 nm helium-neon laser. Emission signals were detected using an analogue PMT (photomultiplier tube) detector for Alexa Fluor 488 labeled structures or an avalanche photodiode detector and a 630 nm reflection short pass filter for ATTO 647N labeled nanoparticles. Hoechst stained nuclei were excited with a pulsed infrared laser (MaiTai, Spectra Physics, United States) running at 800 nm, and detected with a PMT detector.

For quantification of nanoparticle uptake, 2D-images with an area of 246 μ m x 246 μ m (2048 x 2048 pixels with 120 nm x 120 nm per pixel) were acquired. The confocal z-section was placed 2-3 μ m above the cover-slip in order to image intracellular nanoparticles (Figure 4 A). Imaging parameters like laser power (3%), detector gain (100) and scanning speed (200 Hz) were kept constant throughout the experi-

ments to allow for quantitative analysis of the fluorescence intensity in the nanoparticle channel. Stretched and control samples without nanoparticles were prepared and analysed equally in order to subtract contribution of the cellular (auto-) fluorescence from the total fluorescence intensity.

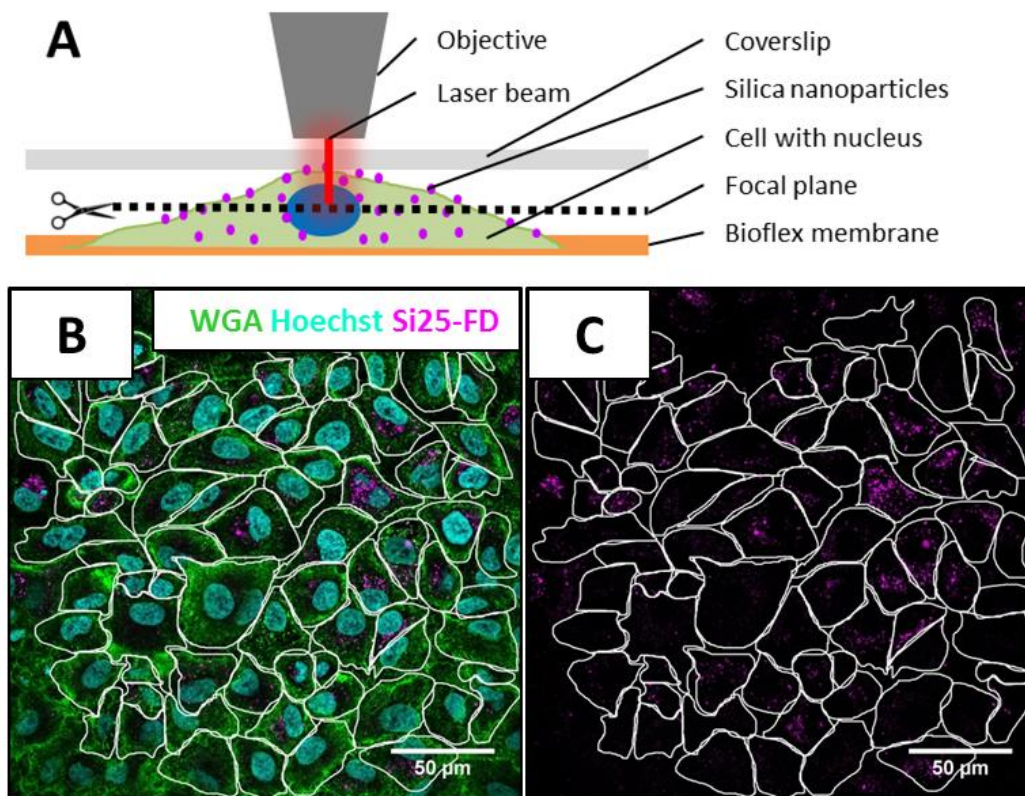


Figure 4: Imaging setup for confocal microscopy and quantitative analysis of nanoparticle accumulation. A549 cells were exposed to Si25-FD ($100 \mu\text{g SiO}_2 \text{ ml}^{-1}$) for 2, 5, and 24 h under static and dynamic conditions. After staining of the cell membrane with WGA, and the nucleus with Hoechst dye (B), samples were analyzed by 2D imaging in a z-plane 2-3 μm above the BioFlex membrane (A), sampling for fluorescence emitted by the fluorescently labeled nanoparticles (C). The fluorescence intensity in the nanoparticles channel was analyzed with ImageJ for quantification of Si25-FD accumulation. Brightness and contrast of the images were enhanced for presentation. Cell segmentation is relevant for Figure 15 and was performed manually with ImageJ 1.51j8.

5.10.3 Image processing with ImageJ 1.51j8

For overall nanoparticle uptake analysis, the total fluorescence intensity (sum of all pixel values (gray values)) in the image was determined using ImageJ's analysis tool 'measure Raw Integrated Density'. Background fluorescence was measured in respective control images that were not exposed to Si25-FD. Background intensity was subtracted from all other samples. Background corrected fluorescence intensity values were then divided by the corresponding number of nuclei, which were counted with ImageJ, to correct for cell number. Final results are given as 'average nanoparticle fluorescence intensity per cell' in arbitrary units [a. u.].

To obtain additional information on nanoparticle uptake under stretch, a single cell analysis was performed. Unlike in the overall nanoparticle uptake analysis where the nanoparticle fluorescence intensity was measured over the complete image, here, intensity was measured in single, manually segmented cells. Corresponding background fluorescence in the nanoparticle channel, which was determined in control samples without nanoparticles, was subtracted from the image prior to analysis. Cell segmentation was based on the WGA membrane staining. Cells on the edge of an image were not included (Figure 4). For each cell the total fluorescence intensity (Raw Integrated Density) was measured using ImageJ 1.51j8. Cells were grouped into 6 groups with different fluorescence intensities ranging from less than 10 a.u., considered as cells with no nanoparticle uptake, to up to 10^6 a.u.

5.10.4 Statistical analysis

If not stated otherwise, data are based on at least 3 independent experiments (biological replicates; N) with 3 technical replicates (measurements) each. Data are shown as mean \pm standard deviation (SD). Two sample, two tailed Student's t-test was applied to compare two groups; analyses of variance (ANOVA) was used to compare more than two groups. *P*-values ≤ 0.05 were considered as statistically significant.

6 Part I: Mechanical strain alters gene expression in A549 cells treated with 25 nm silica particles

The following chapter is based on a peer reviewed publication by Schmitz *et al.* (2019). The work with the title “Mechanical Strain Mimicking Breathing Amplifies Alterations in Gene Expression Induced by SiO² nanoparticles in Lung Epithelial Cells” was performed by scientists from INM – Leibniz Institute for New Materials (Saarbrücken, Germany), the Department of Pharmacy, Pharmaceutical Biology, Saarland University (Saarbrücken, Germany), IfADo—Leibniz Research Centre for Working Environment and Human Factors (Dortmund, Germany) and the Department of Statistics, TU Dortmund (Dortmund, Germany).

6.1 Introduction

Potential adverse effects of nanomaterials on human health are an intensively studied field of research (Gebel *et al.*, 2014). With regard to the great diversity of nanomaterials, the identification of their biological modes of action and the identification of factors that modify the susceptibility of cells to nanomaterials are of high relevance. Therefore, the use and development of advanced, rapid and significant *in vitro*-assays are regarded as essential tasks.

In this study, colloidal silica nanoparticles were used as model material. Synthetic amorphous silica (SAS), comprising fumed silica as well as silica prepared by wet-chemical routes, including colloidal silica, are produced in industrial scales (Fruijtier-Polloth, 2012). A global consumption of 1.5 million tons encompassing all types of SAS was estimated for 2010 (European Union, 2012). Colloidal silica nanoparticles are used in the paper industry, as polishing agents, for catalysis and coatings in the textile industry, for food production, as well as for drug delivery (Vallet-Regi and Balas, 2008; European Union, 2012), but are not authorised as food additives in the EU (EFSA Panel on Food Additives and Nutrient Sources added to Food (ANS), 2018).

Amorphous silica nanoparticles have been regarded to exert a rather low toxicity due to their low bio persistence (Sachverständigenrat für Umweltfragen, 2011). Nevertheless, a kinetic model for worst-case dietary exposure to synthetic amorphous silica estimated silicon concentrations in liver that were similar to liver concentrations in animal studies where adverse effects were observed (van Kesteren *et al.*, 2015). *In vivo* studies focussing on the inhalative route have shown that amorphous silica nanoparticles induce transient lung inflammation and granuloma formation (Napierska *et al.*, 2010). *In vitro*, colloidal silica nanoparticles have been shown to induce cytotoxicity, apoptosis, oxidative stress, as well as pro-inflammatory responses (Murugadoss *et al.*, 2017). Apart from dose, size and surface properties of the nanoparticles, these effects seem to be dependent on the culture conditions and the cell type investigated. Notably, the culture conditions appear to influence the outcome and sensitivity of *in vitro* assays. For example, pyrogenic silica induced a weaker response in A549 cells grown at the air-liquid interface as compared to A549 under submerged conditions (Panas *et al.*, 2014). A modulation of pro-inflammatory responses induced by silica nanoparticles could also be observed in lung co-culture models (Kasper *et al.*, 2011; Napierska *et al.*,

2012). Although co-culture models as well as ALI cultures are regarded as more realistic models compared to conventional monocultures, they still do not provide the dynamic environment of the deep lung, namely the mechanical stimuli lung cells encounter during breathing. Mechanical strain has been described to induce surfactant release from alveolar type II cells (Edwards, 2001), secretion of pro-inflammatory cytokines (Yamamoto *et al.*, 2002) as well as modulation of gene expression patterns in A549 cells (Weber *et al.*, 2014).

This study investigated the effects of colloidal silica nanoparticles on gene expression of A549 cells grown under dynamic conditions (equibiaxial cyclic stretch) compared to static conditions.

6.2 Results

6.2.1 SiO₂ nanoparticle properties

Two variants of amorphous, colloidal SiO₂ nanoparticles of similar size were synthesized: unlabeled SiO₂ nanoparticles (Si25) and fluorescently labeled SiO₂ nanoparticles (Si25-FD). The far-red emitting dye ATTO 647N was used for labeling in order to allow detection of the nanoparticles by fluorescence microscopy. No significant leaching (< 5 %) was measured for labeled particles (Supplementary Figure 36). The mean particle diameter as determined by analysis of TEM micrographs (Figure 5) is listed in Table 5. The hydrodynamic diameter (D_z) of the particles corresponded well with the diameter determined by electron microscopy (Table 5).

Table 5: Physicochemical properties of unlabeled (Si25) and fluorescently labeled (Si25-FD) nanoparticles used in chapter 6. The hydrodynamic diameter D_z was calculated based on the intensity distribution of the particle scattering signals.

SiO ₂ nanoparticles	Labeling Fully dyed (FD)	Diameter ± SD (TEM) [nm]	Hydrodynamic diameter (D_z) [nm]	Zeta potential [mV]	SiO ₂ Concentration of stock dispersion [g L ⁻¹]
Si25 (G)	-	22.4 ± 2	25 ± 6	-27	9.101
Si25 (N)	-	29.0 ± 3	32 ± 4	-35	9.302
Si25-FD	Atto 647N	27.0 ± 2	28 ± 6	-41	8.111

To study the behavior of the synthesized SiO₂ nanoparticles under experimentally relevant conditions, the particle stability and agglomerate content was tested in cell culture media and ultrapure water. The number weighted hydrodynamic diameter (D_n) increased in presence of medium. However, the agglomerate content increased only slightly to 0.3% (Si25-FD) and 1.3% (Si25) after dispersion of the particles in cell culture medium (Table 6). Thus, for both nanoparticle types no significant agglomeration was observed. This is in line with results from previous studies (Peuschel *et al.*, 2015; Tavernaro *et al.*, 2017).

The nanoparticles used in this study exhibited a negative zeta potential in water, indicating electrostatic stabilization under these conditions (Table 5). In a previous study, a reduction of the absolute zeta potential was observed after dispersion of the nanoparticles in cell culture medium, indicating adsorption of ions or molecules to the particle surface (Peuschel *et al.*, 2015).

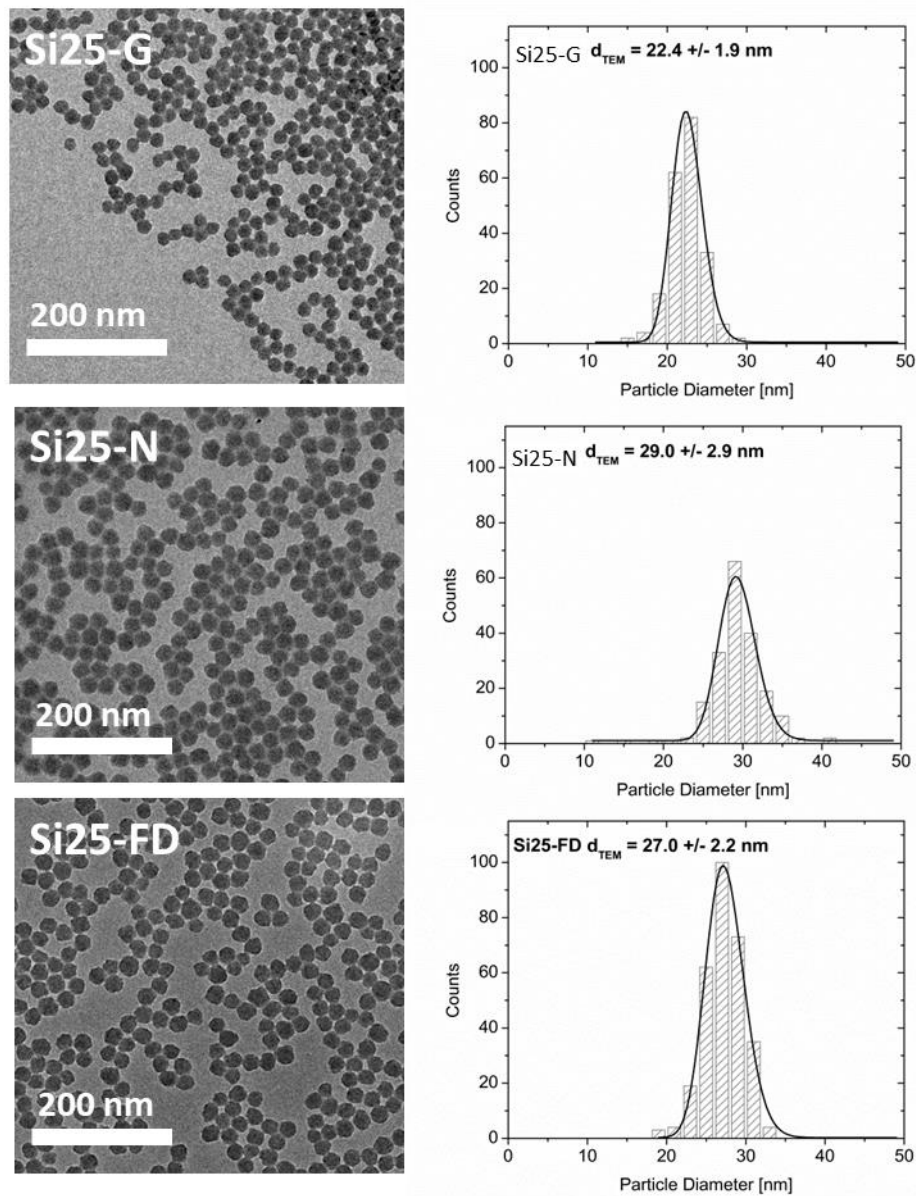


Figure 5: Transmission electron micrographs of Si25 (batch G and N) and Si25-FD particles with particle size histograms from ImageJ based diameter evaluation and leaching measurement for labeled Si25 nanoparticles.

Table 6: Stability of silica nanoparticles at a concentration of $100 \mu\text{g SiO}_2 \text{ ml}^{-1}$ in ultrapure water or cell culture medium (DMEM +10% FBS) measured by dynamic light scattering. The number weighted hydrodynamic diameter D_n was calculated. Numbers in brackets represent the diameter dispersity in %.

SiO ₂ nanoparticles	Hydrodynamic Diameter (D_n) [nm]		Agglomerate Content [%]	
	H ₂ O	Medium	H ₂ O	Medium
Si25-FD	22 (21)	42 (14)	0	0.3
Si25 (N)	24 (21)	39 (11)	0	1.3

The SiO₂ concentration of the synthesized nanoparticles was 9.1 mg SiO₂ ml⁻¹ (Si25 (G)), (9.3 mg SiO₂ ml⁻¹ for Si25 (N)) and 8.1 mg SiO₂ ml⁻¹ (Si25-FD). From these values, the nanoparticle number concentration was calculated based on the particle diameter. At 100 µg SiO₂ ml⁻¹, the particle number concentration, corresponding to the applied dose, was calculated to be 15.7 nmol l⁻¹ (9.5 × 10¹² NP ml⁻¹, Si25 (N)), 7.3 nmol l⁻¹ (4.4 × 10¹² NP ml⁻¹, Si25 (G)) and 9.0 nmol l⁻¹ (5.4 × 10¹² NP ml⁻¹, Si25-FD).

6.2.2 Compatibility of the culture conditions (matrix coating, strain, and nanoparticles)

The BioFlex plates used for cell cultivation exhibit a flexible bottom made of a silicon elastomer. Preliminary growth experiments revealed that A549 cells equally grew on laminin as well as collagen type I coated plates. However, laminin was chosen as a matrix coating because it is distributed in a uniform pattern along the epithelial basement membrane and because it is more abundant than type I collagen in the healthy lung. In comparison, collagen type I is more prominent in diseased lungs, especially in fibrosis (Raghu *et al.*, 1985) or lung tumors (Hendricks *et al.*, 2012). Furthermore, laminin is considered to prevent transdifferentiation of primary alveolar type II cells into type I cells (Guo *et al.*, 2001), whereas collagen type I has been described to promote epithelial-to-mesenchymal transition *in vitro* (Shintani *et al.*, 2008).

At the beginning of this study, the influence of mechanical strain (sinusoidal, equibiaxial strain with 15% surface area expansion at a frequency of 0.25 Hz) on growth and morphology of A549 cells, compared to static conditions, was investigated. Growth experiments using A549 cells indicated that cell division started approximately 24 hours (t = 0) after seeding and that the cells actively grew at the beginning of the experiments (data not shown). At that time (t = 0), either strain was applied, or cells were exposed to nanoparticles, or both. At t = 24 hours, after application of strain for 24 hours, no significant difference in the cell morphology was observed as compared to static cultures. At that time, cultures appeared to be confluent (Figure 6). No significant impact of stretching on cell proliferation could be observed (Figure 7).

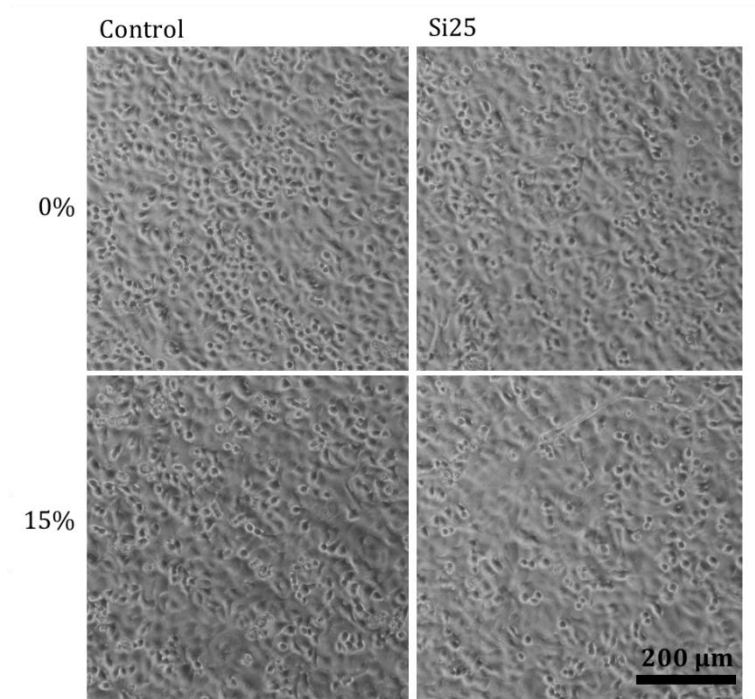


Figure 6: Confluent submerge A549 culture under static (0%) or dynamic (15%) conditions either untreated, or exposed to Si25 (100 μg ml⁻¹, 24 h).

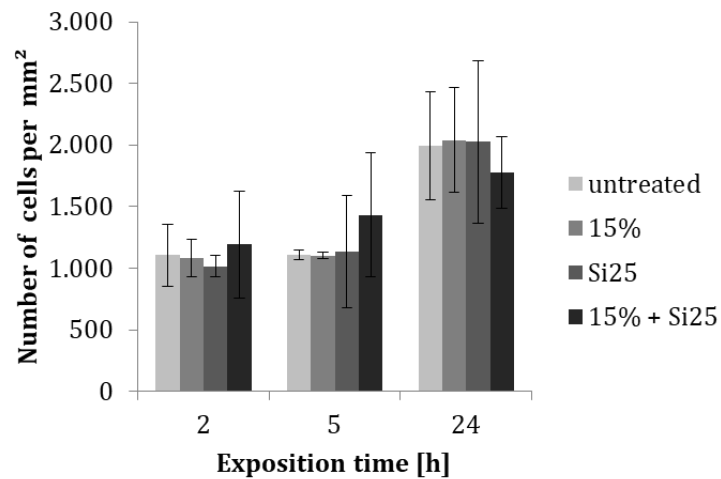


Figure 7: A549 were grown on laminin-coated flexible membranes and treated with Si25 under static (0% stretch) or dynamic (15% stretch) conditions for up to 24 h. Cell counting was performed via nucleic staining and microscopy. Proliferation was related to the initial number of cells at $t = 2$ h. Data represent mean \pm SD. $N = 3$.

6.2.3 Membrane integrity is not affected by SiO₂ nanoparticles, mechanical strain or both

Nanoparticles have been reported to influence membrane integrity under certain conditions (Lesniak *et al.*, 2012). Similarly, mechanical stimulation is also considered to influence membrane integrity (Rouse *et al.*, 2008). As shown in a previous study, the lactate dehydrogenase (LDH) based membrane integrity assay is well suited to determine SiO₂ nanoparticle induced cytotoxicity (Peuschel *et al.*, 2015). Therefore, this assay was used to analyze nanoparticle and strain induced effects on A549 cells. LDH release measurements revealed that Si25 nanoparticles up to a concentration of 800 µg SiO₂ ml⁻¹ did not affect the membrane integrity of A549 cells, neither in the absence nor in the presence of mechanical strain (Figure 8). The further experiments were conducted at an even lower mass concentration of 100 µg SiO₂ ml⁻¹. This concentration was chosen in order to allow for comparison with other studies, e.g. Murugadoss *et al.* (2017). However, Geiser and Kreyling (2010) have estimated that *in vivo*, an alveolar surface cell receives between 120 and 2,400 nanoparticles per hour at maximum, corresponding to a delivered dose of maximally 6×10^{10} nanoparticles per 24 hours and 10^6 cells. In a previous study, according to the *in vitro* sedimentation, diffusion and dosimetry (ISDD) model (Hinderliter *et al.*, 2010), the delivered dose was estimated to be ≈25% of the applied Si25 nanoparticles within 5 hours (Peuschel *et al.*, 2015). From this, it can be estimated that at an administered dose of 100 µg ml⁻¹, the cells receive a 10-fold particle overload (compared to Geiser and Kreyling's estimation) within 5 hours.

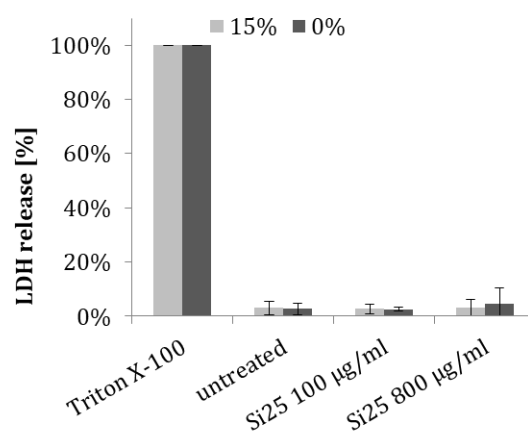


Figure 8: A549 were grown on laminin-coated flexible membranes and treated with 25 nm SiO₂ nanoparticles under static (0% stretch) or dynamic (15% stretch) conditions for 24 h. LDH release into culture medium was measured. Data represent mean ± SD. N = 4.

6.2.4 Determination of treatment exposition time to analyze short term changes in gene expression

Because *CXCL8* is known to be upregulated by silica nanoparticles quickly (Skuland *et al.*, 2014), it was chosen as a target to determine a reasonable exposition time for further analyses. Treatment with stretch or Si25 alone caused slight upregulation of *CXCL8* within 2 hours (4-fold; 4-fold), while a combined treatment caused a significant upregulation to the 13-fold ($p = 0.013$). All effects cleared within the next 3 hours; similar results were obtained for *CCL20* expression (Figure 9).

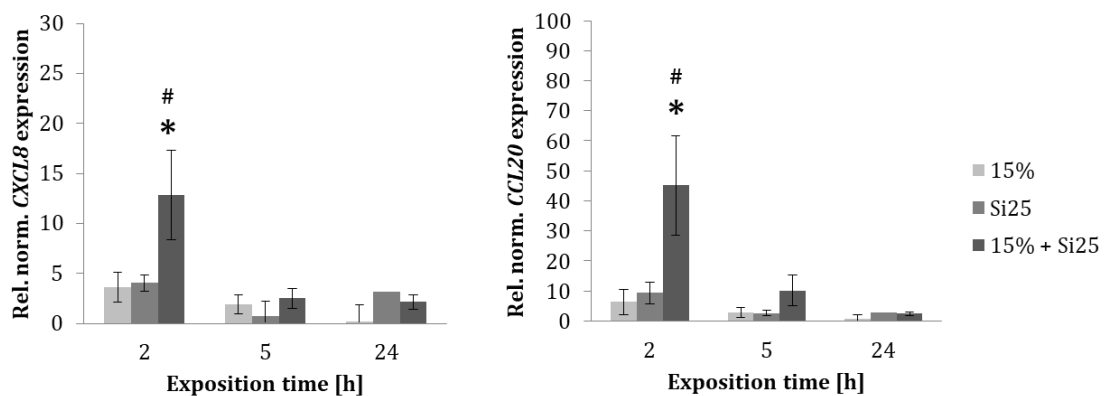


Figure 9: A549 cells were cultured on laminin-coated flexible membranes and treated with 15% equibiaxial strain (stretch), Si25 or both. Cytokine expression was normalized to GAPDH expression and related to expression levels of untreated controls. A statistically significant difference was present between combined treatment and both 15% stretch alone (#) and Si25 (*) alone after 2 hours. (ANOVA and Student's *t*-test with $\alpha = 0.05$. For 2 h data $N = 7$, for 5 h and 24 h data. $N = 3$.)

6.2.5 Genome-wide gene expression alterations

Microarray analyses were performed to identify gene expression changes early after incubation of A549 cells with either Si25 nanoparticles or mechanical strain or the combination of both. As shown before (Figure 9) and according to recent literature (Dos Santos *et al.*, 2004; Rysa *et al.*, 2018), significant gene expression changes were expected to occur early (after 2 h).

Combined exposure to Si25 and stretch led to 41 significantly (false discovery rate adjusted) upregulated probesets (Figure 10: left) representing 34 genes (Table 7). Only one gene (*MAFF*) was upregulated by Si25 alone and one (*CXCL8*) by stretch alone. A similar scenario was obtained for the downregulated genes (Figure 10: right; Table 8). Combined exposure caused decreased expression of 32 probesets representing 29 genes. In contrast, neither Si25 alone, nor stretch alone induced significant decrease of any other gene. Six of the 29 genes were also downregulated when applying stretch alone. Therefore, genome-wide analysis revealed that mechanical strain

strongly enhances the effect caused by Si25 nanoparticles alone.

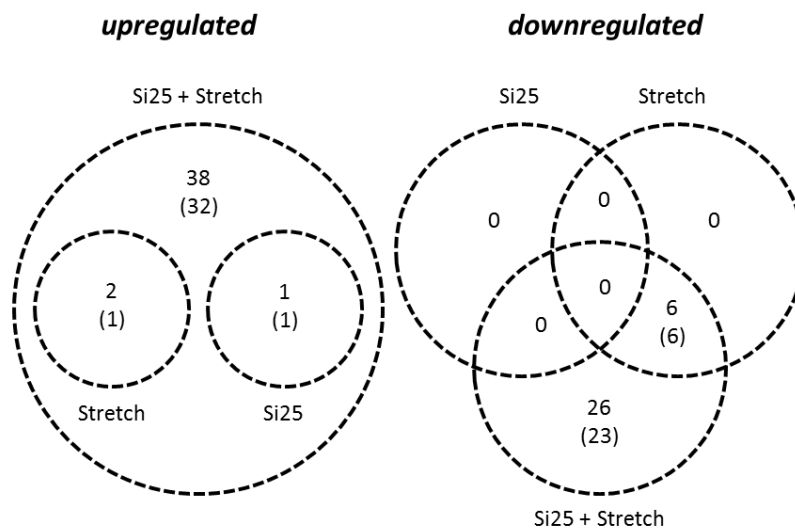


Figure 10: Venn diagram showing the significantly up- and downregulated probesets (genes) in the A549 cells after the application of Si25 nanoparticles, 15% stretch, and the combined treatment (Si25 + stretch). Genes annotated NA were included and counted as individual genes.

6.2.6 Nanoparticle exposure under mechanical strain increases expression of inflammation-associated genes

Among the genes upregulated by Si25 + stretch were six genes encoding chemokines/cytokines as well as three genes related to inflammation (*IL6*, *PTX3*, *ICAM1*) (Table 7). *CXCL8* was the only gene induced under stretch alone. Further genes upregulated by Si25 + stretch were related to signalling, stress, or apoptosis (*EFNA1*, *DUSP5*, *SOD2*, *PPP1R15A*) or have been described as transcription factors or related to transcription. Out of the latter group, *MAFF* was the only gene induced by Si25 alone. Interestingly, all of the nine genes encoding for chemokines/cytokines, as well as additional four genes have been described to be induced by treatment of A549 cells with TNF (Dos Santos *et al.*, 2004). Further, three upregulated genes are related to NF- κ B signalling. The corresponding gene products are known to be involved in either the upregulation of the canonical NF- κ B pathway (*IRAK2*), or inhibition of this pathway (*TNFAIP3*, *BIRC3*), as well as in the alternative NF- κ B pathway (*NFKB2*).

In summary, amorphous silica nanoparticles, when applied under mechanical strain, induced upregulation of a number of genes related to a pro-inflammatory response. This response exhibited a substantial overlap to the response elicited in A549 cells by TNF.

Table 7: Up-regulation of genes by combined treatment of A549 cells with Si25 (100 µg SiO₂ ml⁻¹) + 15% stretch for 2 hours.

FC	Name	
chemokines/cytokines, inflammation related		
CCL2	2	C-C motif chemokine ligand 2 *
CCL20	15	C-C motif chemokine ligand 20 *
CXCL1	2	C-X-C motif chemokine ligand 1 *
CXCL2	2	C-X-C motif chemokine ligand 2 *
CXCL3	2	C-X-C motif chemokine ligand 3 *
CXCL8	7	C-X-C motif chemokine ligand 8 *, s
ICAM1	2	intercellular adhesion molecule 1 *
IL6	3	interleukin 6 *
PTX3	4	pentraxin 3 *
NF-κB related		
IRAK2	2	interleukin 1 receptor associated kinase 2
NFKB2	3	nuclear factor kappa B subunit 2
TNFAIP3	3	TNF alpha induced protein 3 *
BIRC3	2	baculoviral IAP repeat containing 3 *
signaling, stress or apoptosis		
BCL2A1	3	BCL2 related protein A1 *
DUSP5	2	dual specificity phosphatase 5
PPP1R15A	2	protein phosphatase 1 regulatory subunit 15A
EFNA1	2	ephrin A1 *
SOD2	2	superoxide dismutase 2
transcription factors or related to transcription		
ATF3	4	activating transcription factor 3
CITED2	2	Cbp/p300 interacting transactivator with Glu/Asp rich carboxy-terminal domain 2
MAFF	3	MAF bZIP transcription factor F n
NR4A1	2	nuclear receptor subfamily 4 group A member 1
NR4A2	5	nuclear receptor subfamily 4 group A member 2
NR4A3	2	nuclear receptor subfamily 4 group A member 3
others		
ARL14	2	ADP ribosylation factor like GTPase 14
CTGF	2	connective tissue growth factor
FLJ16734	2	
STC1	2	stanniocalcin 1

* = Also induced by TNFa (Dos Santos *et al.*, 2004);

s = also induced under stretch conditions in absence of nanoparticles;

n = also induced by nanoparticle treatment in absence of stretch;

FC = fold change compared to untreated control;

= Six genes identified by the GeneArray were annotated NA and are not given here.

6.2.7 Nanoparticle exposure under mechanical strain decreases expression of proliferation-associated genes

Downregulated genes by treatment with Si25 + stretch included genes for regulation of translation and splicing, regulation of transcription, DNA or nucleotide binding, cell division, apoptosis, ubiquitination, recombination, and double strand repair, as well as calcium signaling (Table 8). This is a typical transcriptional pattern of cells that respond to stress with cell cycle arrest and repair processes, accompanied by altered transcription and translation, in order to survive an acute challenge by exposure to toxic com-

pounds.

Table 8: Down-regulation of genes by combined treatment of A549 cells with Si25 (100 $\mu\text{g SiO}_2 \text{ ml}^{-1}$) + 15% stretch for 2 hours.

Gene#	FC	Name
translation regulation/splicing		
<i>DDX6</i>	0.4	DEAD-box helicase 6
<i>DDX17</i>	0.5	DEAD-box helicase 17
<i>GAS6-AS1</i>	0.4	GAS6 antisense RNA 1
transcription regulation/DNA or nucleotide binding		
<i>ID2</i>	0.5	inhibitor of DNA binding 2
<i>ID3</i>	0.5	inhibitor of DNA binding 3, HLH protein
<i>ID1</i>	0.2	inhibitor of DNA binding 4, HLH protein
<i>ID4</i>	0.4	inhibitor of DNA binding 4, HLH protein
<i>ZNF480</i>	0.3	zinc finger protein 480
<i>BCOR</i>	0.4	BCL6 corepressor
<i>BDP1</i>	0.3	B double prime 1, subunit of RNA polymerase III transcription initiation
<i>HINT3</i>	0.5	histidine triad nucleotide binding protein 3
<i>ESCO1</i>	0.5	establishment of sister chromatid cohesion N-acetyltransferase 1
<i>ZNF770</i>	0.5	zinc finger protein 770
<i>MORF4L2</i>	0.4	mortality factor 4 like 2
cell division/apoptosis		
<i>HIST1H1</i>	0.5	histone cluster 1 H1 family member c
<i>ASPM</i>	0.5	abnormal spindle microtubule assembly
ubiquitination/protein interaction		
<i>TTC37</i>	0.5	tetratricopeptide repeat domain 37
<i>RC2C</i>	0.5	proline rich coiled-coil 2C
<i>LTN1</i>	0.4	listerin E3 ubiquitin protein ligase 1
<i>LONRF2</i>	0.5	LON peptidase N-terminal domain and ring finger 2
<i>OTUD4</i>	0.5	OTU deubiquitinase 4
<i>STYX</i>	0.5	serine/threonine/tyrosine interacting protein
recombination/double strand repair		
<i>OGEN1</i>	0.5	GEN1 Holliday junction 5' flap endonuclease
calcium signaling		
<i>AHNAK2</i>	0.5	AHNAK nucleoprotein 2

FC = fold change compared to untreated control

= Five genes identified by the GeneArray were annotated NA and are not given here

6.2.8 Confirmation of cytokine expression by qPCR

Among the genes tested with the microarray, *CCL20* and *CXCL8* were those with the highest relative expression in cells treated with Si25 + stretch compared to untreated controls. To obtain more reliable data on relative expression levels, *CCL20* and *CXCL8* expression were analyzed by qPCR (Figure 11). According to microarray data, *CCL20* was upregulated to the 15-fold and *CXCL8* to the 7-fold under treatment with Si25 + stretch. Quantitative PCR data indicated an even stronger upregulation upon treatment with Si25 + stretch. *CCL20* was upregulated to the 45-fold, *CXCL8* to the 13-fold. In accordance with the microarray data, treatment with only stretch alone or Si25 alone caused less upregulation (*CCL20*: 6-; 9-fold; *CXCL8*: 4-; 4-fold) (Figure 11).

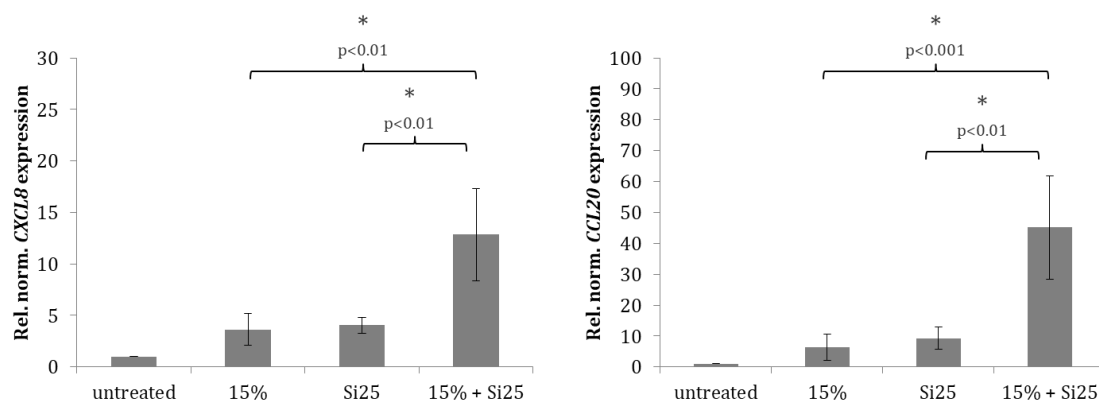


Figure 11: A549 were grown on laminin-coated flexible membranes and treated with Si25 under static (0% stretch) or dynamic (15% stretch) conditions for 2 hours. Cytokine expression was normalized to GAPDH expression and related to expression levels of untreated controls. ANOVA and Student's t-test determined significant ($\alpha = 0.05$) differences. Data represent means \pm SD. N = 6.

6.2.9 Nanoparticle exposure under mechanical strain increases IL8 secretion

In order to investigate whether increased *CXCL8* expression resulted in higher protein levels, the secretion of its gene product IL8 was analyzed by ELISA (Figure 12). After 2 hours of treatment, the Si25 alone, stretch alone, or Si25 + stretch only caused minor, statistically insignificant changes. After 5 h and 24 h, however, an accumulation of IL8 in the cell culture medium could be observed. Untreated cells had secreted ≈ 500 pg ml⁻¹ after 5 hours and ≈ 750 pg ml⁻¹ after 24 hours. Stretch alone did not significantly increase the level of secreted IL8 compared to the untreated controls (≈ 680 pg ml⁻¹ after 5 h; ≈ 980 pg ml⁻¹ after 24 h). Si25 treatment resulted in doubling of the amount of secreted IL8 as compared to untreated controls (≈ 990 pg ml⁻¹ after 5 h; ≈ 1400 pg ml⁻¹ after 24 h). Treatment with Si25 + stretch resulted in the highest secretion (≈ 1300 pg ml⁻¹ after 5 h; ≈ 1600 pg ml⁻¹ after 24 h). The delayed increase in protein

secretion in presence of strain suggests that this strain-induced process may be regulated at the transcriptional level, since the level of protein secretion lags behind the level of mRNA formation. For comparison, the secretion of cells treated with TNF (2 ng ml^{-1}) was also analyzed. The effects of TNF exceeded those induced by the nanoparticle and strain by factors of five to six (Figure 27, Serum A, page 86).

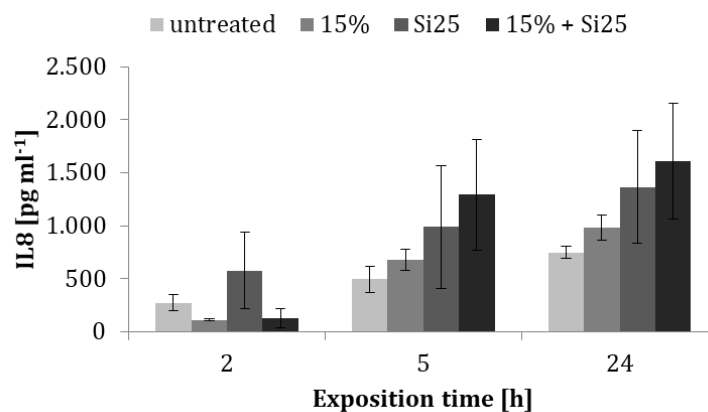


Figure 12: A549 cells were cultured on laminin-coated flexible membranes and treated with 15% stretch, Si25, or both. Cytokine secretion (IL8) was determined by ELISA. ANOVA showed no significant ($\alpha = 0.05$) differences between groups. Data represent means \pm SD. $N = 3$.

6.2.10 Cellular accumulation of Si25 nanoparticles is not affected by stretching

Uptake and intracellular accumulation of nanoparticles are important steps in the induction of toxic effects (Nel *et al.*, 2009). Here, the question was raised whether mechanical strain caused an increased nanoparticle accumulation that was responsible for the altered expression profile under combined treatment. The amount of internalized Si25-FD nanoparticles in A549 over time was analyzed by measuring the overall fluorescence intensity in the nanoparticle imaging channel within a section comprising ≈ 50 -100 cells. As can be seen in Figure 13, an increasing number of bright spots accumulated within the cells over time. After 24 hours of treatment, nearly all cells showed fluorescence from labeled nanoparticles with a tendency to accumulate in the perinuclear region (Supplementary Figure 32). Quantitative analysis confirmed that the average fluorescence intensity per cell increased over time (Figure 14), indicating increased nanoparticle accumulation by the cells. The quantitative evaluation of the fluorescence images did not indicate a significant difference in Si25-FD uptake between stretched or unstretched A549 cells (Figure 14).

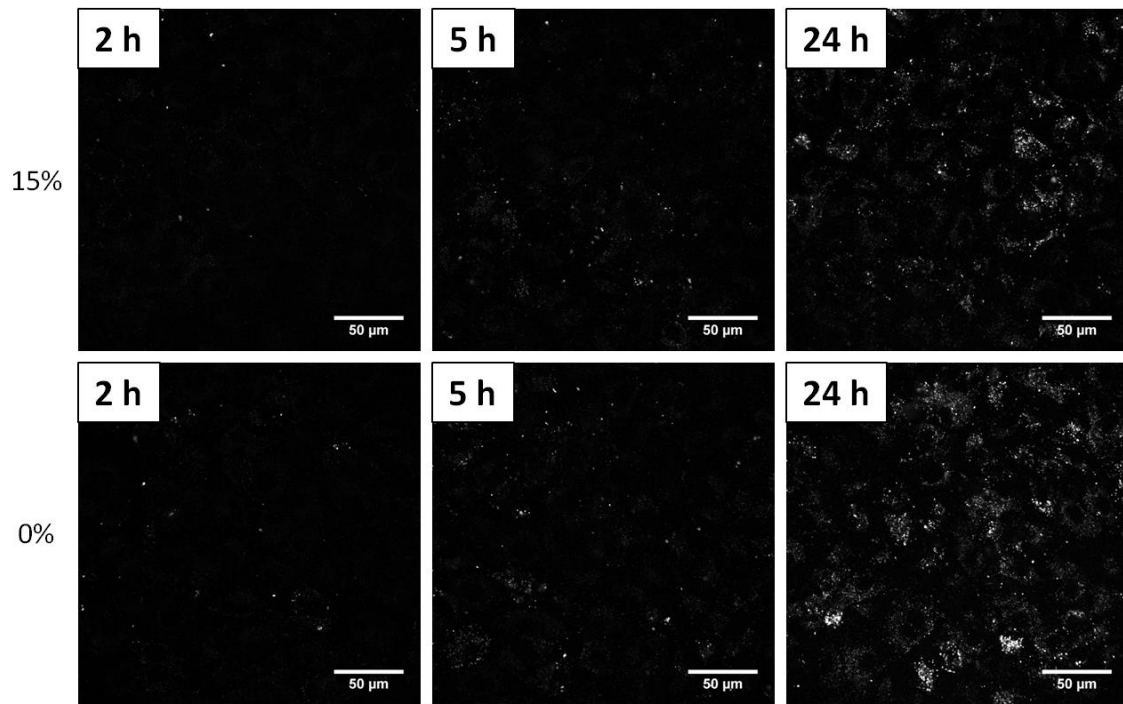


Figure 13: Mechanical strain (15% stretch) did not lead to an increased uptake of Si25-FD over 24 h. A549 cells were exposed to Si25-FD ($100 \mu\text{g SiO}_2 \text{ ml}^{-1}$; 2-24 h) under dynamic (15% stretch) or static (0% stretch) conditions. Brightness and contrast were enhanced for presentation, still only the brightest spots are clearly visible to the eye. Images show representative data taken from three independent experiments with one biological replicate (= microscopy sample from one 6 well) each. Per sample, three images at three different positions were acquired. Brightness and contrast were enhanced for presentation.

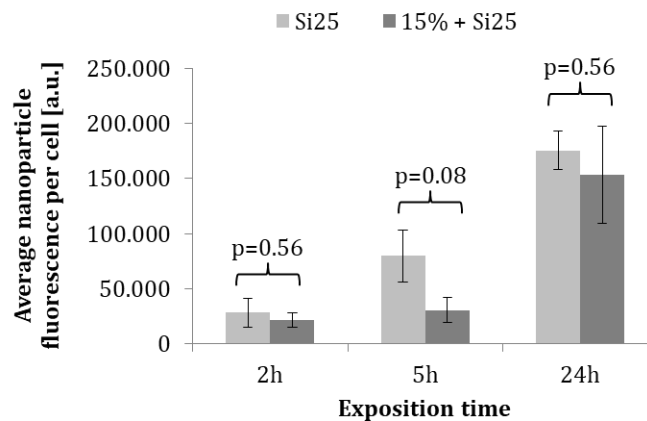


Figure 14: Mechanical strain (15% stretch) did not cause a significant change in the uptake of Si25-FD by A549 within 24 h compared to unstretched controls. The average nanoparticle fluorescence intensity of internalized Si25-FD related to the number of cells was quantified by image processing of confocal images that were acquired by a standardized procedure. Data represent mean values \pm SD from three independent experiments with one biological replicate (\cong microscopy sample from one 6 well) each. Student's *t*-test was performed to determine statistically significant differences between groups ($\alpha = 0.05$).

In order to further determine if all cells internalized similar amounts of Si25-FD, a single cell analysis was performed. Histograms were obtained, displaying the distribution of cells that exhibited different levels of fluorescence intensities (Figure 15). At all times, histogram shapes did not differ much when comparing stretched with un-

stretched cells. Cells with no or very low intensities ($<10^1$ or $<10^2$ a.u.) accounted for only a small proportion in both groups: Already after two hours, nanoparticle fluorescence signals were detected in more than 70% of the stretched cells, and in more than 90% of the unstretched group. This trend continued with time: under both conditions, more than 70% of the cells seemed to have accumulated particles after 5 h and 24 h. A shift of the histogram to the right from 2 h to 24 h also indicated that over time all cells accumulate more nanoparticles. In conclusion, stretching did not severely alter the number of cells that accumulated nanoparticles, nor did it enhance the overall uptake of nanoparticles per cell.

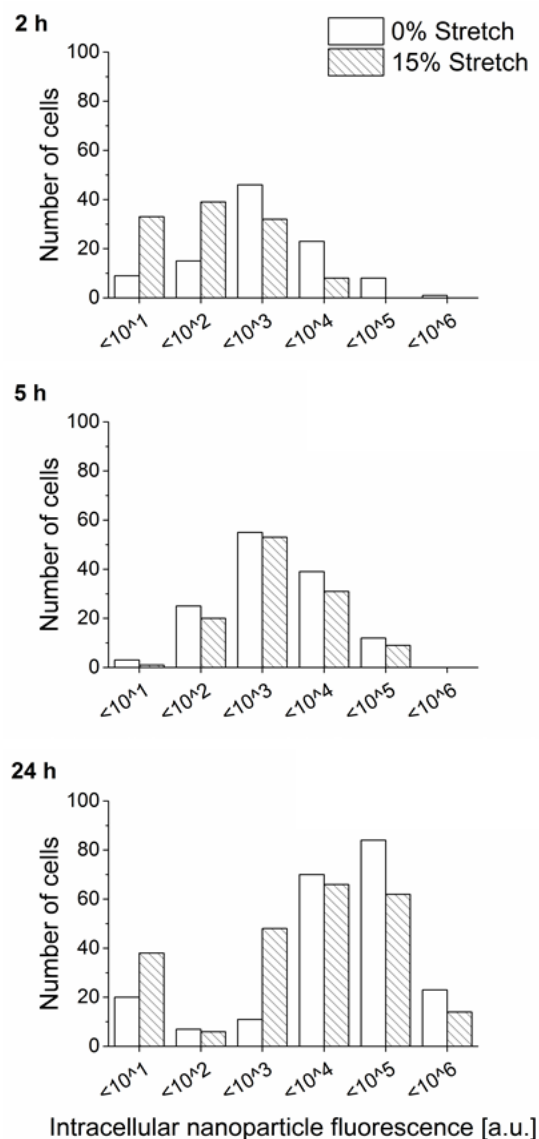


Figure 15: Histograms display the distribution of A549 cells (y-axis: absolute cell number) exhibiting different fluorescence intensities (x-axis: arbitrary fluorescence units). Given data represent two independent experiments with one image of one sample each. Each dataset comprises ca. 100-200 cells, depending on the respective point in time.

6.2.11 No NF- κ B translocation upon Si25 treatment, stretching or both

As described above, the observed gene expression profile showed significant overlap with the gene expression profile induced by TNF (Dos Santos *et al.*, 2004). TNF is known to activate the NF- κ B signaling pathway (Karin and Greten, 2005). According to Dos Santos *et al.* (2004), TNF treatment of A549 cells not only causes induction of *NFKB1* (p105/p50) and *NFKBIA*, coding for its cytoplasmic inhibitor I κ B α , but also of *TNFAIP3/A20* and *BIRC3/IAP2*, which are involved in the inhibition of TNF induced NF- κ B signaling by an auto-feedback loop. Of these genes, only *TNFAIP3/A20* and *BIRC3/IAP2* were upregulated upon treatment of A549 with Si25 + stretch. Instead, the *NFKB2* gene, coding for the NF- κ B2 p100/p52 subunits, was induced according to expression analysis. Translocation of the three subunits NF- κ B p65, NF- κ B1 p105/p50 and NF- κ B2 p100/p52 was analysed by immune fluorescence staining and confocal microscopy (Figure 16, Figure 17, Figure 18).

NF- κ B p65 represents the major NF- κ B heterodimer consisting of RelA (p65)-p50 dimers and is involved in the canonical (classical) NF- κ B signal transduction pathway (Gilmore, 2006). An increase in the nuclear fluorescence intensity compared to untreated cells was not observed and therefore did not indicate a significant accumulation of NF- κ B p65 in the nuclei of A549 cells after 2 hours (Figure 16). In comparison, cells treated with TNF (20 ng ml⁻¹, 1 h) exhibited a bright nuclear fluorescence, indicating translocation of NF- κ B p65. A translocation of NF- κ B1 p105/p50, which is also involved in the canonical pathway, could neither be confirmed nor ruled out by microscopy (Figure 17). These results indicate that the treatment of A549 cells with Si25 + stretch does not result in a marked activation of the classical NF- κ B signaling pathway.

Unlike expected from the expression analysis (Table 7), microscopy could not confirm translocation of NF- κ B2 p100/p52 (*NFKB2*) (Figure 18) upon treatment with Si25 + stretch.

A detailed overview of the translocation kinetics of the analyzed NF- κ B subunits in response to different inducers can be found in the supplementary information (Figure 42, Figure 43, Figure 44).

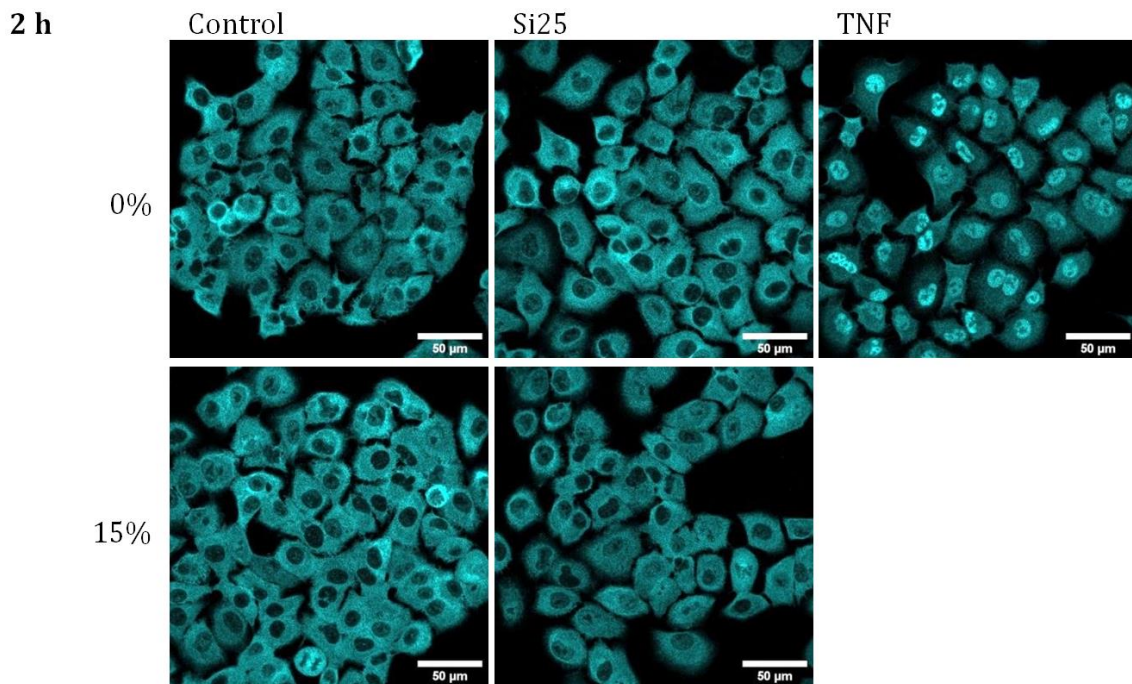


Figure 16: A549 cells were cultured on laminin-coated flexible membranes and treated with 15% stretch, Si25, or both for 2 hours (positive controls: human recombinant TNF, 20 ng ml⁻¹). Cells were fixed and immuno stained for NF-κB p65. Images show representative data taken from one experiment with one biological replicate (= microscopy sample from one 6 well). Per sample, three images at three different positions were acquired. Brightness and contrast were enhanced for graphical presentation. Scale = 50 μm.

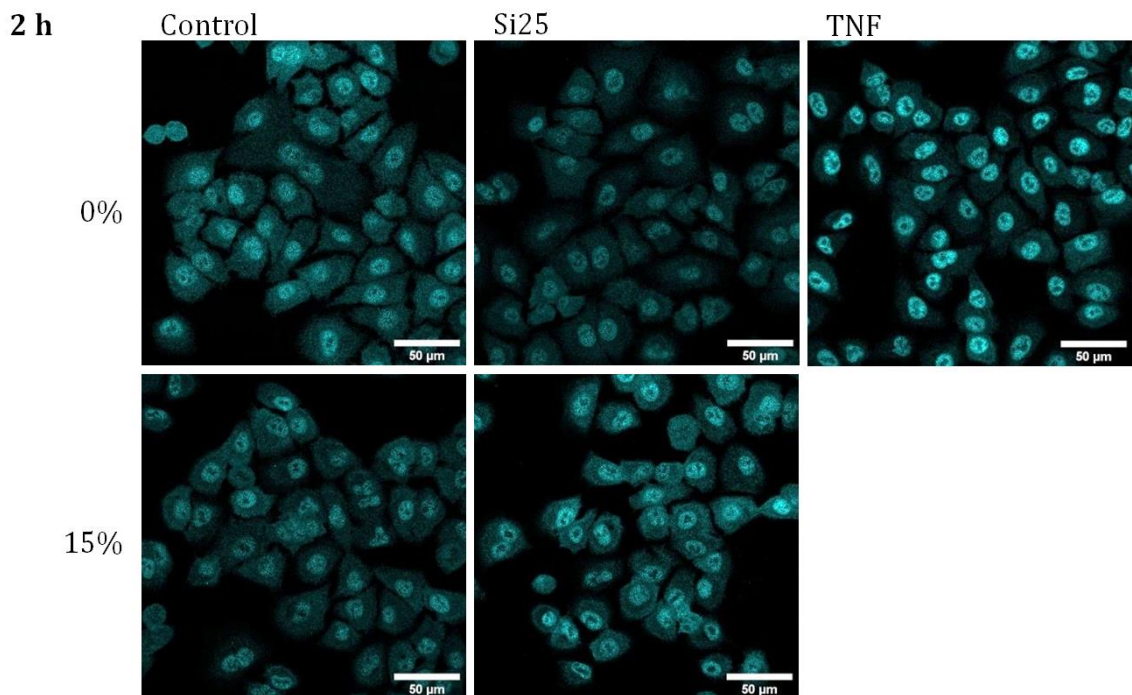


Figure 17: A549 cells were cultured on laminin-coated flexible membranes and treated with 15% stretch, Si25, or both for 2 hours (positive controls: human recombinant TNF, 20 ng ml⁻¹). Cells were fixed and immuno stained for NF-κB1 p105/p50. Images show representative data taken from one experiment with one biological replicate (= microscopy sample from one 6 well). Per sample, three images at three different positions were acquired. Brightness and contrast were enhanced for graphical presentation. Scale = 50 μm.

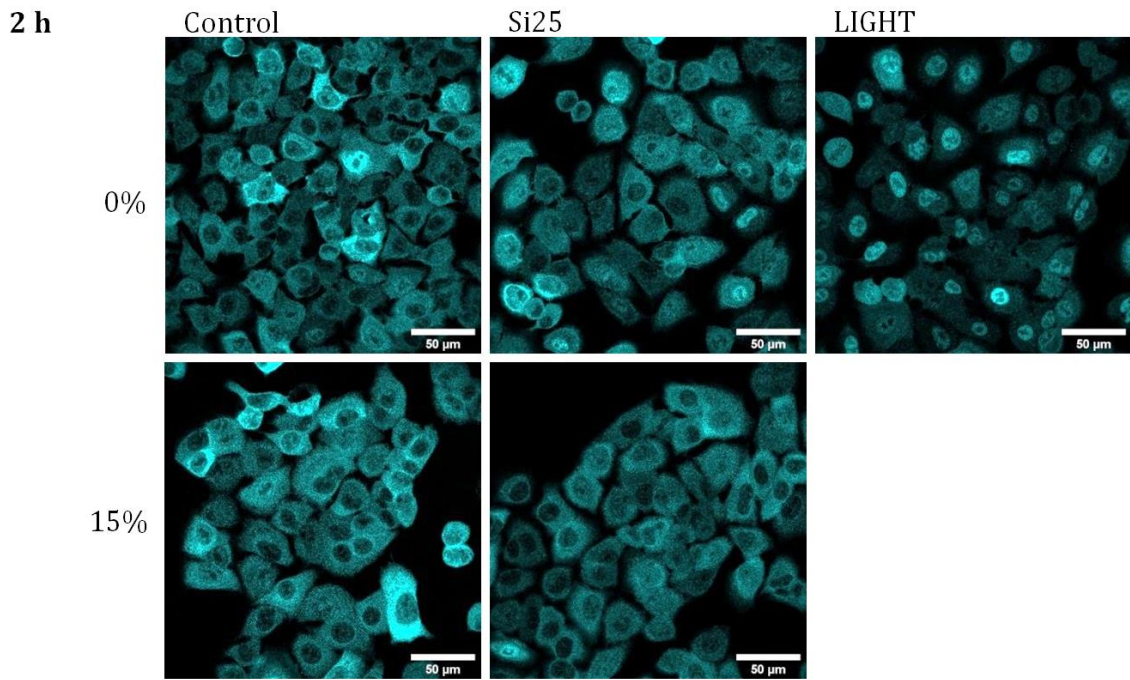


Figure 18: A549 cells were cultured on laminin-coated flexible membranes and treated with 15% stretch, Si25, or both for 2 hours (positive controls: human recombinant LIGHT (TNFSF14, 100 ng ml⁻¹). Cells were fixed and immuno stained for NF- κ B2 p100/p52. Images show representative data taken from one experiment with one biological replicate (= microscopy sample from one 6 well). Per sample, three images at three different positions were acquired. Brightness and contrast were enhanced for graphical presentation. Scale = 50 μ m.

6.3 Discussion

6.3.1 SiO₂ nanoparticle uptake is not enhanced under mechanical strain

Nanoparticle exposure under mechanical strain increased the expression of inflammation-associated genes, especially *CCL20* and *CXCL8*. In order to address the question whether the accumulation of nanoparticles is responsible for the observed amplified responses under mechanical strain, we quantitatively analyzed the intracellular accumulation of fluorescently labeled SiO₂ nanoparticles. No significant difference in cellular nanoparticle accumulation was observed, indicating that mechanical strain amplified the inflammatory effect of nanoparticles independently from their intracellular accumulation. Since the amplitude and frequency of mechanical strain was chosen to resemble the motion of normal breathing in the lung, it is possible that a similar amplification of nanoparticle-induced inflammation also occurs in alveolar epithelial cells *in vivo*.

Previously published studies on the influence of mechanical forces on intracellular accumulation of nanoparticles obtained inconsistent results. Two studies reported an increased accumulation of nanoparticles (made of polystyrene and quantum dots) upon mechanical stimulation of bovine aortic endothelial cells and human epidermal keratinocytes (Rouse *et al.*, 2008; Hu and Liu, 2015). In both studies, uptake was quantified by fluorescence measurements of cell lysates. This approach may only have insufficiently distinguished between internalized and cell-associated nanoparticles. An increase in nanoparticles accumulation under mechanical stimulation was also observed by Huh *et al.* (2010). In their study, confocal microscopy was used to determine the number of nanoparticle-positive NCI H441 alveolar epithelial cells in a lung on a chip model mimicking alveolar distension by application of unidirectional cyclic strain. The authors reported an increased number of cells that had taken up nanoparticles when mechanically stimulated, as well as an increased translocation of nanoparticles across the alveolar barrier from epithelial to endothelial cells. Furthermore, in the study by Huh *et al.* (2010), a strain-induced increase in the fraction of cells internalizing nanoparticles was observed, whereas in absence of strain only 7% of the cells seemed to have accumulated nanoparticles. This trend was not confirmed here. Nevertheless, evidence for a higher number of cells internalizing nanoparticles is qualitatively different from the finding of a larger amount of nanoparticles internalized by a distinct

number of cells. In the current study, nanoparticle uptake was quantified by standardized confocal microscopy analysis of 2D slices of confluent cell layers, ensuring that fully internalized nanoparticles rather than membrane bound nanoparticles are included in the analysis.

Freese *et al.* (2017), did not report an increased uptake of gold nanoparticles in human umbilical vein endothelial cells (HUVEC) using similar stretching parameters. The same authors even observed decreased accumulation of SiO₂ nanoparticles in stretched HUVEC (Freese *et al.*, 2014).

6.3.2 The pro-inflammatory response of A549 cells induced by SiO₂ nanoparticles under mechanical strain seems independent from the canonical NF-κB pathway

Under mechanical strain, Si25 induced upregulation of 13 genes (Table 7) that have also been reported to be upregulated after adding TNF to A549 cells (Dos Santos *et al.*, 2004). Nine of these genes are coding for pro-inflammatory chemokines/cytokines or molecules related to inflammation. The TNF induced response in A549 cells has been described to induce upregulation of *NFKBIA* (IκBα) and *NFKB1* (p105/p50) (Dos Santos *et al.*, 2004). Both genes are involved in the canonical pathway of NF-κB activation, which is induced by TNF (Gilmore, 2006). Expression of these two genes was not influenced by Si25 plus stretch. Similar to the TNF induced response, *TNFAIP3* (*A20*) and *BIRC3* (*IAP2*) were upregulated by Si25 + stretch. The products of these genes have been described to be involved in an auto-inhibition of NF-κB activation by negative feedback (Dos Santos *et al.*, 2004). The upregulation of genes involved in NF-κB signaling led us to investigate the translocation of NF-κB in response to the treatment of A549 cells. TNF is well-known to induce the canonical pathway of NF-κB activation (Gilmore, 2006), including the translocation of p65 into the nucleus of A549 cells (Dos Santos *et al.*, 2004). In contrast, Si25 + stretch did not induce a marked translocation of p65 into the nucleus. However, qualitative microscopy could not rule out involvement of NF-κB1 p105/p50. At this point it seems unlikely that the canonical pathway is involved in the induction of the observed pro-inflammatory response.

Unlike the TNF induced response observed by Dos Santos *et al.* (2004), *NFKB2* (p100/p52) expression was induced by Si25 + stretch. As this might indicate involvement of an alternative NF-κB pathway, the translocation of p52 (a proteolysis product

of p100) was investigated. However, no marked translocation of this component was detected, suggesting that this pathway is also not directly involved in the observed pro-inflammatory response.

6.3.3 Mechanical strain amplifies Si25-induced effects on expression of genes related to inflammation in A549 cells

In this study, mechanical strain with the extent of normal breathing as well as Si25 nanoparticles only led to minor changes in gene expression. Combining both treatments resulted in a severely altered gene expression, suggesting a synergistic or amplifying way of cell stimulation. This demonstrates that culture conditions mimicking the mechanical strain encountered by alveolar epithelial cells during normal breathing may be relevant to identify cellular responses that do not occur under conventional static *in vitro* conditions.

Similarly, under static conditions, modulation of the cellular response to nanoparticles occurs depending on the kind of culture system. Current lung *in vitro* culture systems are either submerge mono- or co-cultures or systems grown at the air-liquid-interface (ALI) as mono- or co-cultures (Clippinger *et al.*, 2018). As shown by Kasper *et al.* (2015), for example, a submerge co-culture model of epithelial and endothelial cells exhibited a more sensitive release of inflammatory markers in response to application of $60 \mu\text{g ml}^{-1}$ SiO₂ nanoparticles compared to the mono-culture. Panas *et al.* (2014) observed a reduced toxicity induced by SiO₂ nanoparticles when exposing A549 cells at the ALI. In contrast, the pro-inflammatory response of A549 cells was induced when cells were grown at the ALI. Generally, ALI systems are regarded to represent the *in vivo* exposure conditions more realistically than standard approaches (Rothen-Rutishauser *et al.*, 2005; Wu *et al.*, 2017; Lacroix *et al.*, 2018). However, conventional ALI systems based on permeable substrates do not incorporate the influence of mechanical stimuli (Huh *et al.*, 2010; Schürch *et al.*, 2014).

Under *in vivo* conditions, in which alveolar cells are constantly exposed to stretch due to breathing, amorphous silica has been shown to result in transient lung inflammation, involving an increase of pro-inflammatory cytokines and chemokines (Fruijtier-Polloth, 2012; Pavan and Fubini, 2016). In contrast, most *in vitro* studies focussing on the effects of amorphous silica nanoparticles on lung cells are performed under static conditions, not addressing the impact of mechanical stimuli. Under static conditions,

amorphous silica nanoparticles have been described to induce a broad range of cellular responses. This is partially caused by the multitude of types of silica used for nanotoxicological studies. The physicochemical properties of amorphous silica particles related to toxicity, including particle size and morphology, aggregation state, porosity, hydrophobicity/hydrophilicity and solubility are to a great extent variable and depend on the preparation process and surrounding conditions (Napierska *et al.*, 2010). Accordingly, various *in vitro* studies reported on the induction of oxidative stress responses, activation of MAP kinase and NF- κ B pathways, release of pro-inflammatory cytokines and chemokines, or even cytotoxicity (Fruijtier-Polloth, 2012).

The colloidal silica nanoparticles used in this study are regarded to be hydrophilic and covered by mutually H-bonded silanols (Napierska *et al.*, 2010; Pavan and Fubini, 2016). Such silica nanoparticles are regarded as non-membranolytic and therefore not involved in the induction of a persistent lung inflammation responsible for the induction of lung cancer, silicosis, or autoimmune diseases (Pavan and Fubini, 2016). In line with this proposal, the silica nanoparticles used in this study did not result in membrane damage or cytotoxicity as measured by LDH release from the cells (Figure 8).

In this study, for the first time, the effects of silica nanoparticles on gene expression of mechanically stretched lung epithelial cells were analyzed. Only under the combined treatments (Si25 + stretch) upregulation of nine genes related to pro-inflammatory responses (Table 7) was induced. According to gene array data, chemokine *CCL20* was among the strongest upregulated genes. *CCL20* is known to recruit immature dendritic cells and subpopulations of T-lymphocytes and B-cells (Schutyser *et al.*, 2003). *CXCL8*, encoding for the neutrophil attracting chemokine IL8, was also markedly upregulated (Table 7). In comparison, no increase in the secretion of IL8 by stretched and silica nanoparticle-treated primary endothelial cells (HUVEC) was found by Freese *et al.* (2014). In addition, in this study, a moderate (2-4-fold) upregulation was observed for *CCL2*, *CXCL1*, *CXCL2*, *CXCL3*, *IL6*, *ICAM1* and *PTX3*. An augmented expression of *ICAM1* induced by silica nanoparticles combined with mechanical strain was also found in endothelial cells (Huh *et al.*, 2010).

Furthermore, a similar gene expression pattern to the one observed in this study was found after exposure of BEAS-2B cells to crystalline silica under static conditions, showing upregulation of *CCL20*, *CXCL8*, *CXCL1*, *CXCL3* and *IL6* together with further

cytokines and chemokines (Ovrevik *et al.*, 2009). The same study also revealed that A549 cells showed an attenuated induction of *CXCL8* in response to crystalline silica as compared to BEAS-2B cells, an immortalized human bronchial epithelial cell line.

In conclusion, this part revealed an amplifying effect on gene expression (inflammatory responses in particular) upon of Si25 and stretch, when simultaneously applied to submerge A549 cells. An indirect effect from impaired membrane integrity or increased nanoparticle uptake upon stretch could be excluded. Involvement of NF- κ B signalling cannot be ruled out at this point. ^

7 Part II: Influence of silica nanoparticle size and stretching amplitude on cytokine release in alveolar type II cells

7.1 Introduction

In the following chapter, two aspects of the previously utilized dynamic lung *in vitro* model for nanotoxicity testing (Schmitz *et al.*, 2019) were evaluated more closely: First, it was investigated if the synergistic effect of nanoparticle treatment in combination with mechanical strain on cytokine expression is specific for the administered particle size (25 nm). Second, it was elucidated if this synergistic effect can be enhanced by stronger, supposedly non-physiological mechanical strain.

7.1.1 Particle size

In pulmonary toxicology research, nanoparticle size is an important parameter as it determines nanoparticle deposition, clearance and translocation (Schmid *et al.*, 2009). For *in vivo* inhalation is known that particles of different sizes and masses deposit in different regions of the lungs depending on their diffusion and sedimentation behaviour (Heyder and Svartengren, 2002). A larger diameter of nanoparticles can limit cellular internalization and intracellular distribution (Lu *et al.*, 2009; Schübbe *et al.*, 2012). Several studies (Hetland *et al.*, 2001; Napierska *et al.*, 2012; Lag *et al.*, 2018) reported stronger inflammatory responses upon exposition to smaller particles, higher total surface areas and higher mass concentrations. Size dependent effects could often be observed for particles with diameter differences of only few nanometers. It is also known that the surface area plays a crucial in nanotoxicity by determine the contact interface between nanoparticles and biological entities like proteins or whole cells (Hetland *et al.*, 2001; Lee *et al.*, 2011). Based on this knowledge it was expected that A549 cells would respond less to Si80 than to Si25 nanoparticles.

When it comes to comparing different particle sizes with each other, an important question arises: Should one administer the different particles at similar mass concentration or at similar particle number concentration. Here, two comparable SiO₂ particles with differing diameters were administered at similar mass concentration of 100 µg SiO₂ ml⁻¹. Consequently, the smaller Si25 particles were delivered at higher particle number concentration (98-fold) and higher total surface area (13-fold) compared to the larger Si80 particles. This supports the hypothesis that Si25 treatment would stimulate stronger responses than Si80 treatment.

Both particle types were within a size range that is preferably internalized *via*

endocytosis, and quickly accumulate in the perinuclear region (Lu *et al.*, 2009; Yuan and Zhang, 2010; Schübbe *et al.*, 2012) (Supplementary Figure 32). As reported by Schumann *et al.* (2012) and Peuschel *et al.* (2015), no major differences in uptake or intracellular transport characteristics were observed in A549 cells. Therefore, it was assumed that potentially different responses upon Si25 or Si80 exposition would not result from a difference in internalization.

7.1.2 Mechanical strain in *in vitro* models

Considering that *in vitro* lung models may represent healthy or pathologic lungs, it is important to be able to mimic physiological and non-physiological mechanical strain. The latter occurs, for example, under invasive mechanical ventilation in the lungs of patients that suffer from acute lung failure (Slutsky, 1999).

While in common *in vitro* models the respiratory rate can simply be translated to cycling frequency, it is still not entirely clear what degree (amplitude) of area expansion (stretch) in the *in vitro* system resembles physiology *in vivo*. A review on estimates of alveolar deformation from 2011 (Roan and Waters) summarized that $\approx 10\%$ stretch ($\epsilon \approx 5\%$) takes place under normal breathing within tidal volume, – more in diseased lungs or when exploiting total lung capacity. A consecutive review of the same authors (Waters *et al.*, 2012) gave a valuable overview of studies that observed responses to mechanical strain in lung epithelial cells. In terms of cell death and injury they suggest that A549 are less vulnerable with tolerable stretching amplitudes of up to 35% ($\epsilon \leq 16\%$) as compared to primary alveolar epithelial cells. Waters *et al.* give profound estimations that below 12% stretch ($\epsilon \leq 6\%$) alveolar epithelial cells are not affected, while stretch between 12% and 21% ($\epsilon = 6\%$ to 10%) may trigger some cellular responses. Stretch of more than 21% can therefore be considered as injurious. In particular, for inflammatory responses Waters *et al.* recapitulate that mechanical strain can indeed cause reactions in lung cells, but an evaluation of necessary degrees of stretching was not possible at that point.

Several studies observed stretch induced or stretch amplified inflammatory responses in the range between 5% and 35% stretch with a risk for cytotoxic reactions at higher stretch intensities (Vlahakis *et al.*, 1999; Dos Santos *et al.*, 2004; Jafari *et al.*, 2004; Ning and Wang, 2007; Doryab *et al.*, 2020). As shown in chapter 6, 15% stretch

alone does not affect A549 cells significantly. Therefore, comparable experiments were performed with higher stretch amplitudes. Stretch was increased to the maximum possible extent (25% stretch) to stimulate a significantly stronger reaction compared to previously performed experiments with 15% stretch.

7.2 Results

7.2.1 Silica nanoparticles of 25 or 80 nm in diameter cause similar responses in A549 cells

Si80 alone caused minor changes in *CXCL8* (4-fold) and *CCL20* (9-fold) expression (Figure 19). There was no significant difference when compared to Si25 treated cells. When stretch was applied, Si80 induced *CXCL8* expression to the 15-fold and *CCL20* to the 48-fold, comparable to the treatment with Si25 + stretch.

Analyses of IL8 secretion after 5 hours of treatment resembled qPCR data (Figure 20), however, the extent of amplification by combining stretch + NP exposition was less pronounced for secretion. Stretch + NP (1,293 pg ml⁻¹ for Si25 + 15%; 1,257 pg ml⁻¹ for Si80 + 15%) exceeded secretion values of treatments with nanoparticles alone (987 pg ml⁻¹ for Si25; 993 pg ml⁻¹ for Si80), or stretch alone (681 pg ml⁻¹). Cellular responses were similar for Si25 and Si80.

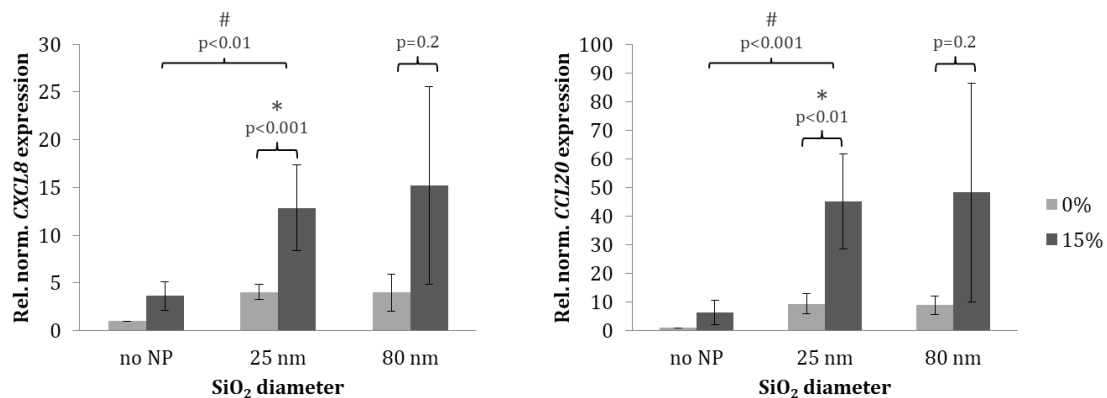


Figure 19: A549 cells were cultured on laminin-coated flexible membranes and treated with 15% stretch, Si25, or Si80 (100 $\mu\text{g ml}^{-1}$), or a combination for 2 hours. Cytokine expression was normalized to GAPDH expression and related to expression levels of untreated controls. ANOVA and Student's *t*-test determined significant ($\alpha = 0.05$) differences from respective stretch only (#) or nanoparticle only (*) controls. Data are given as mean \pm SD. $N = 7$ for no NP and Si25, $N = 3$ for Si80.

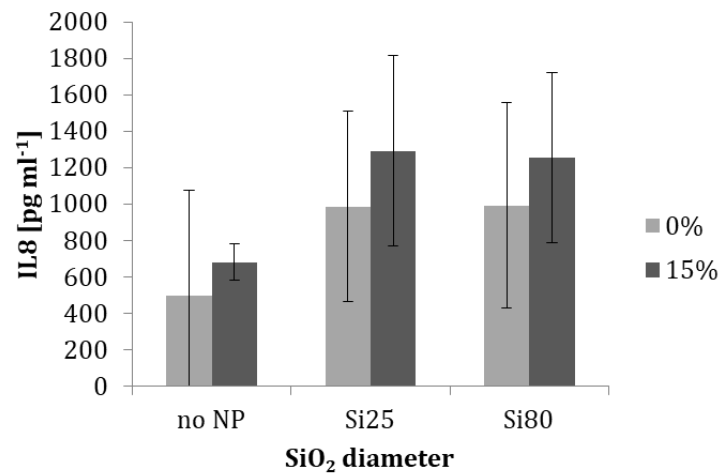


Figure 20: A549 cells were cultured on laminin-coated flexible membranes and treated with 15% stretch, Si25, or Si80 ($100 \mu\text{g ml}^{-1}$), or a combination. IL8 secretion was determined by ELISA after 5 hours of exposition. ANOVA determined no significant ($\alpha = 0.05$) differences between Si25 and Si80 groups. Data are given as mean \pm SD. $N = 3$.

7.2.2 Increasing stretching amplitude from 15% to 25% does not lead to stronger inflammatory response of A549 cells

A non-physiologically strong mechanical strain was applied to A549 cells for 2 hours. Limited by the stretching setup used for this work, 25% stretch (ΔS_A) was applied to the cells in the same frequency (0.25 Hz) and sinusoidal shape as for 15% stretch. Measurement as described in chapter 5.3 and supplementary Figure 33 revealed actual applied area expansion values of 17% (at 15%) and \approx 27% (at 25%). Cell morphology and confluency did not differ between treatments. Without nanoparticle treatment, there was no difference between cells stretched at 15% or 25% (*CXCL8*: 3.6-fold vs. 3.4-fold with $p = 0.3$; *CCL20*: 6.4-fold vs. 5.2-fold with $p = 0.5$) (Figure 21). Combining Si25 + 25% stretch did not raise cytokine expression compared to Si25 + 15% stretching (*CXCL8*: 12.9-fold vs. 12.1-fold with $p = 0.8$; *CCL20*: 45.1-fold vs. 39.7-fold with $p = 0.6$). Again, IL8 secretion data supported results from expression analysis. IL8 secretion was not significantly changed by increasing the stretching amplitude from 15% to 25%.

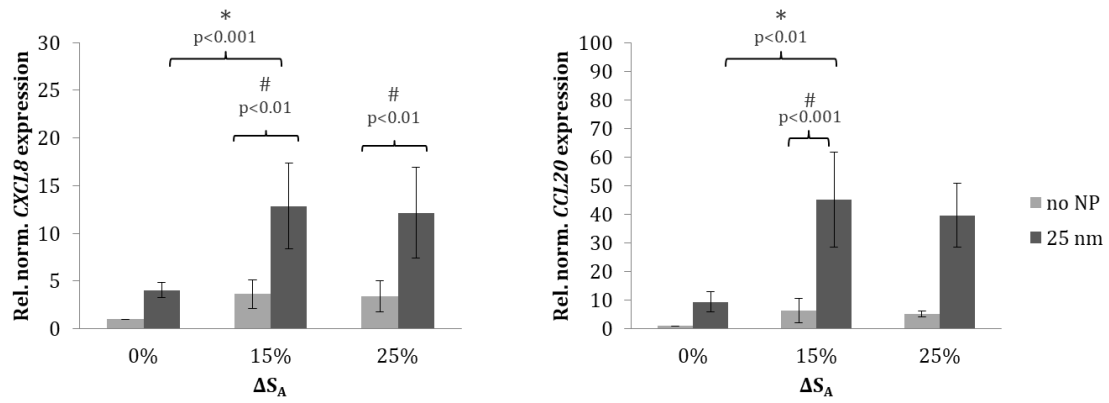


Figure 21: A549 cells were cultured on laminin-coated flexible membranes and treated with 15% or 25% stretch, Si25 ($100 \mu\text{g ml}^{-1}$), or a combination for 2 hours. Cytokine expression was normalized to GAPDH expression and related to expression levels of untreated controls. ANOVA and Student's *t*-test determined significant ($\alpha = 0.05$) differences from respective stretch only (#) or nanoparticle only (*) controls. Data are given as mean \pm SD. $N = 7$ for 0% and 15%, $N = 3$ for 25%.

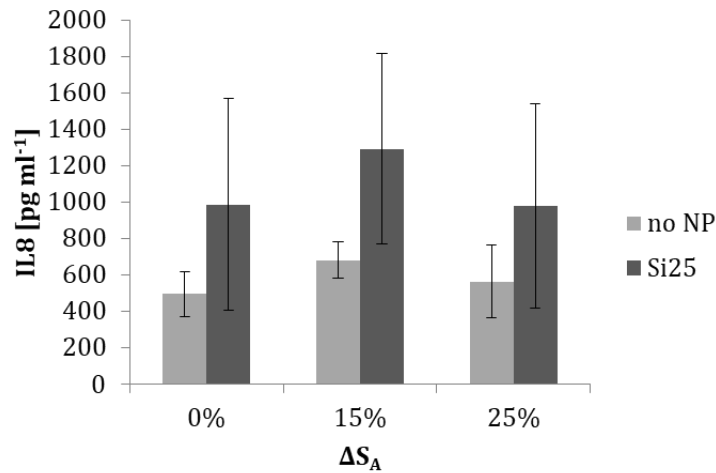


Figure 22: A549 cells were cultured on laminin-coated flexible membranes and treated with 15% or 25% stretch, Si25 ($100 \mu\text{g ml}^{-1}$), or both. IL8 was determined by ELISA after 5 hours of exposition. ANOVA determined no significant ($\alpha = 0.05$) differences between 15% and 25% stretching groups. Data are given as mean \pm SD. $N = 3$.

7.3 Discussion

7.3.1 Particle delivery

To evaluate whether the size of SiO₂ nanoparticles affects cellular response under static or dynamic conditions, A549 cells were treated with SiO₂ nanoparticles of different diameters (Si25 = 22.4 nm, Si80 = 91.5 nm) at similar SiO₂ mass concentrations (100 µg ml⁻¹), but consequently different particle concentrations (Si25 = 9.5 × 10¹² ml⁻¹, Si80 = 1.4 × 10¹¹ ml⁻¹).

Based on the computational model of particle sedimentation, diffusion, and target cell dosimetry for *in vitro* toxicity studies (ISDD) by Hinderliter *et al.* (2010), Peuschel *et al.* (2015) calculated delivered doses for similar nanoparticles as follows: the fraction of deposited particles was 26.5% for Si25 and 20.4% for Si85 particles after 5 h of exposition, assuming no agglomeration. Apart from their longer exposition time compared to this work, Peuschel *et al.* calculated with lower administered doses (Si25 = 1.2 µg ml⁻¹, Si85 = 50 µg ml⁻¹) and higher medium fill level (5 mm or 3 mm). Disregarding that in this in dynamic *in vitro* model cell culture medium is constantly moving and thereby certainly affecting particle sedimentation and diffusion, the approximation by Peuschel *et al.* will be used to estimate the delivered doses (Si25 = 7.9 × 10⁶ particles per cell, Si80 = 0.08 × 10⁶ particles per cell; Table 9). Based on BET (Brunauer–Emmett–Teller) gas adsorption measurements of the SiO₂ nanoparticles (Peuschel *et al.*, 2015), the delivered surface area was calculated. With 109 m² g⁻¹ specific surface area for Si25 and 11 m² g⁻¹ for Si80 it can be estimated that the finally delivered total particle surface area per cell are ≈ 9000 µm² for Si25 and 700 µm² for Si80 – knowing that the cell monolayer is confluent. Depending on the assumed packing density of the nanoparticles it can be estimated that for Si25, 3-4 layers of nanoparticles cover the confluent cell layer. For Si80 is estimated that the cell layer is only covered 60-70%.

*Table 9: Physicochemical properties of unlabeled (Si25) and fluorescently labeled (Si25-FD) nanoparticles. The hydrodynamic diameter D_z was calculated based on the intensity distribution of the particle scattering signals using DLS. Number of particles per cell seeded refers to $0.96 * 10^6$ cells that were seeded per well.*

SiO ₂ nanoparticles	Diameter ± SD (TEM) [nm]	Hydrodynamic diameter (D_z) [nm]	Zeta potential [mV]	Number of particles administered per cell seeded	Estimated number of particles delivered within 2 h per cell seeded	Estimated surface area delivered per cell seeded [μm^2 per cell]
Si25 (G)	22.4 ± 2	25 ± 6	-27	29.6 * 10 ⁶	7.9 * 10 ⁶	9000
Si80 (M)	91.5 ± 3	98 ± 19	-34	0.4 * 10 ⁶	0.08 * 10 ⁶	700

7.3.2 Interplay between stretch and nanoparticles may take place at the cell membrane

Hetland *et al.* (2001) studied the effect of silica particle size and surface area on cytokine release in A549 cells. Different sizes of quartz and fumed amorphous microsilica were administered. For quartz, they observed that the total administered surface area rather than particle size determined the cellular response. They also concluded that when comparing crystalline and non-crystalline silica at low concentrations, different cytokines are induced. Non-crystalline silica (0.3 μm) was more potent for IL6, similarly sized quartz (0.4 μm) was more potent for IL8. With increasing concentrations, crystallinity rather than particle size or surface area determined toxicity. However, more recent evidence suggested that independent of crystallinity, disorganized silanol groups on the surface of silica nanoparticles can affect membrane integrity (Pavan and Fubini, 2016; Pavan *et al.*, 2019). Focussing on colloidal amorphous silica nanoparticles, Rabolli *et al.* (2010) studied the 'Influence of size, surface area and microporosity on the *in vitro* cytotoxic activity of amorphous silica nanoparticles in different cell types'. They observed that vulnerability to physico-chemical nanoparticle properties can vary between cell types. Macrophages (murine, J774), for example, were sensitive to large surface areas and small micropore volumes. In contrast, for endothelial cells (human, EA.hy926) and fibroblasts (murine, 3T3), primarily surface roughness and small particle diameter affected viability. A study by Lag *et al.* (2018) investigated size-dependent cytokine release upon amorphous silica nanoparticle exposition in two bronchial epithelial cell lines (human, BEAS-2B; human, HBEC3-KT). They observed similar cytokine response patterns for both cell lines and both particle sizes (10 nm vs. 50 nm) involving p38 MAPK, TACE and the NF- κ B pathway. Independent of the administered surface

area, particles with smaller diameter were more potent in inducing cytokines than larger particles.

Based on this knowledge on silica toxicity it was hypothesized that A549 would respond less to $100 \mu\text{g Si80 ml}^{-1}$ than to the same mass of Si25 for multiple reasons: larger diameter, smaller total surface area, and fewer particles. As both particle types originate from comparable syntheses (protocol and starting material) their surface chemistry was expected to be similar and therefore probably not responsible for any varying effect on cellular response.

Surprisingly, data shown in Figure 19 and Figure 20 could not verify the hypothesis that Si25 and Si80 affect A549 in a size dependent manner. In the two scenarios that were compared here, cells were either fully covered with multiple layers (3-4) of Si25 in large numbers, or only partially covered (60-70%) with fewer Si80 nanoparticles. At a mass concentration of $100 \mu\text{g ml}^{-1}$, a size difference does not seem to play a role at first sight. For a conclusion about the contribution of particle number and total particle surface area, further experiments are necessary. Experiments with similar particle concentration or similar total surface area could help to elucidate, if in this setup particle size is a relevant factor. Preferably, administered doses should stepwise cover more and more of the cell surface up to multiple layers as already studied for Si25 here. This could provide insight whether the proportion of 'covered' cell surface is a decisive factor for the observed inflammatory response.

Adding 15% stretch to the Si80 treatment resulted in a similarly amplified response as previously shown for Si25 + stretch. Assuming that particle uptake is similar for Si25 and Si80 (Peuschel *et al.*, 2015), and that stretch does not affect uptake rate (Schmitz *et al.*, 2019), it can be hypothesized that the short-term synergistic interplay between stretch and nanoparticles takes place at the first contact site between cells and particles – the cell membrane. Potential interaction mechanisms between nanoparticles and the cell membrane will be discussed in chapter 9.

7.3.3 Cell type specific robustness to mechanical strain needs to be considered for *in vitro* models

The following studies reported stretch-induced or stretch-amplified cytokine release in A549 cells: Vlahakis *et al.* (1999) used a predecessor of the stretching setup used here to show that stretch alone can induce cytokine release in alveolar epithelial cells. Ex-

posing cells to 20% stretch did not cause a significant increase of IL8 release ($7.8 \pm 44\%$). Thirty percent stretch, however, did so ($49 \pm 34\%$). Both conditions did not affect proliferation or viability. They could also show that TNF-induced IL8 release can be amplified by 30% stretch if TNF exposition time was 48 h and dosing was $< 0.1 \text{ ng ml}^{-1}$. IL8 induction from higher doses of TNF was not affected by additional stimulation from stretch – supposedly because the maximum response was already triggered. They confirmed their results with analyses of gene expression where 30% stretch for 4 hours led to a 4-fold upregulation of *CXCL8*. As an indicator for the magnitude of the cellular response under static conditions Vlahakis *et al.* determined a maximum upregulation of *CXCL8* to the 16-fold by treatment with TNF at 10 ng ml^{-1} . It is notable that Vlahakis *et al.* applied cyclic sinusoidal stretch with higher frequencies (0.33 or 0.66 Hz) compared to this work (0.25 Hz). Dos Santos *et al.* (2004) published similar results that were obtained with a similar setup. Cytokine induction with TNF (10 ng ml^{-1}) could not be raised by 20% stretch (0.5 Hz). Another study by Jafari *et al.* (2004) observed IL8 release after 4 hours in A549 cells that were stretched cyclically (0.33 Hz) to 32%, but not in cells that were stretched with less than 21%. Synergistic effects on IL8 release and *CXCL8* expression by LPS (lipopolysaccharides) and mechanical strain was observed by Ning and Wang in 2007. They also observed amplitude (5%, 15%, 30% stretch) and frequency (0.2 Hz, 0.5 Hz, 1 Hz) dependent IL8 increase in A549 after 4 hours. Describing a new “stretchable” ALI lung *in vitro* model, Doryab *et al.* (2020) reported no change in proliferation or cell viability of A549 under 21% stretch, but a reduction of both under 35% stretch at 0.33 Hz. Furthermore, they confirmed Vlahakis’ observations on an intensified TNF induced IL8 release upon 35% stretch, but not upon 21% stretch. It is worth mentioning that Doryab *et al.* induced IL8 with 15 ng ml^{-1} of TNF.

Based on Waters’ estimation from 2012 and the above listed studies, it can be suspected that stretch above $\approx 21\%$ affects A549 cells only slightly, with serious effects appearing with increasing stretch. Here, 15% stretch, previously shown not to affect proliferation, membrane integrity, or gene expression, was compared to 25% stretch. Both amplitudes caused similarly moderate cytokine upregulation in A549 cells after short exposition time of 2 hours. Again, these results support Waters *et al.* (2012) saying that A549 cells are, compared to primary alveolar cells, robust against relatively

high degrees of mechanical strain and may result in an underestimation of the impact of mechanical strain. In combination with nanoparticle treatment, no difference between 15% and 25% area expansion could be observed either, although maximum response was not yet reached.

Assuming that these, from a technical point of view, minor changes in gene expression should be detectable, it can be summarized that increasing stretch from 15% to 25% did not lead to a further increase in cytokine expression, neither with nor without nanoparticles present. Within this range of stretching amplitude, the synergistic contribution of stretching is probably regulated like an on/off switch rather than an adjustable response.

A distinct feature of A549 cells is a mutation of the *K-ras* gene (Kirsten Rat Sarcoma Viral Proto-Oncogene), which leads to a permanently upregulated *CXCL8* expression and IL8 secretion (Valenzuela and Groffen, 1986; Sparmann and Bar-Sagi, 2004). Even though A549 cells may be less sensitive to mechanical strain compared to primary alveolar cells, it is conceivable that a higher baseline expression/secretion of *CXCL8* could lower their relative response amplitude as well as their response threshold towards stretch or nanoparticle stimuli. Comparable experiments with primary alveolar epithelial cells or a cell line without *K-ras* mutation could determine the contribution of A549 specific behavior to this study's outcome. Preliminary results (Supplementary Figure 41) from an experiment with human pulmonary alveolar epithelial cells (HPAEPiC) indicate that primary cells may overall respond less to stretch and nanoparticles. As this experiment was performed under 10% only, and as no viability or toxicity data are available yet, these results are to be interpreted with caution.

8 Part III: Experimental reproducibility with the dynamic lung *in vitro* model

8.1 Introduction

In vitro models for nanotoxicity research aim at high levels of reproducibility. The previously utilized dynamic *in vitro* lung model (Schmitz *et al.*, 2019) comprises two variable factors that may affect reproducibility of test results, besides proper functioning of the Flexcell stretching setup. i) An extensively studied immortalized cell line (A549) was chosen instead of using primary cells, which are less uniform in their behaviour. Cell behavior, though, can be influenced strongly by composition of the cell culture medium (van der Valk *et al.*, 2018). Supplementation with antibiotics was renounced, however, fetal bovine serum (FBS) was added (10%). ii) Toxicity of nanoparticles of the same type may vary between batches (e.g. due to change in bulk material) and way of administration (e.g. submerge vs. air-liquid (Panas *et al.*, 2014; Lovén *et al.*, 2021). Thorough characterization of all used batches is essential, considering that under lab scale the product of one synthesis may not suffice for a complete toxicity screening.

The employed submersed cell culture model lets nanoparticles interact with the cell culture medium first, before an interaction with the cells can take place. If present, proteins from the biological milieu that surround nanoparticles, e.g. blood or lymph fluid *in vivo*, or cell culture medium *in vitro*, can adsorb to their surface. This may not only affect particle properties like zeta-potential and thereby colloidal stability, but also conformation of the bound proteins. An altered nanoparticle-cell interaction is consequential. This concept has long been known as ‘protein-lipid corona’ on nanoparticles (Lundqvist and Cedervall, 2020). In an *in vitro* setup, FBS is the main source for proteins, such as growth factors, immunoglobulins, or serum albumin.

With regard to silica nanoparticles, Lesniak *et al.* (2012) could show that when administered under serum-free conditions, silica nanoparticles adhere more strongly to the cell membrane and are internalized more efficiently by cells compared to serum-containing conditions. Under serum-free conditions, they observed more cell membrane damage, and particle uptake did not seem to be limited to the vesicular endolysosomal pathway, but nanoparticles that were applied under serum-free conditions also grew protein coronas, however, in their composition they differed significantly from those coronas grown on nanoparticles in FBS-containing medium. They exhibited cytosolic and cytoskeleton or membrane related proteins in their corona rather than immunoglobulins, complement proteins, or apolipoproteins – probably

released upon cell damage. For the amorphous colloidal Si25 particles used in this work, Peuschel *et al.* (2015) reported no LDH leakage up to concentrations of $200 \mu\text{g ml}^{-1}$ for A549 cells grown in DMEM supplemented with 10% FBS. Under serum-free conditions, though, this concentration caused a cytotoxic LDH leakage.

Not only the presence or absence of FBS in *in vitro* models has been shown to affect experimental outcome. As FBS is an uncontrolled and inadequately characterized animal product that varies strongly depending on origin, season and processing, batch to batch variations can affect cell behavior in the *in vitro* model (Gstraunthaler *et al.*, 2013; Barosova *et al.*, 2021). Critical components can be endotoxins, or simply too many bovine proteins (e.g. γ -globulins or haemoglobin). Especially controversial is FBS supplementation in cancer or stem cell research as well as in *in vitro* toxicity testing. Research quality and animal protection are reasons to find alternatives to supplementing cell culture medium with FBS. First achievements have been made, however, FBS is still widely used (van der Valk *et al.*, 2018).

In this chapter, reproducibility of the previously observed results was tested when using another batch of FBS and another batch of Si25 nanoparticles.

8.2 Results

8.2.1 Nanoparticles and fetal bovine serum

During the experimentation period, a new FBS from a different provider as well as new synthesis batches of Si25 were introduced. Serum 'A' (FBS Gold from PAA Laboratories, Austria) was replaced with serum 'B' (FBS Gold from PAN-Biotech GmbH, Germany). Further reproducibility tests were performed with serum 'C' (FBS Standard from PAA Laboratories, Austria) (Table 2, page 25). According to manufacturers, albumin concentrations did not differ much while serum 'B' contained slightly more protein in total. Synthesis batch Si25 (G) was replaced with batch Si25 (N). All other experimental settings and analysis methods were performed as previously described (Chapter 5). Nanoparticles from different batches were considered comparable. Physicochemical characteristics can be found in Table 10 and were analysed as described in chapter 5.1.

Table 10: Physicochemical properties of unlabeled Si25 used in chapter 8. The hydrodynamic diameter D_z was calculated based on the intensity distribution of the particle scattering signals.

SiO ₂ nanoparticles	Diameter ± SD (TEM) [nm]	Hydrodynamic diameter (D _z) [nm]	Zeta potential [mV]	SiO ₂ Concentration of stock dispersion [g L ⁻¹]
Si25 (G)	22.4 ± 2	25 ± 6	-27	9.101
Si25 (L)	21.0 ± 2	21 ± 5	-24	5.841
Si25 (N)	29.0 ± 3	32 ± 4	-35	9.302

8.2.2 Culture conditions may alter particle-induced effects on cytokine expression

Under condition A (Serum A / Si25 (G)), treatment with stretch or Si25 caused minor *CXCL8* upregulation in A549 cells (3.6-fold vs. 4.1-fold with $p = 0.54$). Under condition B (Serum B / Si25 (N)), cells responded to stretch, but not to Si25 exposition (2.7-fold vs. 0.3-fold with $p < 0.001$ (§)). Under condition A, a combined treatment with stretch + Si25 (12.9-fold) exceeded effects of stretch alone (#, $p < 0.01$) and Si25 alone (*, $p < 0.01$). Under condition B, a combined treatment with stretch + Si25 (2.6-fold) did not exceed stretch alone ($p = 0.93$). A similar pattern was observed for the expression of *CCL20* (Figure 23). Apparently, the amplifying effect of combining stretch + Si25 that was observed under condition A could not be reproduced under condition B. Comparing the response to stretch alone for serum 'A' and 'B' revealed minor but insignificant differences (Figure 23). The most obvious differences were the missing re-

sponse to Si25 alone and stretch + Si25 under condition B.

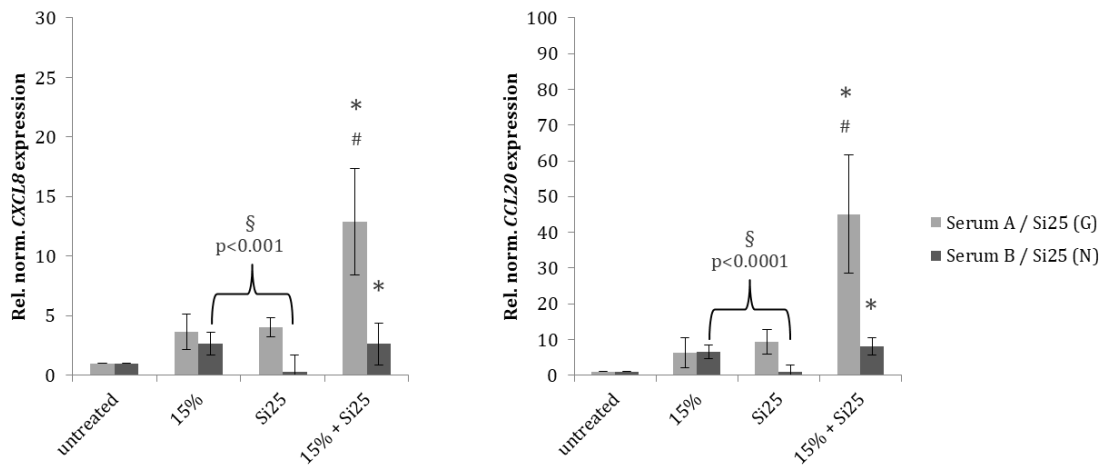


Figure 23: A549 cells were cultured on laminin-coated flexible membranes in medium supplemented with FBS from two different suppliers and treated with 15% stretch, Si25 ($100 \mu\text{g ml}^{-1}$), or both for 2 hours. Cytokine expression (CXCL8, CCL20) was normalized to GAPDH expression and related to expression levels of untreated controls. ANOVA and Student's *t*-test determined significant differences ($\alpha = 0.05$) between treatments (* combined treatment vs. Si25, # combined treatment vs. stretch, § stretch vs. Si25). Data are given as mean \pm SD. $N = 7$ for Serum A/Si25(G) and $N = 10$ for Serum B/Si25(N).

To evaluate baseline expression, untreated controls under serum 'B' were related to untreated controls under serum 'A' (Figure 24). A549 seemed to express slightly less CXCL8 under serum 'B' than under serum 'A'.

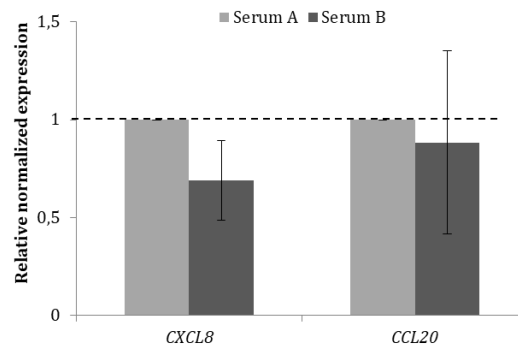


Figure 24: A549 cells were cultured on laminin-coated flexible membranes in medium supplemented with FBS from two different suppliers for 2 hours. Cytokine expression (CXCL8, CCL20) was normalized to GAPDH expression and related to expression levels of untreated controls under Serum A. $N = 3$.

It should be mentioned here that at this time of the experimentation period neither serum 'A' nor Si25 from batch 'G' were available any longer. Therefore, an independent exchange of the two factors was not possible.

To determine if the absent response to Si25 with serum 'B' was caused by the change in particle batch or FBS batch, the experiment was repeated with two different

Si25 batches ('L' vs. 'N'). Figure 25 shows that when cultured with serum 'B', neither Si25 from batch 'L' nor from batch 'N' caused an increase in *CXCL8* or *CCL20* expression compared to untreated controls. Adding stretch to Si25 (L) or Si25 (N) treated cells did not induce a significantly stronger response than observed for stretch alone. This indicated that a change in nanoparticle batches was not the reason for an altered experimental result. However, as the original serum is no longer available, solid evidence could not be produced.

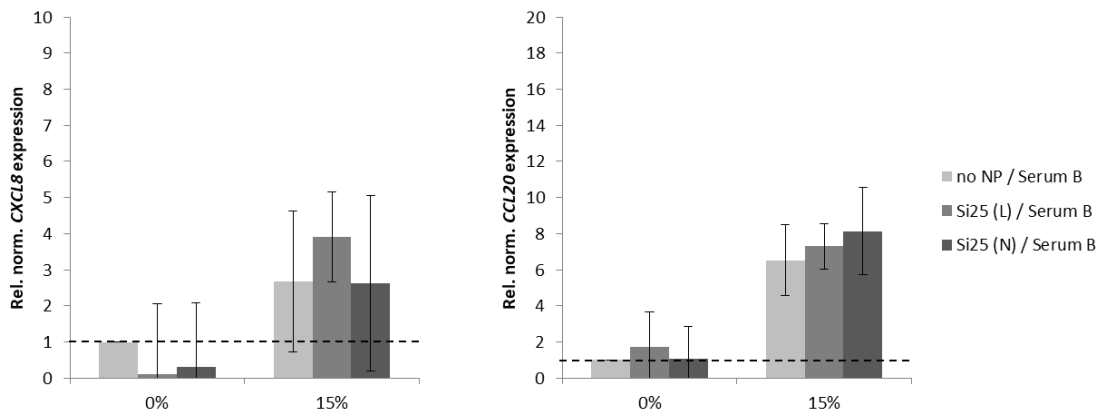


Figure 25: A549 cells were cultured on laminin-coated flexible membranes in medium supplemented with serum 'B' and exposed to Si25 of two different batches (Si25(L) or Si25(N), $100 \mu\text{g ml}^{-1}$) with (15%) or without stretch. Cytokine expression (*CXCL8*, *CCL20*) was normalized to GAPDH expression and related to expression levels of untreated controls. ANOVA did not reveal significant difference between Si25 batches. Data are given as mean \pm SD. $N = 10$ for no NP/Serum B, $N = 3$ for Si25(L)/Serum B and $N = 7$ for Si25(N)/Serum B.

IL8 secretion corresponded with *CXCL8* expression in both experimental setups, when related to the respective baseline IL8 secretion (Supplementary Figure 37). Similar to the comparison of baseline expression (Figure 24), baseline IL8 secretion differed between both conditions: Under serum 'B', untreated cells only secreted half the amount of IL8 within 24 hours compared to untreated cells under serum 'A' (369 vs. 746 pg ml^{-1}) (Figure 26). This difference became even more pronounced when cells were treated with TNF for 24 hours (Figure 27).

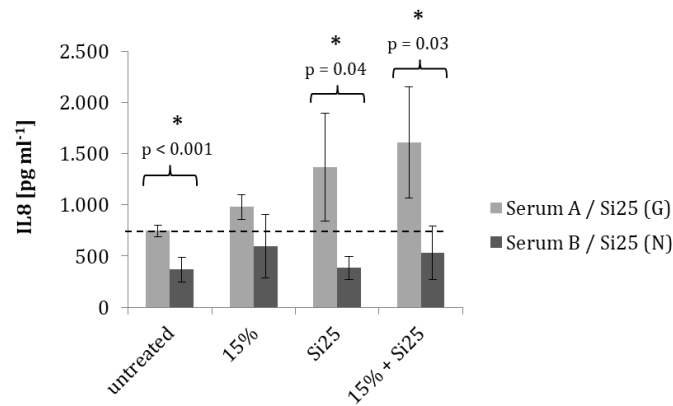


Figure 26: A549 cells were cultured on laminin-coated flexible membranes and treated with 15% stretch, Si25 of different batches ($100 \mu\text{g ml}^{-1}$), or both. Two different experimental setups are compared here: cells cultured in medium supplemented with serum 'A' and exposed to Si25(G) and cells cultured in medium supplemented with serum 'B' and exposed to Si25(N). Cytokine secretion (IL8) was determined by ELISA after 24 hours of exposition. ANOVA and Student's *t*-test with $\alpha = 0.05$ determined significant differences (*) between experiments from different setups. $N = 3$.

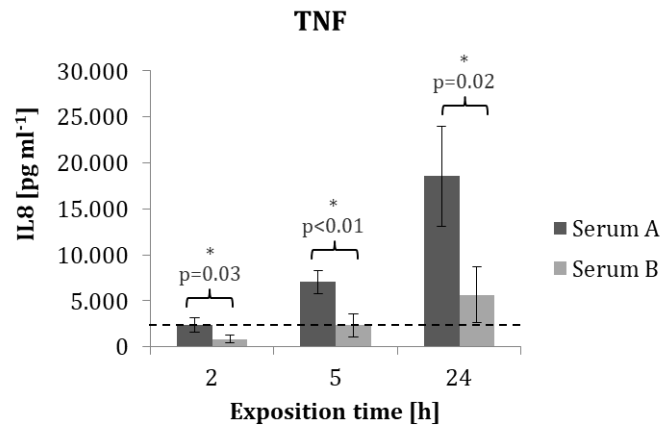


Figure 27: Cells were treated with TNF (2 ng ml^{-1}) in DMEM with different FBS batches. Baseline IL8 secretion at $t = 2 \text{ h}$ was $273 \pm 76 \text{ pg ml}^{-1}$ with serum 'A' and $141 \pm 97 \text{ pg ml}^{-1}$ with serum 'B'. IL8 secretion was determined by ELISA. Data represent mean values \pm SD from three independent experiments. Student's *t*-test determined significant differences (*, $\alpha = 0.05$) between respective samples from different setups.

Light microscopy did not reveal a difference in cell morphology between both FBS supplements (Supplementary Figure 38).

8.2.3 Impact of FBS change on NF- κ B translocation

As described in chapters 6.2.11 and 6.3.2, NF- κ B signaling may play a role in the inflammatory response caused by Si25 exposition under mechanical strain. In chapter 6, NF- κ B translocation experiments were performed with fetal bovine serum 'C'^d. According to the gene expression analysis (chapter 6.2.5), *RELA* (coding for subunit NF- κ B p65) was not upregulated, although the general response pattern was similar to that caused by TNF, which is known to activate NF- κ B p65 signaling. Microscopy did not show NF- κ B p65 translocation either. These results could be reproduced when culturing cells with serum 'B' (Figure 28). Similar to the experiments in chapter 6, an increased expression or translocation of subunit NF- κ B1 p105/p50 (*NFKB1*) could neither be confirmed nor ruled out with this method. A slight difference between 15% stretch or Si25 alone compared to 15% + Si25 may be visible in Figure 29. However, slight nuclear presence of this subunit is always visible. Subunit NF- κ B2 p100/p52, whose corresponding gene *NFKB2* was upregulated to the 3-fold (Chapter 6.2.6) just as in the previous experiments, did not translocate to the nucleus when cells were cultured with serum 'B' (Figure 30).

In summary, qualitative analysis by confocal microscopy did not show involvement of NF- κ B signaling upon treatment with Si25, stretch, or both when A549 were cultured with different fetal bovine serum batches.

^d Serum C was considered comparable to serum 'A' as it was provided by the same manufacturer in the same year. Serum A was no longer available for these experiments. Respective cytokine expression data can be found in supplementary Figure 40.

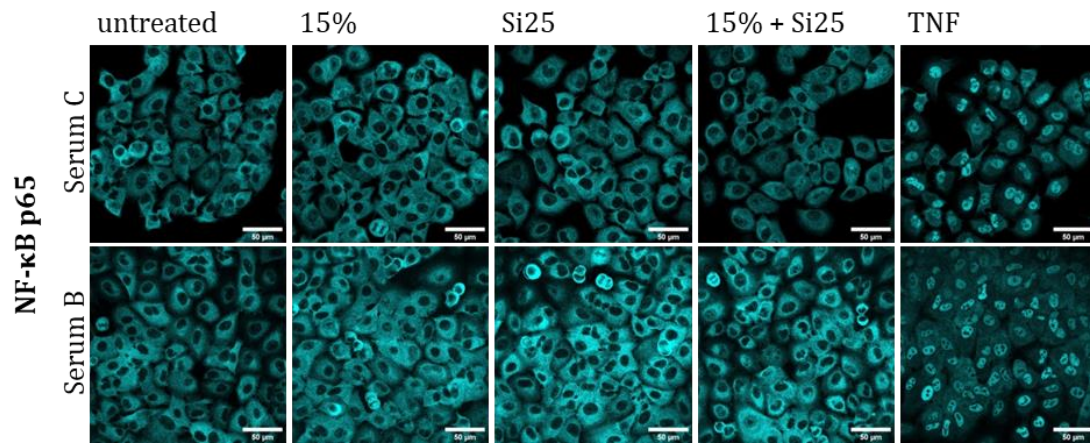


Figure 28: Confocal fluorescence microscopy of A549 cells that were cultured with different batches of FBS on laminin-coated flexible membranes and treated with 15% stretch, Si25, or both for 2 hours (positive controls: human recombinant TNF (20 ng ml^{-1})). Cells were fixed and immune-stained for NF- κ B p65. Images represent one experiment for serum 'C' and three independent experiments for serum 'B'. Brightness and contrast were enhanced for graphical presentation. Scale bar is $50 \mu\text{m}$.

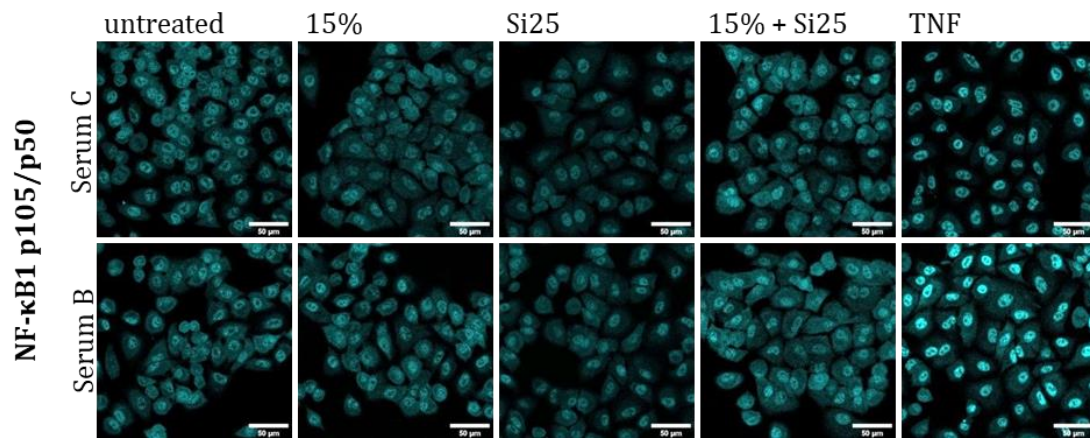


Figure 29: Confocal fluorescence microscopy of A549 cells that were cultured with different batches of FBS on laminin-coated flexible membranes and treated with 15% stretch, Si25, or both for 2 hours (positive controls: human recombinant TNF (20 ng ml^{-1})). Cells were fixed and immune-stained for NF- κ B1 p105/p50. Images represent one experiment for serum 'C' and two independent experiments for serum 'B'. Brightness and contrast were enhanced for graphical presentation. Scale bar is $50 \mu\text{m}$.

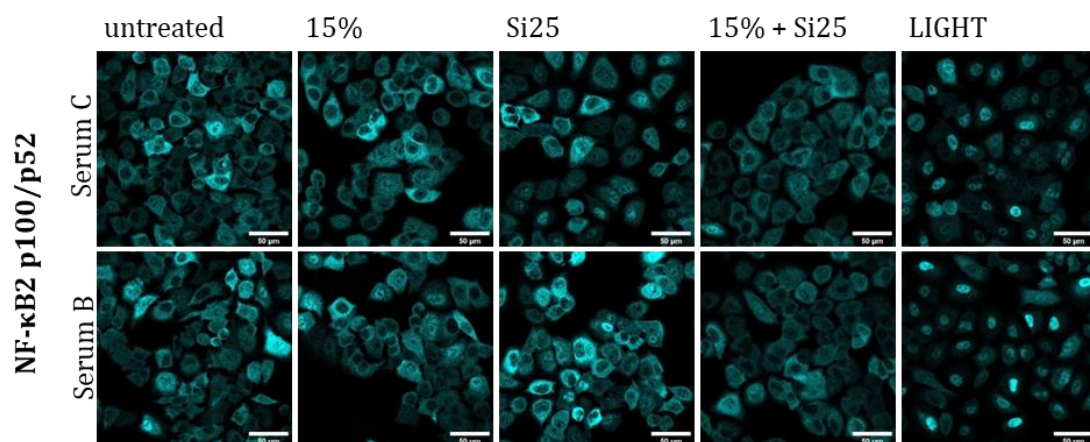


Figure 30: Confocal fluorescence microscopy of A549 cells that were cultured with different batches of FBS on laminin-coated flexible membranes and treated with 15% stretch, Si25, or both for 2 hours (positive controls: human recombinant LIGHT (TNFSF14), 100 ng ml^{-1}). Cells were fixed and immune-stained for NF- κ B2 p100/p52. Images represent two independent experiments for serum 'C' and three for serum 'B'. Brightness and contrast were enhanced for graphical presentation. Scale bar is $50 \mu\text{m}$.

8.3 Discussion

Reproduction of the previously described cytokine expression analysis (Chapter 6) with another fetal bovine serum batch indicated that FBS as a supplement to cell culture medium affects the outcome of *in vitro* experiments with regard to inflammatory responses. The response to stretch alone was similar under both serum conditions while the response to nanoparticles differed (Figure 23): With serum 'A', A549 cells responded slightly to Si25 exposition by overexpressing *CXCL8* and *CCL20*. With serum 'B', no response to Si25 was observed. Accordingly, with serum 'B' the response to Si25 + stretch did not exceed the response to stretch alone. A contribution by a change in Si25 batches is unlikely as demonstrated in chapter 8.2.1 (Table 10, Figure 25).

When related to untreated controls, the IL8 secretion analysis (Supplementary Figure 37) corresponded well with the respective expression analysis (Figure 23) for both FBS batches. Absolute values, however, revealed that when kept with serum 'A', A549 cells produced higher levels of baseline IL8 compared to serum 'B' (Figure 26). Under both conditions, a treatment with TNF (2 ng ml⁻¹) resulted in a ≈7 fold increase in IL8 secretion within 24 hours, but still, cells under serum 'B' produced less IL8 than those under serum 'A' (Figure 27). Compared to the response to TNF, the response to Si25 + stretch was rather small in both scenarios. Similar observations were made by Veranth *et al.* (2008) who reported that IL6 secretion of untreated and soil dust treated BEAS-2B cells was not only increasing with increasing FBS concentration, but also depended on the composition of the cell culture medium.

The following paragraphs will discuss potential differences of the applied FBS batches that may have contributed to the different experimental outcome. Based on manufacturer information from analysis certificates, endotoxin content was acceptably low in all three sera (Table 2). According to Kirikae *et al.* (1997) who analysed endotoxin content of 40 different FBS batches, median endotoxin levels were ≈46 pg ml⁻¹. One fifth of the tested FBS batches contained more than 1 ng ml⁻¹ endotoxin. After the dilution of FBS in cell culture medium, endotoxin concentrations in this work ranged between 10 - 40 pg ml⁻¹. Referring to Standiford *et al.* (1990) who reported that IL8 could not be induced by LPS at concentrations up to 10 µg ml⁻¹ in A549 cells, it seems unlikely that the here present minor endotoxin concentrations caused the observed varying baseline IL8 secretion.

Interestingly, serum 'B' contained significantly more immunoglobulin G (IgG, $411 \mu\text{g ml}^{-1}$) than serum 'A' or 'C' ($88 \mu\text{g ml}^{-1}$, $63 \mu\text{g ml}^{-1}$). IgG molecules that rapidly adsorb to silica particles tend to be replaced in large parts by complex bovine serum proteins, if present, within minutes (Frost *et al.*, 2017). After 2 hours of incubation, immunoglobulins make up for only $\approx 5\text{-}10\%$ of the protein corona on amorphous silica nanoparticles (Tenzer *et al.*, 2013). However, Frost *et al.* (2017) also demonstrated that when exposed to IgG alone, dispersed silica nanoparticles aggregate. Here, a supplementation with 10% FBS provided sufficient complex proteins to compete with IgG for adsorption on the silica surface. However, the $\approx 5\text{-fold}$ IgG concentration in serum 'B' compared to serum 'A' may have led to more nanoparticle aggregation thereby reducing the amount of dispersed particles that interacted with the cells. This may explain why under serum 'B', A549 cells hardly responded to Si25 exposition.

Further should be mentioned that fetal bovine serum is an undefined product that contains many more molecules than those analysed for quality control. It is not unlikely that an unknown component affected the experimental outcome as well. For instance, Niederstaetter *et al.* (2021) recently identified eicosanoids, a group of signaling molecules, to vary strongly between FBS batches. This is particularly interesting as these molecules have complex inflammatory functions (Calder, 2020). Hydroxyeicosatetraenoic acids, for example, have been shown to inhibit mucin production and NF- κ B translocation in human mucoepidermoid pulmonary carcinoma cells (Song *et al.*, 2015), but also to activate TNF and IL8 secretion *via* the canonical NF κ B signaling pathway in THP-1 human monocytic cells (Liu *et al.*, 2020). As their impact on alveolar epithelial cells is still unclear, it remains unanswered whether varying eicosanoid concentrations in FBS have affected these experiments.

The FBS batch 'Serum A' may have been involved in undeclared blending with bovine serum albumin (BSA) (Gstraunthaler *et al.*, 2014). BSA can act protectively when involved in nanoparticle-cell interactions (Gualtieri *et al.*, 2012; Peuschel *et al.*, 2015). Compared with serum 'B' (presumed to not contain additional amounts of BSA), cells in serum 'A' may have been protected from nanoparticles by BSA. Against these expectations, cells responded to Si25 under serum 'A' but not under serum 'B'. Accordingly, under serum 'B' no amplified effect by adding stretch to nanoparticle exposition was observed (Figure 23). It is known that already small amounts of BSA alone can

protect cells from silica induced damage as much as 10% FBS supplementation does (Peuschel *et al.*, 2015). Considering that this work was performed with 10% FBS supplementation, it seems unlikely that additional BSA could have increased “protection” from particle induced damage. Further, compared to fetal bovine serum, BSA (usually gained from adult animals) contains more IgG. As discussed above, in presence of sufficient other complex serum proteins IgG may play a role for nanoparticle aggregation.

In conclusion, moderate fluctuations in serum albumin content from blending with BSA could be ruled out as an interfering factor as albumin accounts for roughly three quarters of the total protein content in FBS anyhow. Similarly, endotoxins which are part of regular FBS quality analysis were present in concentration ranges that are unlikely to affect A549 cells. Immunoglobulins (i.p. IgG) may affect nanoparticle aggregation and thereby reduce the amount of dispersed nanoparticles that are finally delivered to the cells. Other active molecules (e.g. eicosanoids) that are not part of regular FBS quality analysis may vary strongly between batches and cannot be ruled out as interfering factors in these experiments.

Expression and secretion experiments with heat inactivated FBS were not performed as cell attachment and morphology were affected in initial experiments (Supplementary Figure 39). Additional investigations on the exact FBS composition, its overall impact on gene expression, as well as a detailed characterization of the nanoparticle-protein coronas are necessary to draw further conclusions. This test for experimental reproducibility again demonstrates that FBS and its varying composition of active molecules is a source for inconsistent study results *in vitro*.

9 Conclusion and Outlook

In this work, mechanical strain was found to intensify silica nanoparticle-induced gene expression in A549 cells without increasing intracellular uptake of nanoparticles. This indicates that under *in vitro* conditions that mimic mechanical stimulation, nanoparticles might induce more pronounced effects than observed under conventional static *in vitro* conditions. Presumably, integration of mechanical strain into predictive nanotoxicity *in vitro* models can improve *in vitro-in vivo* correlation compared to static submerged model systems.

Furthermore, this work defined limitations of the utilized dynamic *in vitro* model: with A549 cells modelling alveolar epithelial cells, this setup was not able to mimic pathologically heavy extents of mechanical strain as would occur under mechanical ventilation or certain respiratory diseases. A549 were robust to 25% area expansion, which was the maximum technically achievable stretch, and supposedly harmful for other cell types. With respect to pharmaceutical nanoparticle applications in the diseased respiratory system, the robustness of model cell types to mechanical strain should be considered.

Regarding the colloidal amorphous silica nanoparticles (Si25 or Si80), no direct size-dependent effects on A549 cells could be shown when administered at the same mass concentration.

Interestingly, a supplier change for FBS led to the insight that batch-to-batch variations may affect nanoparticles, cells and their interaction. It remains unresolved whether the observed stretch-independent nanoparticle accumulation described in chapter 6.2.10 was also influenced by batch-to-batch variations, as these experiments were performed with serum 'B', unlike the associated gene expression experiments in chapter 6.2.5 that were performed with serum 'A'.

In summary, this work has shown that the interaction of nanoparticles and cells can be influenced by mechanical stimulation. Further research is needed to identify the exact 'site of interplay' between nanoparticles and mechanical stimulation.

Some studies already focused on the interaction between nanoparticles and several cell membrane components: in a murine type II alveolar epithelial cell line (C10) Orr *et al.* (2009) found that 500 nm silica nanoparticles are coupled to actin filaments

upon interaction with the transmembrane heparan sulfate proteoglycan syndecan-1. The authors also suggested that silica nanoparticles trigger their own uptake *via* macropinocytosis, which is a possible internalization route for silica in A549 cells (Nowak *et al.*, 2014), by clustering these transmembrane proteins. Tsugita *et al.* (2017) and Nishijima *et al.* (2017) identified scavenger receptors to bind and recognize amorphous and crystalline silica and to mediate internalization, IL1 β secretion and inflammasome activation in macrophages. For airway epithelium Sanchez *et al.* (2017) observed an inhibition of the cation channel Transient Receptor Potential Vanilloid 4 (TRPV4) by amorphous silica nanoparticles, leading to an impaired ciliary function.

Knowing that clathrin-dependent endocytosis and macropinocytosis are important uptake mechanisms for amorphous nano silica in lung epithelial cells (Hsiao *et al.*, 2014; Nowak *et al.*, 2014; Kümper, 2017) and that the cytoskeleton, particularly actin filaments, play an important role in these mechanisms (Robertson *et al.*, 2009) makes the following findings even more interesting: in pulmonary epithelial cells, stretch induced gene expression is related to rearrangements of cytoskeletal actin filaments (Geiger *et al.*, 2006). The stability of microtubules (Geiger *et al.*, 2009) as well as tight junction distribution (Cavanaugh *et al.*, 2001; Jacob and Gaver, 2012; Doryab *et al.*, 2020) may also be affected by mechanical strain. Even though it was shown that for amorphous silica nanoparticles, caveolin-dependent endocytosis plays a secondary role in A549 cells (Hsiao *et al.*, 2014), it should be mentioned that formation of caveolae and related signalling can also be altered by mechanical strain (Gervasio *et al.*, 2011; Nassoy and Lamaze, 2012). However, Diem *et al.* (2020) stated that *in vivo*, where alveolar type II cells account for less than 10% of the epithelial surface, it is known that the cytoskeleton is involved in signaling, membrane interactions (Mattila *et al.*, 2016), internalization (Orr *et al.*, 2007) and intracellular endosome transport (Matteoni and Kreis, 1987).

For the dynamic lung *in vitro model* presented here, however, the point of intersection between nanoparticle-induced and stretch-induced cellular response remains to be identified. Bionanomechanic approaches (Septiadi *et al.*, 2018) combined with super resolution microscopy (Hansel *et al.*, 2020) may help to study the interactions of i) nanoparticles with the cell membrane, ii) nanoparticles with the cytoskeleton and extracellular matrix, iii) stretching with cell adhesion and the cytoskeleton. The interac-

tion of fluorescent silica nanoparticles with integrins, focal adhesions, or cytoskeletal fibers before and after mechanical stimulation could, for instance, be visualized.

10 References

- Abdel-Halim, M., Darwish, S.S., ElHady, A.K., Hoppstädter, J., Abadi, A.H., Hartmann, R.W., Kiemer, A.K. & Engel, M., 2016. Pharmacological inhibition of protein kinase C (PKC) ζ downregulates the expression of cytokines involved in the pathogenesis of chronic obstructive pulmonary disease (COPD). *European Journal of Pharmaceutical Sciences*, 93, 405-409.
- Bachofen, H., Schurch, S., Urbinelli, M. & Weibel, E., 1987. Relations among alveolar surface tension, surface area, volume, and recoil pressure. *Journal of Applied Physiology*, 62, 1878-1887.
- Barosova, H., Meldrum, K., Karakocak, B.B., Balog, S., Doak, S.H., Petri-Fink, A., Clift, M.J.D. & Rothen-Rutishauser, B., 2021. Inter-laboratory variability of A549 epithelial cells grown under submerged and air-liquid interface conditions. *Toxicology in Vitro*, 75, 105178.
- Brochard, L., Slutsky, A. & Pesenti, A., 2017. Mechanical ventilation to minimize progression of lung injury in acute respiratory failure. *American journal of respiratory and critical care medicine*, 195, 438-442.
- Calder, Philip C., 2020. Eicosanoids. *Essays in Biochemistry*, 64, 423-441.
- Cavanaugh, K.J., Jr., Oswari, J. & Margulies, S.S., 2001. Role of stretch on tight junction structure in alveolar epithelial cells. *American journal of respiratory cell and molecular biology*, 25, 584-591.
- Chapman, K.E., Sinclair, S.E., Zhuang, D., Hassid, A., Desai, L.P. & Waters, C.M., 2005. Cyclic mechanical strain increases reactive oxygen species production in pulmonary epithelial cells. *Am J Physiol Lung Cell Mol Physiol*, 289, L834-41.
- Clippinger, A.J., Allen, D., Jarabek, A.M., Corvaro, M., Gaca, M., Gehen, S., Hotchkiss, J.A., Patlewicz, G., Melbourne, J., Hinderliter, P., Yoon, M., Huh, D., Lowit, A., Buckley, B., Bartels, M., Berube, K., Wilson, D.M., Indans, I. & Vinken, M., 2018. Alternative approaches for acute inhalation toxicity testing to address global regulatory and non-regulatory data requirements: An international workshop report. *Toxicology In Vitro*, 48, 53-70.
- Costa, A., de Souza Carvalho-Wodarz, C., Seabra, V., Sarmiento, B. & Lehr, C.M., 2019. Triple co-culture of human alveolar epithelium, endothelium and macrophages for studying the interaction of nanocarriers with the air-blood barrier. *Acta Biomaterialia*, 91, 235-247.
- Crapo, J.D., Barry, B.E., Gehr, P., Bachofen, M. & Weibel, E.R., 1982. Cell number and cell characteristics of the normal human lung. *American Review of Respiratory Disease*, 126, 332-337.
- Crapo, J.D., Young, S.L., Fram, E.K., Pinkerton, K.E., Barry, B.E. & Crapo, R.O., 1983. Morphometric characteristics of cells in the alveolar region of mammalian lungs. *American Review of Respiratory Disease*, 128, 42-46.
- da Silva, A.B., Minitier, M., Thom, W., Hewitt, R.E., Wills, J., Jugdaohsingh, R. & Powell, J.J., 2020. Gastrointestinal Absorption and Toxicity of Nanoparticles and Microparticles: Myth, Reality and Pitfalls explored through Titanium Dioxide. *Current opinion in toxicology*, 19, 112-120.
- Del Favero, G. & Kraegeloh, A., 2020. Integrating Biophysics in Toxicology. *Cells*, 9, 1282.
- Diem, K., Fauler, M., Fois, G., Hellmann, A., Winokur, N., Schumacher, S., Kranz, C. & Frick, M., 2020. Mechanical stretch activates piezo1 in caveolae of alveolar type I cells to trigger ATP release and paracrine stimulation of surfactant secretion from alveolar type II cells. *The FASEB Journal*, 34, 12785-12804.
- Doak, S.H. & Dusinska, M., 2017. NanoGenotoxicology: present and the future. *Mutagenesis*, 32, 1-4.
- Donahue, N.D., Acar, H. & Wilhelm, S., 2019. Concepts of nanoparticle cellular uptake, intracellular trafficking, and kinetics in nanomedicine. *Advanced drug delivery reviews*, 143, 68-96.
- Donaldson, K., Murphy, F.A., Duffin, R. & Poland, C.A., 2010. Asbestos, carbon nanotubes and the pleural mesothelium: a review of the hypothesis regarding the role of long fibre retention in the parietal pleura, inflammation and mesothelioma. *Particle and fibre toxicology*, 7, 5.

- Donaldson, K., Stone, V., Tran, C.L., Kreyling, W. & Borm, P.J., 2004. Nanotoxicology. *Occupational and Environmental Medicine*, 61, 727-728.
- Doryab, A., Taskin, M.B., Stahlhut, P., Schröppel, A., Wagner, D.E., Groll, J. & Schmid, O., 2020. A Biomimetic, Copolymeric Membrane for Cell-Stretch Experiments with Pulmonary Epithelial Cells at the Air-Liquid Interface. *Advanced Functional Materials*, 31, 2004707.
- Dos Santos, C.C., Han, B., Andrade, C.F., Bai, X., Uhlig, S., Hubmayr, R., Tsang, M., Lodyga, M., Keshavjee, S., Slutsky, A.S. & Liu, M., 2004. DNA microarray analysis of gene expression in alveolar epithelial cells in response to TNF α , LPS, and cyclic stretch. *Physiological genomics*, 19, 331-342.
- Edwards, Y.S., 2001. Stretch stimulation: its effects on alveolar type II cell function in the lung. *Comparative Biochemistry and Physiology, Part A: Molecular & Integrative Physiology*, 129, 245-260.
- EFSA Panel on Food Additives and Nutrient Sources added to Food (ANS), 2018. Re-evaluation of silicon dioxide (E 551) as a food additive. *EFSA J*, 16, e05088.
- European Commission, 2011. Commission recommendation of 18 October 2011 on the definition of nanomaterial (2011/696/EU). *Official Journal of the European Union*. 38-40.
- European Food Safety Authority, 2021. *Titanium dioxide: E171 no longer considered safe when used as a food additive* [online]. <https://www.efsa.europa.eu/en/news/titanium-dioxide-e171-no-longer-considered-safe-when-used-food-additive>, [November 15, 2021].
- European Union, 2012. Types and uses of nanomaterials, including safety aspects. Accompanying the Communication from the Commission to the European Parliament, the Council and the European Economic and Social Committee on the Second Regulatory Review on Nanomaterials. EU Brussels.
- Freese, C., Anspach, L., Deller, R., Richards, S.-J., Gibson, M., Kirkpatrick, C. & Unger, R., 2017. Gold nanoparticle interactions with endothelial cells cultured under physiological conditions. *Biomaterials science*, 5, 707-717.
- Freese, C., Schreiner, D., Anspach, L., Bantz, C., Maskos, M., Unger, R.E. & Kirkpatrick, C.J., 2014. In vitro investigation of silica nanoparticle uptake into human endothelial cells under physiological cyclic stretch. *Particle and fibre toxicology*, 11, 68.
- Frost, R., Langhammer, C. & Cedervall, T., 2017. Real-time in situ analysis of biocorona formation and evolution on silica nanoparticles in defined and complex biological environments. *Nanoscale*, 9, 3620-3628.
- Frujtier-Polloth, C., 2012. The toxicological mode of action and the safety of synthetic amorphous silica-a nanostructured material. *Toxicology*, 294, 61-79.
- Gebel, T., Foth, H., Damm, G., Freyberger, A., Kramer, P.J., Lilienblum, W., Rohl, C., Schupp, T., Weiss, C., Wollin, K.M. & Hengstler, J.G., 2014. Manufactured nanomaterials: categorization and approaches to hazard assessment. *Archives of Toxicology*, 88, 2191-2211.
- Gehr, P., Bachofen, M. & Weibel, E.R., 1978. The normal human lung: ultrastructure and morphometric estimation of diffusion capacity. *Respiration Physiology*, 32, 121-140.
- Geiger, R.C., Kaufman, C.D., Lam, A.P., Budinger, G.R. & Dean, D.A., 2009. Tubulin acetylation and histone deacetylase 6 activity in the lung under cyclic load. *American journal of respiratory cell and molecular biology*, 40, 76-82.
- Geiger, R.C., Taylor, W., Glucksberg, M.R. & Dean, D.A., 2006. Cyclic stretch-induced reorganization of the cytoskeleton and its role in enhanced gene transfer. *Gene Therapy*, 13, 725-731.
- Geiser, M. & Kreyling, W.G., 2010. Deposition and biokinetics of inhaled nanoparticles. *Particle and fibre toxicology*, 7, 2.
- Gervasio, O.L., Phillips, W.D., Cole, L. & Allen, D.G., 2011. Caveolae respond to cell stretch and contribute to stretch-induced signaling. *Journal of cell science*, 124, 3581-3590.

- Gil, J., Bachofen, H., Gehr, P. & Weibel, E.R., 1979. Alveolar volume-surface area relation in air- and saline-filled lungs fixed by vascular perfusion. *Journal of Applied Physiology*, 47, 990-1001.
- Gilmore, T.D., 2006. Introduction to NF-kappaB: players, pathways, perspectives. *Oncogene*, 25, 6680-6684.
- Global Burden of Disease (GBD) 2015 Risk Factors Collaborators, 2016. Global, regional, and national comparative risk assessment of 79 behavioural, environmental and occupational, and metabolic risks or clusters of risks, 1990–2015: a systematic analysis for the Global Burden of Disease Study 2015. *The Lancet*, 388, 1659-1724.
- Gstraunthaler, G., Lindl, T. & van der Valk, J., 2013. A plea to reduce or replace fetal bovine serum in cell culture media. *Cytotechnology*, 65, 791-793.
- Gstraunthaler, G., Lindl, T. & van der Valk, J., 2014. A severe case of fraudulent blending of fetal bovine serum strengthens the case for serum-free cell and tissue culture applications. *Alternatives to Laboratory Animals*, 42, 207-209.
- Gualtieri, M., Skuland, T., Iversen, T.G., Lag, M., Schwarze, P., Bilanicova, D., Pojana, G. & Refsnes, M., 2012. Importance of agglomeration state and exposure conditions for uptake and pro-inflammatory responses to amorphous silica nanoparticles in bronchial epithelial cells. *Nanotoxicology*, 6, 700-712.
- Guo, Y.H., Martinez-Williams, C., Yellowley, C.E., Donahue, H.J. & Rannels, D.E., 2001. Connexin expression by alveolar epithelial cells is regulated by extracellular matrix. *American Journal of Physiology-Lung Cellular and Molecular Physiology*, 280, L191-L202.
- Hansel, C.S., Holme, M.N., Gopal, S. & Stevens, M.M., 2020. Advances in high-resolution microscopy for the study of intracellular interactions with biomaterials. *Biomaterials*, 226, 119406.
- Hartlen, K.D., Athanasopoulos, A.P. & Kitaev, V., 2008. Facile preparation of highly monodisperse small silica spheres (15 to >200 nm) suitable for colloidal templating and formation of ordered arrays. *Langmuir*, 24, 1714-1720.
- Hendricks, P., Diaz, F.J., Schmitt, S., Sitta Sittampalam, G. & Nirmalanandhan, V.S., 2012. Effects of respiratory mechanical forces on the pharmacological response of lung cancer cells to chemotherapeutic agents. *Fundamental & clinical pharmacology*, 26, 632-643.
- Hetland, R.B., Schwarze, P.E., Johansen, B.V., Myran, T., Uthus, N. & Refsnes, M., 2001. Silica-induced cytokine release from A549 cells: importance of surface area versus size. *Human and Experimental Toxicology*, 20, 46-55.
- Heyder, J. & Svartengren, M.U., 2002. Basic principles of particle behavior in the human respiratory tract. *Drug delivery to the lung New York: Marcel Dekker*, 21-45.
- Hinderliter, P.M., Minard, K.R., Orr, G., Chrisler, W.B., Thrall, B.D., Pounds, J.G. & Teeguarden, J.G., 2010. ISDD: A computational model of particle sedimentation, diffusion and target cell dosimetry for in vitro toxicity studies. *Particle and fibre toxicology*, 7, 36.
- Hoppstädter, J., Diesel, B., Zarbock, R., Breinig, T., Monz, D., Koch, M., Meyerhans, A., Gortner, L., Lehr, C.M., Huwer, H. & Kiemer, A.K., 2010. Differential cell reaction upon Toll-like receptor 4 and 9 activation in human alveolar and lung interstitial macrophages. *Respiratory Research*, 11, 124.
- Hsiao, I.-L., Gramatke, A.M., Joksimovic, R., Sokolowski, M., Gradzielski, M. & Haase, A., 2014. Size and cell type dependent uptake of silica nanoparticles. *Journal of Nanomedicine & Nanotechnology*, 5, 1.
- Hu, J. & Liu, Y., 2015. Cyclic Strain Enhances Cellular Uptake of Nanoparticles. *Journal of Nanomaterials*, 2015, 1-8.
- Huh, D., Matthews, B.D., Mammoto, A., Montoya-Zavala, M., Hsin, H.Y. & Ingber, D.E., 2010. Reconstituting organ-level lung functions on a chip. *Science*, 328, 1662-1668.
- Irizarry, R.A., Hobbs, B., Collin, F., Beazer-Barclay, Y.D., Antonellis, K.J., Scherf, U. & Speed, T.P., 2003. Exploration, normalization, and summaries of high density oligonucleotide array probe level data. *Biostatistics*, 4, 249-264.

- Jacob, A.M. & Gaver, D.P., 3rd, 2012. Atelectrauma disrupts pulmonary epithelial barrier integrity and alters the distribution of tight junction proteins ZO-1 and claudin 4. *Journal of applied physiology*, 113, 1377-1387.
- Jafari, B., Ouyang, B., Li, L.F., Hales, C.A. & Quinn, D.A., 2004. Intracellular glutathione in stretch-induced cytokine release from alveolar type-2 like cells. *Respirology*, 9, 43-53.
- Janković, N.Z. & Plata, D.L., 2019. Engineered nanomaterials in the context of global element cycles. *Environmental Science: Nano*, 6, 2697-2711.
- Kagan, V.E., Bayir, H. & Shvedova, A.A., 2005. Nanomedicine and nanotoxicology: two sides of the same coin. *Nanomedicine*, 1, 313-316.
- Karin, M. & Greten, F.R., 2005. NF-kappaB: linking inflammation and immunity to cancer development and progression. *Nature Reviews Immunology*, 5, 749-759.
- Karlsruher Institut für Technologie, 2021a. *DaNa – Informationen zur Sicherheit von neuen, innovativen Materialien und Nanomaterialien* [online]. <https://nanopartikel.info/en/knowledge/materials/>, [April 25, 2021].
- Karlsruher Institut für Technologie, 2021b. *Nanomaterialien in Lebensmitteln* [online]. <https://nanopartikel.info/basics/querschnittsthemen/nanomaterialien-in-lebensmitteln/>, [September 10, 2021].
- Kasper, J., Hermanns, M.I., Bantz, C., Maskos, M., Stauber, R., Pohl, C., Unger, R.E. & Kirkpatrick, J.C., 2011. Inflammatory and cytotoxic responses of an alveolar-capillary coculture model to silica nanoparticles: comparison with conventional monocultures. *Particle and fibre toxicology*, 8, 6.
- Kasper, J.Y., Feiden, L., Hermanns, M.I., Bantz, C., Maskos, M., Unger, R.E. & Kirkpatrick, C.J., 2015. Pulmonary surfactant augments cytotoxicity of silica nanoparticles: Studies on an in vitro air-blood barrier model. *Beilstein journal of nanotechnology*, 6, 517-528.
- Kasper, J.Y., Hermanns, M.I., Unger, R.E. & Kirkpatrick, C.J., 2017. A responsive human triple-culture model of the air-blood barrier: incorporation of different macrophage phenotypes. *J Tissue Eng Regen Med*, 11, 1285-1297.
- Kirikae, T., Tamura, H., Hashizume, M., Kirikae, F., Uemura, Y., Tanaka, S., Yokochi, T. & Nakano, M., 1997. Endotoxin contamination in fetal bovine serum and its influence on tumor necrosis factor production by macrophage-like cells J774.1 cultured in the presence of the serum. *International Journal of Immunopharmacology*, 19, 255-262.
- Knudsen, L., Lopez-Rodriguez, E., Berndt, L., Steffen, L., Ruppert, C., Bates, J.H.T., Ochs, M. & Smith, B.J., 2018. Alveolar Micromechanics in Bleomycin-induced Lung Injury. *American journal of respiratory cell and molecular biology*, 59, 757-769.
- Knudsen, L. & Ochs, M., 2018. The micromechanics of lung alveoli: structure and function of surfactant and tissue components. *Histochemistry and cell biology*, 150, 661-676.
- Kreyling, W.G., Semmler-Behnke, M. & Chaudhry, Q., 2010. A complementary definition of nanomaterial. *Nano today*, 5, 165-168.
- Krug, A.K., Kolde, R., Gaspar, J.A., Rempel, E., Balmer, N.V., Meganathan, K., Vojnits, K., Baquie, M., Waldmann, T., Ensenat-Waser, R., Jagtap, S., Evans, R.M., Julien, S., Peterson, H., Zagoura, D., Kadereit, S., Gerhard, D., Sotiriadou, I., Heke, M., Natarajan, K., Henry, M., Winkler, J., Marchan, R., Stoppini, L., Bosgra, S., Westerhout, J., Verwei, M., Vilo, J., Kortenkamp, A., Hescheler, J., Hothorn, L., Bremer, S., van Thriel, C., Krause, K.H., Hengstler, J.G., Rahnenfuhrer, J., Leist, M. & Sachinidis, A., 2013. Human embryonic stem cell-derived test systems for developmental neurotoxicity: a transcriptomics approach. *Archives of Toxicology*, 87, 123-43.
- Kucki, M., Cavelius, C. & Kraegeloh, A., 2014. Interference of silica nanoparticles with the traditional Limulus amoebocyte lysate gel clot assay. *Innate Immunity*, 20, 327-336.
- Kümper, A., 2017. Einfluss von kolloidalen Silikananopartikeln auf die EGFR-abhängige Signaltransduktion. Universitäts- und Landesbibliothek der Heinrich-Heine-Universität Düsseldorf.

- Lacroix, G., Koch, W., Ritter, D., Gutleb, A.C., Larsen, S.T., Loret, T., Zanetti, F., Constant, S., Chortarea, S., Rothen-Rutishauser, B., Hiemstra, P.S., Frejafon, E., Hubert, P., Gribaldo, L., Kearns, P., Aublant, J.M., Diabate, S., Weiss, C., de Groot, A. & Kooter, I., 2018. Air-Liquid Interface In Vitro Models for Respiratory Toxicology Research: Consensus Workshop and Recommendations. *Applied in vitro toxicology*, 4, 91-106.
- Lag, M., Skuland, T., Godymchuk, A., Nguyen, T.H.T., Pham, H.L.T. & Refsnes, M., 2018. Silica Nanoparticle-induced Cytokine Responses in BEAS-2B and HBEC3-KT Cells: Significance of Particle Size and Signalling Pathways in Different Lung Cell Cultures. *Basic & clinical pharmacology & toxicology*, 122, 620-632.
- Lang, H., 2020. Anatomie und der Atmung. In H. Lang (ed.) *Beatmung für Einsteiger*. Berlin, Heidelberg: Springer Berlin Heidelberg, 3-17.
- Lee, S., Yun, H.-S. & Kim, S.-H., 2011. The comparative effects of mesoporous silica nanoparticles and colloidal silica on inflammation and apoptosis. *Biomaterials*, 32, 9434-9443.
- Lesniak, A., Fenaroli, F., Monopoli, M.P., Aberg, C., Dawson, K.A. & Salvati, A., 2012. Effects of the presence or absence of a protein corona on silica nanoparticle uptake and impact on cells. *ACS nano*, 6, 5845-5857.
- Lieber, M., Smith, B., Szakal, A., Nelson-Rees, W. & G., T., 1976. A Continuous Tumor-Cell Line From a Human Lung Carcinoma With Properties of Type II Alveolar Epithelial Cells. *International Journal of Cancer*, 17, 62-70.
- Liu, G.-Y., Moon, S.H., Jenkins, C.M., Sims, H.F., Guan, S. & Gross, R.W., 2020. A functional role for eicosanoid-lysophospholipids in activating monocyte signaling. *Journal of Biological Chemistry*, 295, 12167-12180.
- Liu, M., Skinner, S.J., Xu, J., Han, R.N., Tanswell, A.K. & Post, M., 1992. Stimulation of fetal rat lung cell proliferation in vitro by mechanical stretch. *Am J Physiol*, 263, L376-83.
- Lovén, K., Dobric, J., Bölükbas, D.A., Kåredal, M., Tas, S., Rissler, J., Wagner, D.E. & Isaxon, C., 2021. Toxicological effects of zinc oxide nanoparticle exposure: an in vitro comparison between dry aerosol air-liquid interface and submerged exposure systems. *Nanotoxicology*, 15, 494-510.
- Lu, F., Wu, S.H., Hung, Y. & Mou, C.Y., 2009. Size effect on cell uptake in well-suspended, uniform mesoporous silica nanoparticles. *Small*, 5, 1408-1413.
- Lundqvist, M. & Cedervall, T., 2020. Three Decades of Research about the Corona Around Nanoparticles: Lessons Learned and Where to Go Now. *Small*, 16, e2000892.
- Matteoni, R. & Kreis, T.E., 1987. Translocation and clustering of endosomes and lysosomes depends on microtubules. *The Journal of Cell Biology*, 105, 1253-1265.
- Mattila, P.K., Batista, F.D. & Treanor, B., 2016. Dynamics of the actin cytoskeleton mediates receptor cross talk: An emerging concept in tuning receptor signaling. *The Journal of Cell Biology*, 212, 267-280.
- Miller, M.R. & Poland, C.A., 2020. Nanotoxicology: The Need for a Human Touch? *Small*, 16, e2001516.
- Mohammadinejad, R., Moosavi, M.A., Tavakol, S., Vardar, D.O., Hosseini, A., Rahmati, M., Dini, L., Hussain, S., Mandegary, A. & Klionsky, D.J., 2019. Necrotic, apoptotic and autophagic cell fates triggered by nanoparticles. *Autophagy*, 15, 4-33.
- Muehlfeld, C., Rothen-Rutishauser, B., Blank, F., Vanhecke, D., Ochs, M. & Gehr, P., 2008. Interactions of nanoparticles with pulmonary structures and cellular responses. *American Journal of Physiology: Lung Cellular and Molecular Physiology*, 294, L817-29.
- Murugadoss, S., Lison, D., Godderis, L., Van Den Brule, S., Mast, J., Brassinne, F., Sebaihi, N. & Hoet, P.H., 2017. Toxicology of silica nanoparticles: an update. *Archives of Toxicology*, 91, 2967-3010.
- Napierska, D., Thomassen, L.C., Lison, D., Martens, J.A. & Hoet, P.H., 2010. The nanosilica hazard: another variable entity. *Particle and fibre toxicology*, 7, 39.

- Napierska, D., Thomassen, L.C., Vanaudenaerde, B., Luyts, K., Lison, D., Martens, J.A., Nemery, B. & Hoet, P.H., 2012. Cytokine production by co-cultures exposed to monodisperse amorphous silica nanoparticles: the role of size and surface area. *Toxicology Letters*, 211, 98-104.
- Nassoy, P. & Lamaze, C., 2012. Stressing caveolae new role in cell mechanics. *Trends in Cell Biology*, 22, 381-389.
- Nel, A.E., Madler, L., Velegol, D., Xia, T., Hoek, E.M., Somasundaran, P., Klaessig, F., Castranova, V. & Thompson, M., 2009. Understanding biophysicochemical interactions at the nano-bio interface. *Nature materials*, 8, 543-557.
- Nho, R., 2020. Pathological effects of nano-sized particles on the respiratory system. *Nanomedicine*, 29, 102242.
- Niederstaetter, L., Neuditschko, B., Brunmair, J., Janker, L., Bileck, A., Del Favero, G. & Gerner, C., 2021. Eicosanoid Content in Fetal Calf Serum Accounts for Reproducibility Challenges in Cell Culture. *Biomolecules*, 11.
- Ning, Q.M. & Wang, X.R., 2007. Response of alveolar type II epithelial cells to mechanical stretch and lipopolysaccharide. *Respiration*, 74, 579-585.
- Nishijima, N., Hirai, T., Misato, K., Aoyama, M., Kuroda, E., Ishii, K.J., Higashisaka, K., Yoshioka, Y. & Tsutsumi, Y., 2017. Human Scavenger Receptor A1-Mediated Inflammatory Response to Silica Particle Exposure Is Size Specific. *Frontiers in Immunology*, 8, 379.
- Nohynek, G.J., Lademann, J., Ribaud, C. & Roberts, M.S., 2007. Grey goo on the skin? Nanotechnology, cosmetic and sunscreen safety. *Critical Reviews in Toxicology*, 37, 251-277.
- Nowak, J.S., Mehn, D., Nativo, P., Garcia, C.P., Gioria, S., Ojea-Jimenez, I., Gilliland, D. & Rossi, F., 2014. Silica nanoparticle uptake induces survival mechanism in A549 cells by the activation of autophagy but not apoptosis. *Toxicology Letters*, 224, 84-92.
- Oberdörster, G., Oberdörster, E. & Oberdörster, J., 2005. Nanotoxicology: an emerging discipline evolving from studies of ultrafine particles. *Environmental Health Perspectives*, 113, 823-839.
- Oberdörster, G., Stone, V. & Donaldson, K., 2009. Toxicology of nanoparticles: A historical perspective. *Nanotoxicology*, 1, 2-25.
- Orr, G., Panther, D.J., Cassens, K.J., Phillips, J.L., Tarasevich, B.J. & Pounds, J.G., 2009. Syndecan-1 mediates the coupling of positively charged submicrometer amorphous silica particles with actin filaments across the alveolar epithelial cell membrane. *Toxicology and Applied Pharmacology*, 236, 210-220.
- Orr, G., Panther, D.J., Phillips, J.L., Tarasevich, B.J., Dohnalkova, A., Hu, D., Teeguarden, J.G. & Pounds, J.G., 2007. Submicrometer and nanoscale inorganic particles exploit the actin machinery to be propelled along microvilli-like structures into alveolar cells. *ACS nano*, 1, 463-475.
- Osman, N.M., Sexton, D.W. & Saleem, I.Y., 2020. Toxicological assessment of nanoparticle interactions with the pulmonary system. *Nanotoxicology*, 14, 21-58.
- Ovrevik, J., Lag, M., Holme, J.A., Schwarze, P.E. & Refsnes, M., 2009. Cytokine and chemokine expression patterns in lung epithelial cells exposed to components characteristic of particulate air pollution. *Toxicology*, 259, 46-53.
- Panas, A., Comouth, A., Saathoff, H., Leisner, T., Al-Rawi, M., Simon, M., Seemann, G., Dossel, O., Mulhopt, S., Paur, H.R., Fritsch-Decker, S., Weiss, C. & Diabate, S., 2014. Silica nanoparticles are less toxic to human lung cells when deposited at the air-liquid interface compared to conventional submerged exposure. *Beilstein journal of nanotechnology*, 5, 1590-1602.
- Pavan, C., Delle Piane, M., Gullo, M., Filippi, F., Fubini, B., Hoet, P., Horwell, C.J., Huaux, F., Lison, D., Lo Giudice, C., Martra, G., Montfort, E., Schins, R., Sulpizi, M., Wegner, K., Wyart-Remy, M., Ziemann, C. & Turci, F., 2019. The puzzling issue of silica toxicity: are silanols bridging the gaps between surface states and pathogenicity? *Particle and fibre toxicology*, 16, 32.
- Pavan, C. & Fubini, B., 2016. Unveiling the variability of "quartz hazard" in light of recent toxicological findings. *Chemical research in toxicology*, 30, 469-485.

- Perez-Gil, J. & Weaver, T.E., 2010. Pulmonary surfactant pathophysiology: current models and open questions. *Physiology (Bethesda, Md)*, 25, 132-141.
- Peuschel, H., Ruckelshausen, T., Cavalius, C. & Kraegeloh, A., 2015. Quantification of Internalized Silica Nanoparticles via STED Microscopy. *BioMed research international*, 2015, 961208.
- Pfaffl, M.W., 2001. A new mathematical model for relative quantification in real-time RT-PCR. *Nucleic Acids Research*, 29, e45.
- Pfaffl, M.W. & Riedmaier, I., 2011. Die Real-Time-RT-PCR-Datenanalyse im Fokus der MIQE-Richtlinie. *BIOspektrum*, 17, 295-297.
- Praphawatvet, T., Peters, J.I. & Williams, R.O., 3rd, 2020. Inhaled nanoparticles-An updated review. *International Journal of Pharmaceutics*, 587, 119671.
- Rabolli, V., Thomassen, L.C., Princen, C., Napierska, D., Gonzalez, L., Kirsch-Volders, M., Hoet, P.H., Huaux, F., Kirschhock, C.E., Martens, J.A. & Lison, D., 2010. Influence of size, surface area and microporosity on the in vitro cytotoxic activity of amorphous silica nanoparticles in different cell types. *Nanotoxicology*, 4, 307-318.
- Raghu, G., Striker, L.J., Hudson, L.D. & Striker, G.E., 1985. Extracellular matrix in normal and fibrotic human lungs. *American Review of Respiratory Disease*, 131, 281-289.
- Reifarth, M., Hoepfener, S. & Schubert, U.S., 2018. Uptake and Intracellular Fate of Engineered Nanoparticles in Mammalian Cells: Capabilities and Limitations of Transmission Electron Microscopy-Polymer-Based Nanoparticles. *Advanced Materials*, 30.
- Riediker, M., Zink, D., Kreyling, W., Oberdörster, G., Elder, A., Graham, U., Lynch, I., Duschl, A., Ichihara, G., Ichihara, S., Kobayashi, T., Hisanaga, N., Umezawa, M., Cheng, T.J., Handy, R., Gulumian, M., Tinkle, S. & Cassee, F., 2019. Particle toxicology and health - where are we? *Particle and fibre toxicology*, 16, 19.
- Roan, E. & Waters, C.M., 2011. What do we know about mechanical strain in lung alveoli? *American Journal of Physiology: Lung Cellular and Molecular Physiology*, 301, L625-L635.
- Robertson, A.S., Smythe, E. & Ayscough, K.R., 2009. Functions of actin in endocytosis. *Cellular and Molecular Life Sciences*, 66, 2049-2065.
- Rothen-Rutishauser, B.M., Kiama, S.G. & Gehr, P., 2005. A three-dimensional cellular model of the human respiratory tract to study the interaction with particles. *American journal of respiratory cell and molecular biology*, 32, 281-289.
- Rouse, J.G., Haslauer, C.M., Lobo, E.G. & Monteiro-Riviere, N.A., 2008. Cyclic tensile strain increases interactions between human epidermal keratinocytes and quantum dot nanoparticles. *Toxicology in Vitro*, 22, 491-497.
- Ruppel, G.L., 2012. What is the clinical value of lung volumes? *Respiratory Care*, 57, 26-38.
- Rysa, J., Tokola, H. & Ruskoaho, H., 2018. Mechanical stretch induced transcriptomic profiles in cardiac myocytes. *Scientific Reports*, 8, 4733.
- Sachverständigenrat für Umweltfragen, 2011. Vorsorgestrategien für Nanomaterialien. *Sondergutachten des SRU*.
- Sanchez, A., Alvarez, J.L., Demydenko, K., Jung, C., Alpizar, Y.A., Alvarez-Collazo, J., Cokic, S.M., Valverde, M.A., Hoet, P.H. & Talavera, K., 2017. Silica nanoparticles inhibit the cation channel TRPV4 in airway epithelial cells. *Particle and fibre toxicology*, 14, 43.
- Savla, U. & Waters, C.M., 1998. Mechanical strain inhibits repair of airway epithelium in vitro. *Am J Physiol*, 274, L883-92.
- Schmid, O., Möller, W., Semmler-Behnke, M., A. Ferron, G., Karg, E., Lipka, J., Schulz, H., Kreyling, W.G. & Stoeger, T., 2009. Dosimetry and toxicology of inhaled ultrafine particles. *Biomarkers*, 14, 67-73.

- Schmitz, C., Welck, J., Tavernaro, I., Grinberg, M., Rahnenfuhrer, J., Kiemer, A.K., van Thriel, C., Hengstler, J.G. & Kraegeloh, A., 2019. Mechanical strain mimicking breathing amplifies alterations in gene expression induced by SiO₂ NPs in lung epithelial cells. *Nanotoxicology*, 13, 1227-1243.
- Schübbe, S., Schumann, C., Cavelius, C., Koch, M., Müller, T. & Kraegeloh, A., 2012. Size-dependent localization and quantitative evaluation of the intracellular migration of silica nanoparticles in Caco-2 cells. *Chemistry of Materials*, 24, 914-923.
- Schumann, C., Schubbe, S., Cavelius, C. & Kraegeloh, A., 2012. A correlative approach at characterizing nanoparticle mobility and interactions after cellular uptake. *Journal of Biophotonics*, 5, 117-127.
- Schürch, D., Vanhecke, D., Clift, M.J., Raemy, D., de Aberasturi, D.J., Parak, W.J., Gehr, P., Petri-Fink, A. & Rothen-Rutishauser, B., 2014. Modeling nanoparticle–alveolar epithelial cell interactions under breathing conditions using captive bubble surfactometry. *Langmuir*, 30, 4924-4932.
- Schutysse, E., Struyf, S. & Van Damme, J., 2003. The CC chemokine CCL20 and its receptor CCR6. *Cytokine & Growth Factor Reviews* 14, 409-426.
- Septiadi, D., Crippa, F., Moore, T.L., Rothen-Rutishauser, B. & Petri-Fink, A., 2018. Nanoparticle-Cell Interaction: A Cell Mechanics Perspective. *Advanced Materials*, 30, e1704463.
- Sharma, N. & Jha, S., 2020. Amorphous nanosilica induced toxicity, inflammation and innate immune responses: A critical review. *Toxicology*, 441, 152519.
- Shintani, Y., Maeda, M., Chaika, N., Johnson, K.R. & Wheelock, M.J., 2008. Collagen I promotes epithelial-to-mesenchymal transition in lung cancer cells via transforming growth factor-beta signaling. *American journal of respiratory cell and molecular biology*, 38, 95-104.
- Singh, N., Nelson, B.C., Scanlan, L.D., Coskun, E., Jaruga, P. & Doak, S.H., 2017. Exposure to Engineered Nanomaterials: Impact on DNA Repair Pathways. *International journal of molecular sciences*, 18, 1515.
- Skuland, T., Øvrevik, J., Låg, M., Schwarze, P. & Refsnes, M., 2014. Silica nanoparticles induce cytokine responses in lung epithelial cells through activation of a p38/TACE/TGF- α /EGFR-pathway and NF- κ B signalling. *Toxicology and applied pharmacology*, 279, 76-86.
- Slutsky, A.S., 1999. Lung injury caused by mechanical ventilation. *Chest*, 116, 9S-15S.
- Slutsky, A.S. & Ranieri, V.M., 2013. Ventilator-induced lung injury. *The New England Journal of Medicine*, 369, 2126-2136.
- Smyth, G.K., 2005. Limma: linear models for microarray data. *Bioinformatics and computational biology solutions using R and Bioconductor*. Springer, 397-420.
- Sohal, I.S., O'Fallon, K.S., Gaines, P., Demokritou, P. & Bello, D., 2018. Ingested engineered nanomaterials: state of science in nanotoxicity testing and future research needs. *Particle and fibre toxicology*, 15, 29.
- Song, Y.-S., Kim, M.S., Lee, D.H., Oh, D.-K. & Yoon, D.-Y., 2015. 15-Hydroxyeicosatetraenoic acid inhibits phorbol-12-myristate-13-acetate-induced MUC5AC expression in NCI-H292 respiratory epithelial cells. *Journal of Microbiology and Biotechnology*, 25, 589-597.
- Sparmann, A. & Bar-Sagi, D., 2004. Ras-induced interleukin-8 expression plays a critical role in tumor growth and angiogenesis. *Cancer Cell*, 6, 447-458.
- Standiford, T.J., Kunkel, S.L., Basha, M.A., Chensue, S.W., Lynch, J.P., 3rd, Toews, G.B., Westwick, J. & Strieter, R.M., 1990. Interleukin-8 gene expression by a pulmonary epithelial cell line. A model for cytokine networks in the lung. *The Journal of clinical investigation*, 86, 1945-1953.
- Stern, S.T. & McNeil, S.E., 2008. Nanotechnology safety concerns revisited. *Toxicological Sciences*, 101, 4-21.
- Strambeanu, N., Demetrovici, L. & Dragos, D., 2015a. Anthropogenic Sources of Nanoparticles. In M. Lungu, A. Neculae, M. Bunoiu & C. Biris (eds.) *Nanoparticles' Promises and Risks*. Cham: Springer International Publishing, 21-54.

- Strambeanu, N., Demetrovici, L. & Dragos, D., 2015b. Natural Sources of Nanoparticles. *Nanoparticles' Promises and Risks*. Springer, 9-19.
- Stucki, J.D., Hobi, N., Galimov, A., Stucki, A.O., Schneider-Daum, N., Lehr, C.M., Huwer, H., Frick, M., Funke-Chambour, M., Geiser, T. & Guenat, O.T., 2018. Medium throughput breathing human primary cell alveolus-on-chip model. *Sci Rep*, 8, 14359.
- Tavernaro, I., Cavalius, C., Peuschel, H. & Kraegeloh, A., 2017. Bright fluorescent silica-nanoparticle probes for high-resolution STED and confocal microscopy. *Beilstein J Nanotechnol*, 8, 1283-1296.
- Tenzer, S., Docter, D., Kuharev, J., Musyanovych, A., Fetz, V., Hecht, R., Schlenk, F., Fischer, D., Kiouptsi, K., Reinhardt, C., Landfester, K., Schild, H., Maskos, M., Knauer, S.K. & Stauber, R.H., 2013. Rapid formation of plasma protein corona critically affects nanoparticle pathophysiology. *Nature nanotechnology*, 8, 772-781.
- Tschumperlin, D.J. & Margulies, S.S., 1999. Alveolar epithelial surface area-volume relationship in isolated rat lungs. *Journal of applied physiology*, 86, 2026-2033.
- Tsugita, M., Morimoto, N., Tashiro, M., Kinoshita, K. & Nakayama, M., 2017. SR-B1 Is a Silica Receptor that Mediates Canonical Inflammasome Activation. *Cell Reports*, 18, 1298-1311.
- Valenzuela, D.M. & Groffen, J., 1986. Four human carcinoma cell lines with novel mutations in position 12 of c-K-ras oncogene. *Nucleic Acids Research*, 14, 843-852.
- Vallet-Regi, M. & Balas, F., 2008. Silica materials for medical applications. *The open biomedical engineering journal*, 2, 1-9.
- van der Valk, J., Bieback, K., Buta, C., Cochrane, B., Dirks, W.G., Fu, J., Hickman, J.J., Hohensee, C., Kolar, R., Liebsch, M., Pistollato, F., Schulz, M., Thieme, D., Weber, T., Wiest, J., Winkler, S. & Gstraunthaler, G., 2018. Fetal Bovine Serum (FBS): Past - Present - Future. *Alternatives to Animal Experimentation*, 35, 99-118.
- van Kesteren, P.C., Cubadda, F., Bouwmeester, H., van Eijkeren, J.C., Dekkers, S., de Jong, W.H. & Oomen, A.G., 2015. Novel insights into the risk assessment of the nanomaterial synthetic amorphous silica, additive E551, in food. *Nanotoxicology*, 9, 442-452.
- Veranth, J.M., Cutler, N.S., Kaser, E.G., Reilly, C.A. & Yost, G.S., 2008. Effects of cell type and culture media on Interleukin-6 secretion in response to environmental particles. *Toxicology in Vitro*, 22, 498-509.
- Vlahakis, N.E., Schroeder, M.A., Limper, A.H. & Hubmayr, R.D., 1999. Stretch induces cytokine release by alveolar epithelial cells in vitro. *American Journal of Physiology: Lung Cellular and Molecular Physiology*, 277, L167-73.
- Waters, C.M., Roan, E. & Navajas, D., 2012. Mechanobiology in lung epithelial cells: measurements, perturbations, and responses. *Comprehensive Physiology*, 2, 1-29.
- Weber, B., Bader, N., Lehnich, H., Simm, A., Silber, R.E. & Bartling, B., 2014. Microarray-based gene expression profiling suggests adaptation of lung epithelial cells subjected to chronic cyclic strain. *Cell Physiol Biochem*, 33, 1452-1466.
- Wirtz, H.R. & Dobbs, L.G., 1990. Calcium mobilization and exocytosis after one mechanical stretch of lung epithelial cells. *Science*, 250, 1266-9.
- Wu, J., Wang, Y., Liu, G., Jia, Y., Yang, J., Shi, J., Dong, J., Wei, J. & Liu, X., 2017. Characterization of air-liquid interface culture of A549 alveolar epithelial cells. *Brazilian Journal of Medical and Biological Research*, 51, e6950.
- Yamamoto, H., Teramoto, H., Uetani, K., Igawa, K. & Shimitsu, E., 2002. Cyclic stretch upregulates interleukin-8 and transforming growth factor- β 1 production through a protein kinase C-dependent pathway in alveolar epithelial cells. *Respirology*, 7, 103-109.
- Yang, Y., Li, W., Kroner, E., Arzt, E., Bhushan, B., Benameur, L., Wei, L., Botta, A., Lu, Y., Lou, J., Jena, D., Nosonovsky, M., Bhushan, B., Søndergaard, T., Sekhar, P.K., Bhansali, S. & Trusov, A.A., 2012. Genotoxicity of Nanoparticles. In B. Bhushan (ed.) *Encyclopedia of Nanotechnology*. Dordrecht: Springer Netherlands, 952-962.

- Yuan, H. & Zhang, S., 2010. Effects of particle size and ligand density on the kinetics of receptor-mediated endocytosis of nanoparticles. *Applied Physics Letters*, 96, 033704.
- Zamprogno, P.G.V., Wüthrich, S., Achenbach, S., Stucki, J., Hobi, N., Schneider-Daum, N., Lehr, C.-M., Huwer, H., Geiser, T. & Schmid, R., 2019. Second-generation lung-on-a-chip array with a stretchable biological membrane. *BioRxiv*.

11 Supplementary Information

11.1 Identity verification of A549 cell line

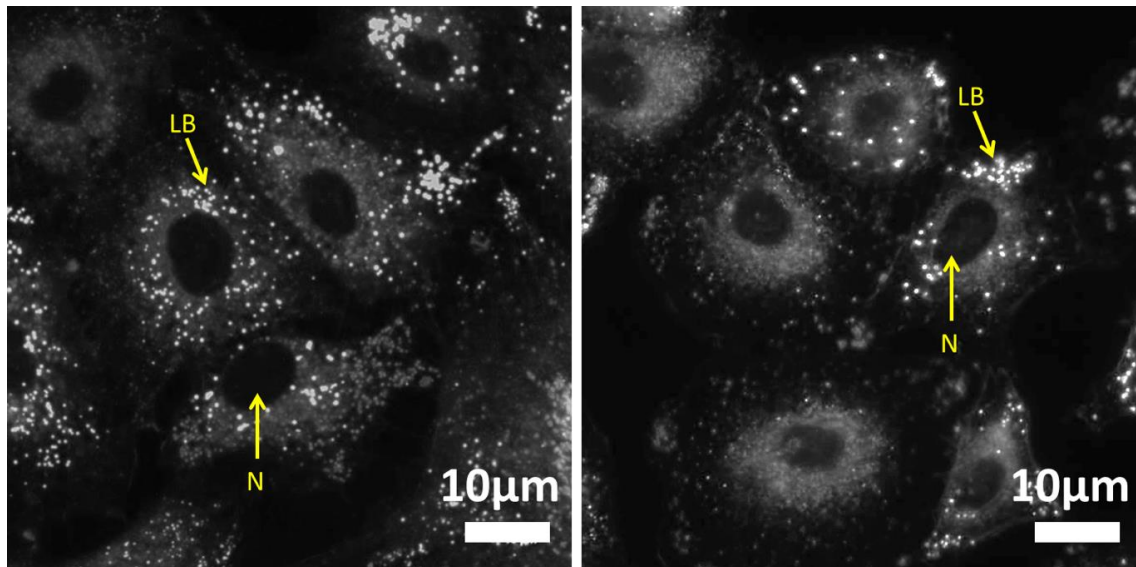


Figure 31: Lamellar bodies (LB) in A549 cells stained with LD540 (left) for fluorescence microscopy, or visualized with darkfield microscopy (right). N = Nucleus.

11.2 Intracellular nanoparticle localization

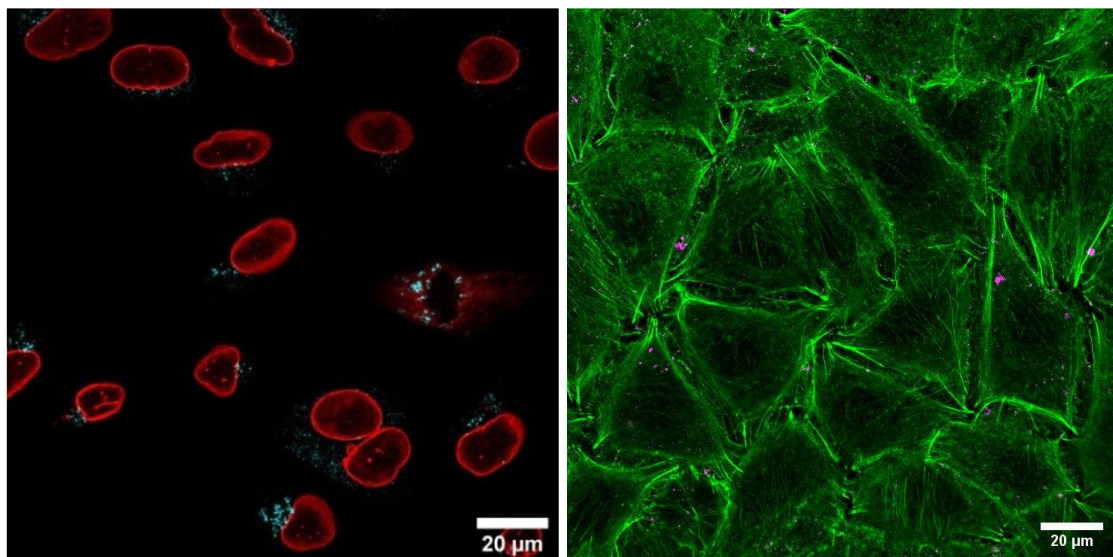


Figure 32: Left: Confocal fluorescence microscopy of A549 treated with fluorescently labeled Si25 at $100 \mu\text{g ml}^{-1}$ for 24 hours. Lamin-B (red) nucleus staining with Si25 labeled with Atto 647N (cyan). Right: Confocal fluorescence microscopy of A549 treated with fluorescently labeled Si25 ($100 \mu\text{g ml}^{-1}$) + 15% stretch for 2 hours. Filamentous actin (green) and Si25 labeled with Atto 647N (magenta).

11.3 Validation of elongation in stretching setup

To validate the manufacturer's specifications on area expansion values, a membrane was marked with five crosses by hand and one picture was taken when the membrane was relaxed and one when the membrane was stretched at a nominal value of 15% (or 25%). With ImageJ 1.51j8, 14 different distances between the crosses were measured to determine the elongation of +8% (or 13%), which results in an effective area expansion of +17% (or 27%).

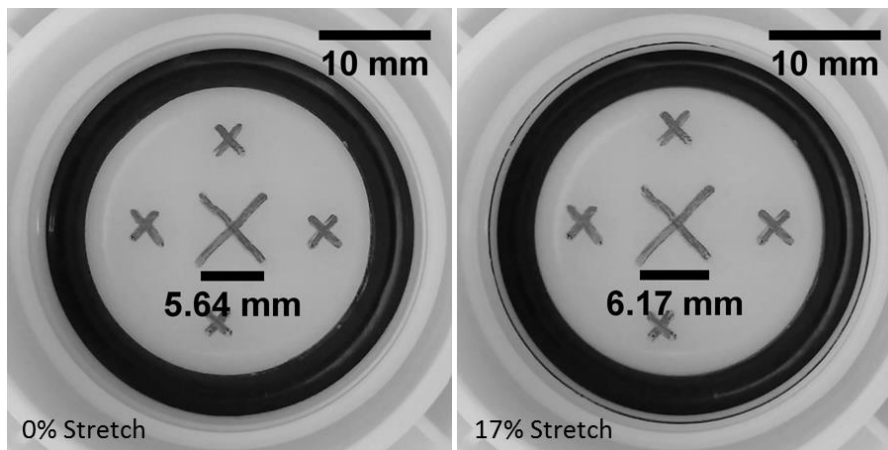


Figure 33: Validation of nominal area expansion.

11.4 Primer validation

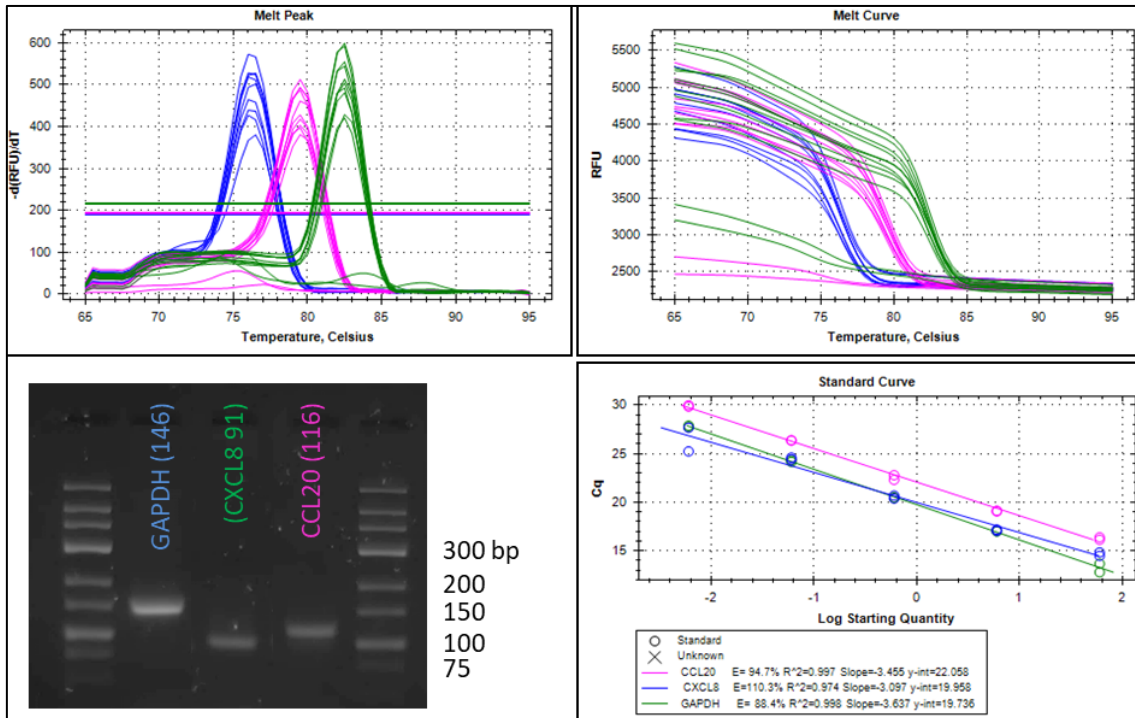


Figure 34: Primer validation: Melting peak, melting curve, electrophoresis, qPCR standard curve.

11.5 LDH degradation

To determine the amount of lactate dehydrogenase that potentially degraded during the 24 hour exposition time, a control experiment was performed. Cells were seeded and grown to confluence in a 96-well plate. Fresh medium was added to both groups and the blank (Medium + FBS) at $t = 0$ min. Triton X-100 was given to both groups at $t = 0$ min. The LDH assay (CytoTox-ONE Homogeneous Membrane Integrity Assay (Promega GmbH, Germany)) was performed with group A at $t = 30$ min and with group B at $t = 24$ h. After 24 h only $\approx 50\%$ of the released LDH could still be detected. Data represent mean values \pm SD of one experiment with 3 technical replicates. Student's t-test with $\alpha = 0.05$ was performed and indicated a significant degradation of LDH within 24 h in blank, untreated controls and triton X-100 treated positive controls.

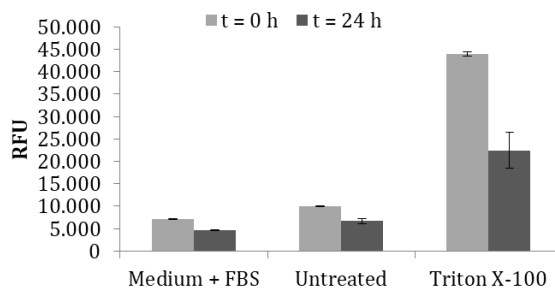


Figure 35: Degradation of LDH within 24 h.

11.6 Leaching of fluorescent SiO₂ nanoparticles

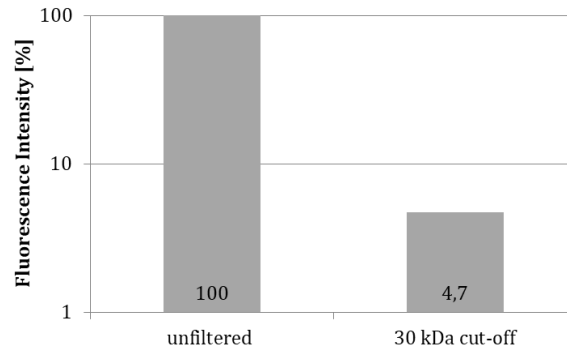


Figure 36: Leaching of the ATTO 647N dye was determined by fluorescence measurements using a centrifugal device with a 30 kDa molecular weight cut-off. No significant leaching was observed.

11.7 Stretch and Si25 induced IL8 secretion

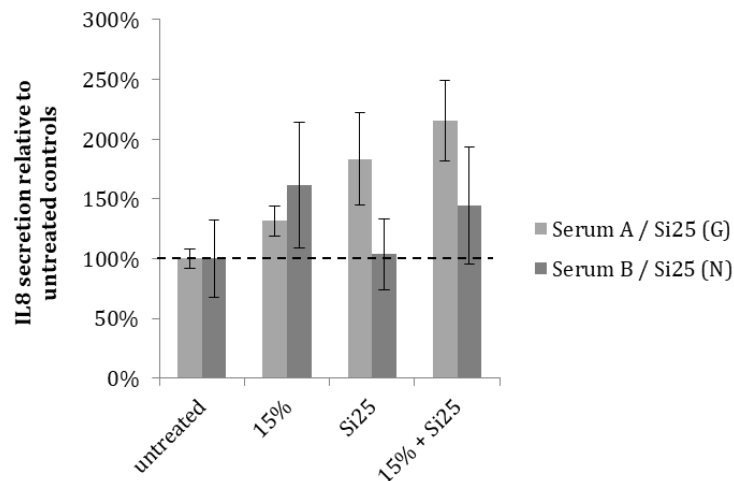


Figure 37: A549 cells were cultured on laminin-coated flexible membranes and treated with 15% stretch, Si25 of different batches ($100 \mu\text{g ml}^{-1}$), or both. Two different experimental setups are compared: cells cultured in medium supplemented with serum 'A' and exposed to Si25 (G) and cells cultured in medium supplemented with serum 'B' and exposed to Si25 (N). Cytokine secretion (IL8) was determined by ELISA after 24 h exposition. $N = 3$.

11.8 Cell morphology under different fetal bovine sera

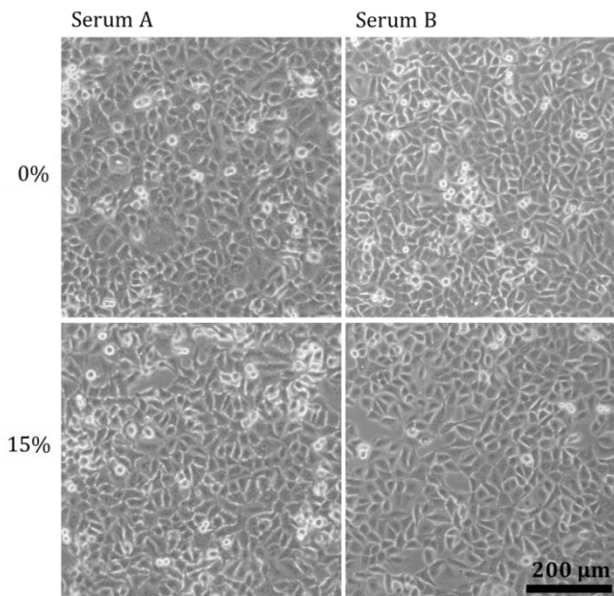


Figure 38: Light microscopy of A549 cells that were cultured on laminin-coated flexible membranes with two different supplements of FBS. Cells were kept under static (0% stretch) or dynamic (15% stretch) conditions for 24 hours.

11.9 Cell morphology under supplementation with heat-inactivated FBS

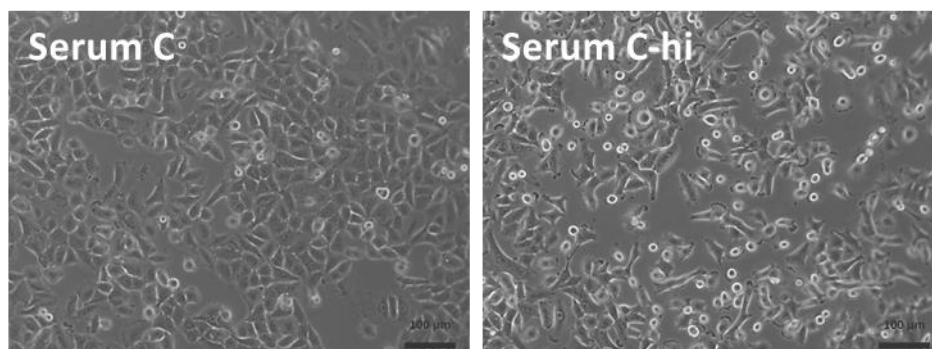


Figure 39: Light microscopy of A549 cells that were cultured on laminin-coated flexible membranes with untreated or heat-inactivated fetal bovine serum 'C' for 24 hours. Serum was heat inactivated at 56°C for 30 minutes before addition to culture medium. Scale indicates 100 µm.

11.10 Cytokine expression under supplementation with heat-inactivated FBS

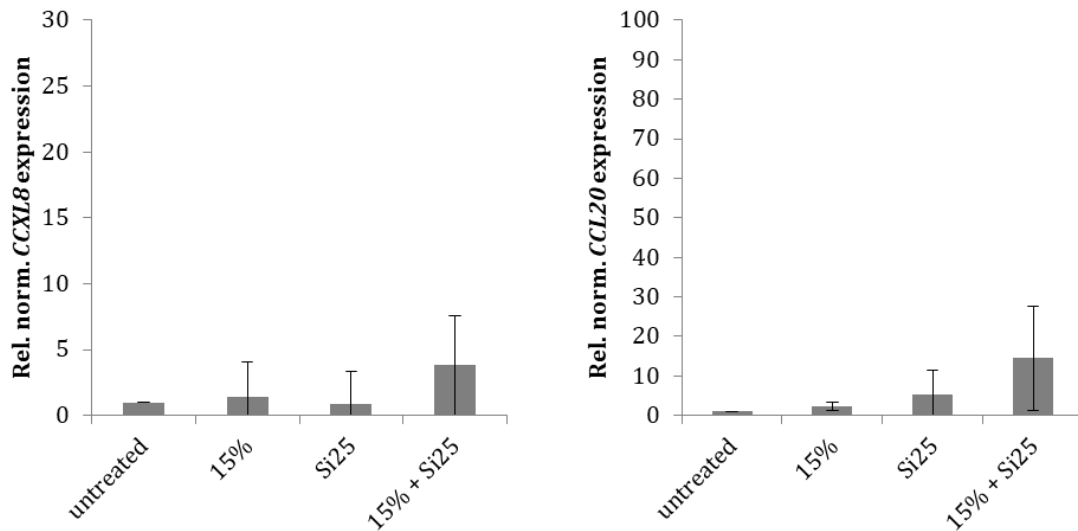


Figure 40: A549 cells were cultured on laminin-coated flexible membranes and treated with 15% stretch, Si25 (batch "N", $100 \mu\text{g ml}^{-1}$), or both. Cell culture medium was supplemented with serum 'C'. Cytokine expression (CXCL8, CCL20) was normalized to GAPDH expression and related to expression levels of untreated controls. $N=3$.

11.11 Effect of nanoparticles and stretch on human pulmonary alveolar epithelial cells

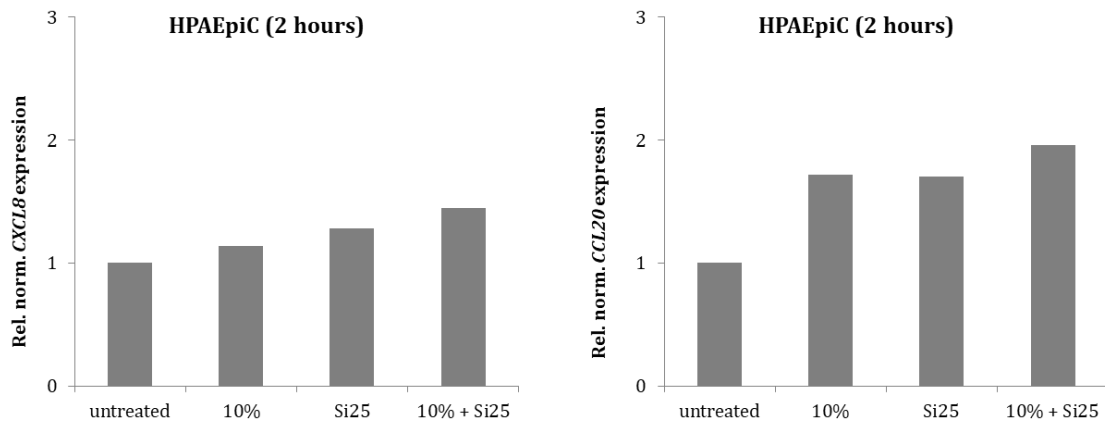


Figure 41: Human pulmonary alveolar epithelial cells (HPAEpiC) were cultured on laminin-coated flexible membranes and treated with 10% stretch, Si25 ($100 \mu\text{g ml}^{-1}$), or both. Cytokine expression (CXCL8, CCL20) was normalized to GAPDH expression and related to expression levels of untreated controls. $N=1$.

11.12 Translocation kinetics of NF- κ B subunits

11.12.1 NF- κ B p65

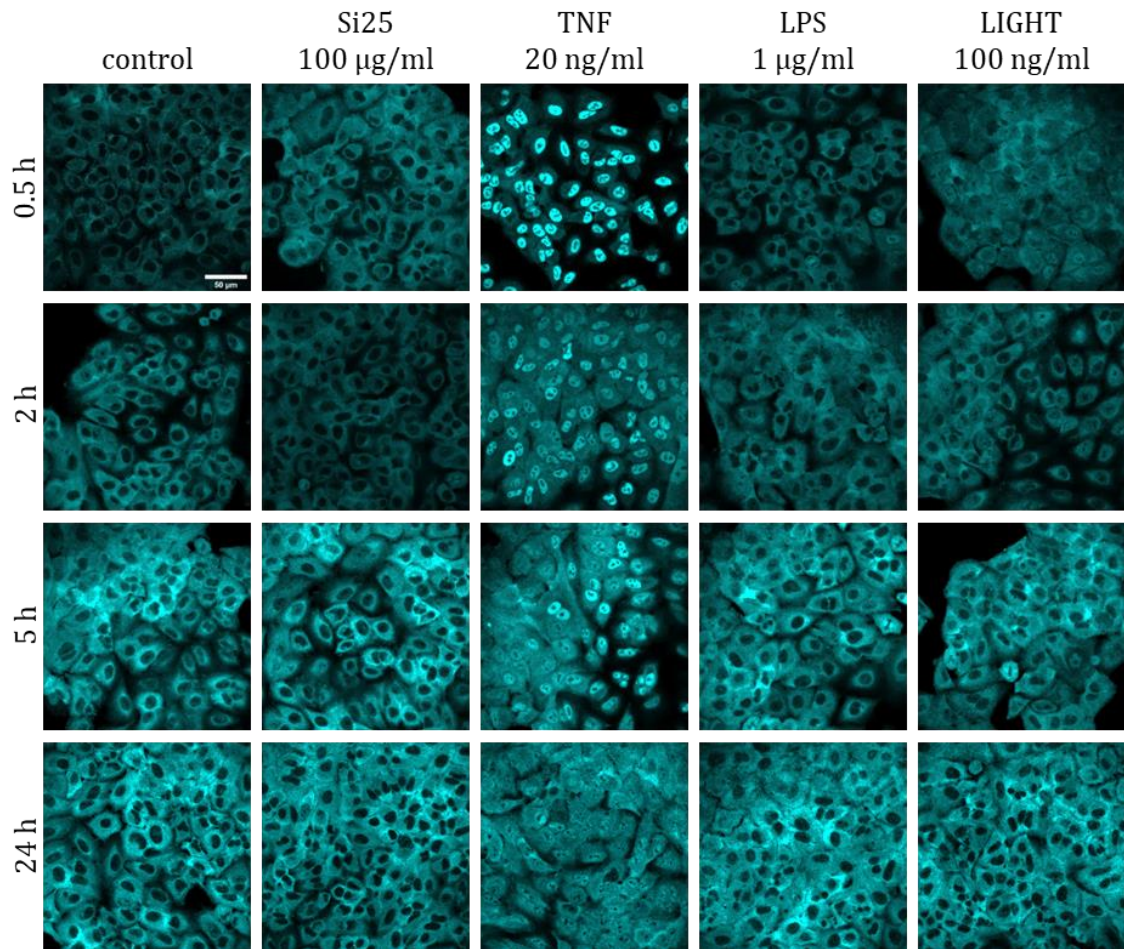


Figure 42: Confocal fluorescence microscopy of A549 cells that were treated with Si25, human recombinant TNF, lipopolysaccharides (LPS, *E. coli* K12), or human recombinant LIGHT (TNFSF14) and fixed and immuno stained for NF- κ B p65 after different incubation times. Images represent one experiment.

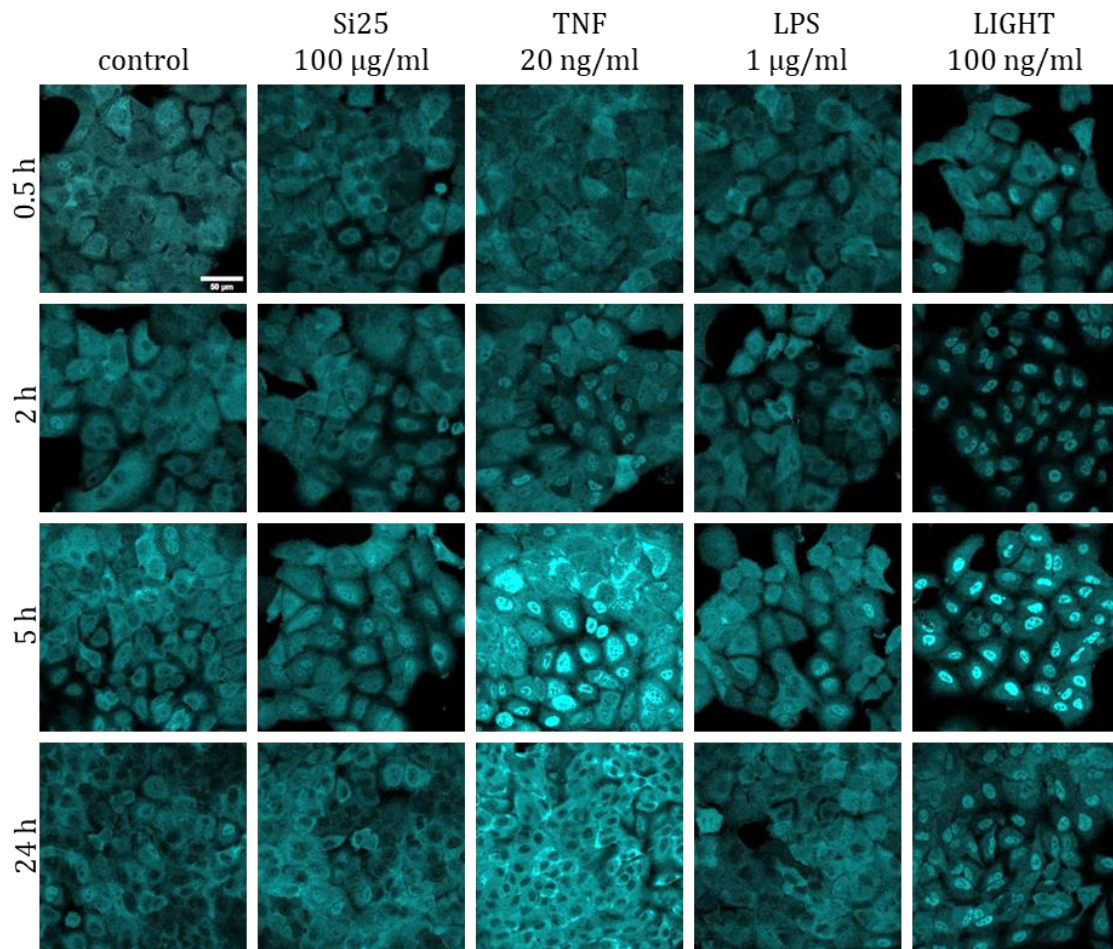
11.12.2 NF- κ B2 p100/p52

Figure 43: Confocal fluorescence microscopy of A549 cells that were treated with Si25, human recombinant TNF, lipopolysaccharides (LPS, *E. coli* K12), or human recombinant LIGHT (TNFSF14) and fixed and immuno stained for NF- κ B2 p100/p52 after different incubation times. Images represent one experiment.

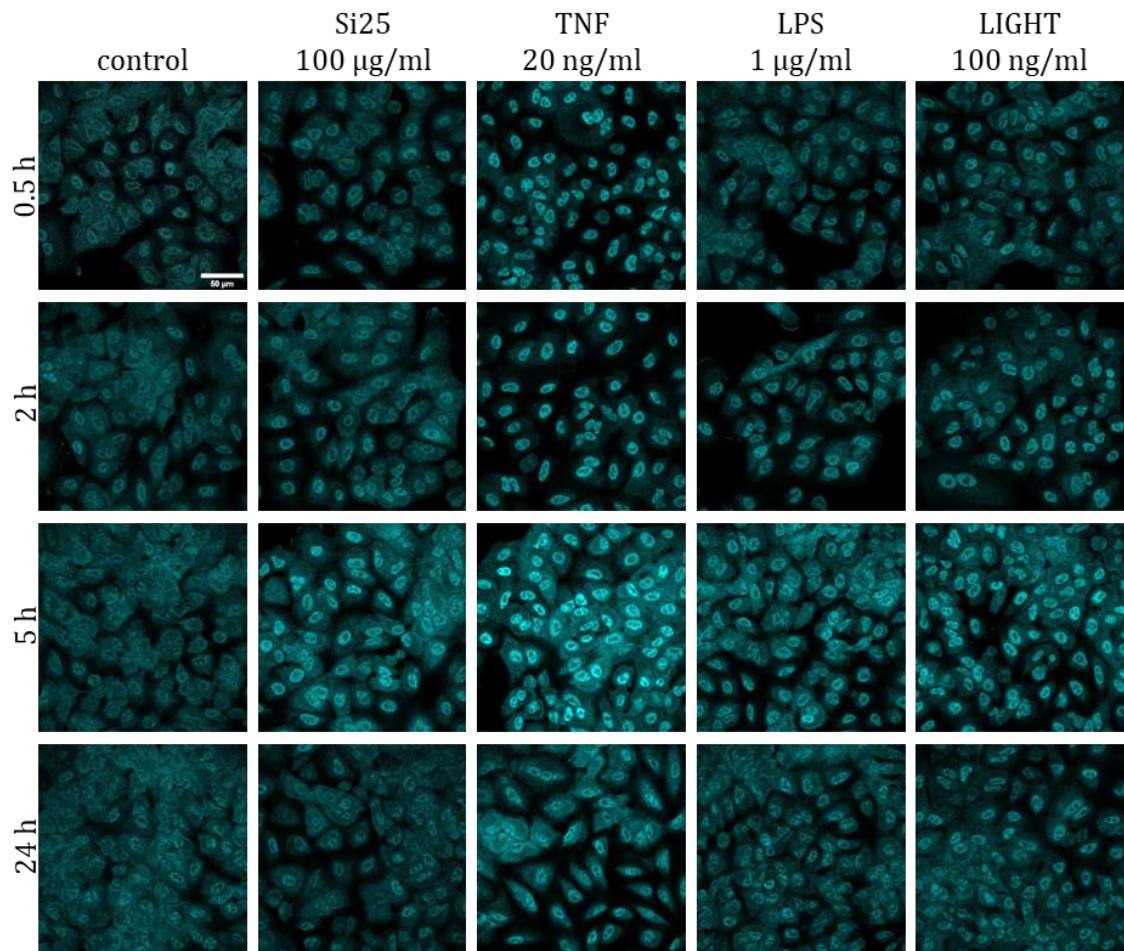
11.12.3 NF- κ B1 p105/p50

Figure 44: Confocal fluorescence microscopy of A549 cells that were treated with Si25, human recombinant TNF, lipopolysaccharides (LPS, *E. coli* K12), or human recombinant LIGHT (TNFSF14) and fixed and immuno stained for NF- κ B1 p105/p50 after different incubation times. Images represent one experiment.

Danksagung

Für die Möglichkeit zur Erarbeitung dieser Doktorarbeit, für die Unterstützung und Förderung, sowie für die vielen anregenden Diskussionen möchte ich mich herzlich bei Frau PD Dr. Annette Kraegeloh bedanken. Ebenso gilt mein Dank Frau Prof. Dr. Alexandra K. Kiemer für Ihre Unterstützung und den wertvollen Austausch in regelmäßigen Seminaren.

Bedanken möchte ich mich bei allen Kollegen und Kolleginnen des INM die zum Erfolg dieser Arbeit beigetragen haben: Frau Jennifer Welck für eine erstklassige Vorarbeit zum Versuchsaufbau und zur Probengewinnung sowie für die Überlassung einiger wertvoller Proben, Frau Silke Kiefer für die umfangreiche und tatkräftige Unterstützung im Labor, Frau Dr. Jana Fleddermann für ihre Unterstützung in Sachen Mikroskopie und die vielen fachlichen Diskussionen, Frau Dr. Isabella Tavernaro und Frau Anja Colbus für all die Synthesen und Charakterisierungen der Nanopartikel, Herrn Dr. Marcus Koch für die Elektronenmikroskopie, Frau Gabi Kliegle für die Unterstützung bei der Durchführung der ELISAs. Mein Dank gilt auch allen Koautoren und Koautorinnen der Publikation die aus dieser Arbeit entstanden ist.

Ebenso möchte ich mich bei allen INM und UDS Kollegen und Kolleginnen für eine gute Zusammenarbeit und das allzeit angenehme Arbeitsklima bedanken. Es war eine schöne Zeit an die ich mich immer gern erinnern werde!

„Danke“ an meine Korrekturleserinnen Eva und Annette S., an meine Familie und besonders an meinen Partner Max für sein Verständnis und die unzähligen Ermutigungen.